Isern, A.R., Anselmetti, F.S., Blum, P., et al., 2002
Proceedings of the Ocean Drilling Program, Initial Reports Volume 194

4. Site 1193[1]

Shipboard Scientific Party[2]

INTRODUCTION

Site 1193 (proposed Site CS-01A) is located on the Marion Plateau, in 348 m of water ~80 km from the south central Great Barrier Reef margin (Fig. F1). The site is positioned at the intersection of regional seismic line MAR13 (SP 4126) (Fig. F2) and local grid line MAR34 (SP 2241). The total sediment thickness at Site 1193 is 540 m. Holes 1193A, 1193B, and 1193C penetrated to total depths of 515, 138, and 548.5 meters below seafloor (mbsf), respectively. Acoustic basement was recovered in Hole 1193C. Site 1193 was the first Ocean Drilling Program (ODP) site at which the advanced diamond core barrel (ADCB) system was used to drill a sedimentary section. This experiment was planned because recovery in platform carbonates generally is extremely low.

Site 1193 was positioned to recover the sediment sequences making up the middle Miocene northern carbonate platform (Fig. F2) (MP2 of Pigram, 1992). This platform is an important element for the reconstruction of Miocene sea level history because its top marks the last platform growth phase before the major middle to late Miocene sea level fall. Seismic data indicates that the top of the northern platform is an irregular, karstic surface buried under a relatively thin cover of hemipelagic drift deposits (Fig. F2). Seismic geometry further indicates that this platform was established on previously deposited prograding slope sediments, as seen by the inclined reflections underneath the platform (Fig. F2).

The northern edge of this platform was drilled during Leg 133 (Davies, McKenzie, Palmer-Julson, et al., 1991). Coring at Sites 816 and 826 showed that the top of the northern platform consisted of a tropical reefal assemblage deposited in water depths ≤20 m. This depth defines the approximate point from which the sea level began to fall near the middle/late Miocene boundary (Pigram et al., 1992). Results from Sites 816 and 826 indicated that the top of the northern carbonate plat-

F1. Bathymetry map, p. 32.

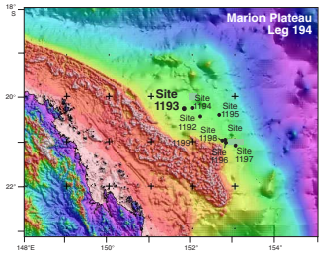

F2. Seismic line MAR13, p. 33.

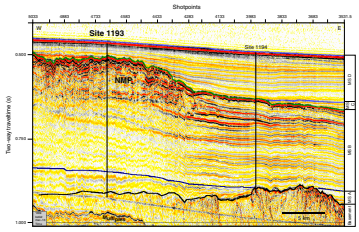

[1]Examples of how to reference the whole or part of this volume.
[2]Shipboard Scientific Party addresses.

form has been subjected to subaerial exposure (Davies, McKenzie, Palmer-Julson, et al., 1991).

Site 1193 provides a record of the total thickness of the eastern edge of this platform, as well as the timing of its growth phases and its exposure. By investigating the hemipelagic sediments overlying the platform, the timing of its burial can be determined. In addition, postcruise analysis on Site 1193 sediments will yield a record of fluid flow and diagenetic processes in this partially dolomitized carbonate platform. The nature of the deeper-water sediments underlying the platform, together with the facies of the basal sediments directly overlying the basement, provide information regarding the timing and processes linked to the initial basement transgression. Finally, Site 1193 provides a lithologic record of the nature of the acoustic basement.

OPERATIONS

Operations at Site 1193 (proposed Site CS-01A) began when a beacon was dropped on site coordinates at 2200 hr on 12 January 2001. The water depth was 352.8 m based on the corrected precision depth recorder.

Hole 1193A

Hole 1193 was spudded with the advanced piston corer (APC) at 0045 hr on 13 January and established a water depth of 348.3 m (Table T2, p. 87, in the "Leg 194 Summary" chapter; Tables T1, T2). Piston coring advanced to 37.1 mbsf, where the carbonate platform was penetrated. The average recovery for the piston-cored interval was 100.8%.

T1. Coring summary, p. 92.

T2. Expanded coring summary, p. 93.

Coring continued with the extended core barrel (XCB) system and advanced to 450.4 mbsf (Core 73X) with generally low recovery. Cores were retrieved at half-interval (~4.8 m) advances to maximize the chances of capturing the elusive reefal debris. The average recovery over this interval was 27.8%. Recovery was below 6% between 50 and 150 mbsf and improved in the interval from 150 to 180 mbsf, ranging between 10% and 60%, apparently as a result of higher amounts of mud in the formation.

Following the recovery of Core 73X, excessive backflow from the drill string resulted in the entire drill floor being sprayed with water. When the driller lowered the kelly into the drill pipe in preparation for making up the next connection, the drawworks mechanical brake did not hold. The driller applied the electric brake to gain control of the traveling assembly, but the assembly had already descended ~2 to 3 ft, thus bending the 20-ft and 30-ft knobbies along with the first joint of 5.5-in drill pipe in the rotary table. Apparently, the immediate cause of the incident was the wet mechanical brakes on the drawworks.

After the severely bent 30-ft knobby was laid out and the slightly bent 20-ft knobby was made up to the drill string, rotation and circulation could not be established. The string was worked with high pull, weight, and torque until rotation was regained. Mud sweeps were circulated to work the tight hole. The wireline was run to retrieve the latest core barrel, and the pipe was worked again until it eventually became free. The top drive and all traveling components were inspected for any damage, and no problems were detected. Coring operations resumed at 0730 hr on 16 January. The total operating time lost as a result of this incident was 7.75 hr.

XCB coring advanced from 450.0 to 515.0 mbsf with an average recovery of 17.2% for this interval. At this depth, hole instability prevented further coring. The pipe got stuck, and another 5 hr was needed to free it. After several wireline fishing trips failed to recover the last core barrel (Core 84X), the hole was displaced with 118 barrels (bbl) of mud, and the bottom-hole assembly (BHA) had to be recovered. The retrieved core barrel was found with a broken latch dog, which had jammed into the latch sleeve. The latter was cracked in several places.

During coring operations on 13 January, the rendezvous boat *Black Samurai* arrived from Mackay, Australia, with three scientists (Gilles Conesa, Gregor Eberli, and Wuchang Wei) and two ODP technicians (Austin Crawford and Gavin Eppard), who stayed on shore so that the Hydraulic Autoclave Coring Equipment (HYACE) engineers could be accommodated during the first 3 days. In addition to the HYACE team, the personnel leaving the *JOIDES Resolution* were Lamont-Doherty Earth Observatory representative Greg Meyers, ODP/Texas A&M University (TAMU) development engineer Eddie Wright, and ODP/TAMU technician Darren Lawrie.

While the drill string was being recovered, a helicopter from Reef Helicopters in Mackay landed on the vessel and removed roughneck Melchoir Pepito, who had been diagnosed with probable kidney stones. The helicopter landed at 1015 hr and departed with the patient at 1028 hr on 17 January.

Hole 1193B

The vessel was offset 20 m east of Hole 1193A. A rotary core barrel (RCB) BHA was lowered, and the seafloor was tagged, indicating a water depth of 348.3 mbsf. Hole 1193B was spudded at 1730 hr on 17 January. After the hole was washed ahead to 35.0 mbsf, rotary coring penetrated the hard cover of the carbonate platform and advanced 53.8 mbsf with 19% recovery. The average rate of penetration for the two cored intervals was 6.5 m/hr. A free-fall funnel (FFF) was deployed after the bit had been pulled back to 20.3 mbsf. The underwater television system was employed to verify that the FFF was visible and not buried in the top of the seafloor.

The pipe was tripped to make up the ADCB system (see **"Sea Trials with the Advanced Diamond Core Barrel,"** p. 2, in the "Explanatory Notes" chapter) with a 7.25-in polycrystalline diamond compact (PDC) bit. The ADCB was deployed in anticipation of improved recovery of reefal limestone. The core barrels were dressed with the new Lexan liner and a combination basket/slip-type catcher. Hole 1193B was reentered with the ADCB (Fig. **F3**), and the bit was advanced to 53.8 mbsf, where coring was initiated. The first core (3Z) was cut in less than 7 min, with an advance of 4.7 m. The mud pump was set at 13 strokes/min, and the rotary speed was set at 40 rpm. The maximum weight on bit used throughout the core run was <3 kilopounds (kips) (average = ~2 kips). Operating pressure during the initial core run was between 300 and 350 psi. The second barrel gave a momentary indication that it landed, but immediately appeared to have lifted off of the seat as a result of a loss in operating pressure. The barrel was recovered and the core lifter case replaced with a standard slip-type catcher. The hole appeared to be packing off, so the pumps were turned up again before the barrel reached the bottom. Because of the softness of the material recovered in the first ADCB core, the decision was made to advance the core barrel, despite the fact that it appeared not to have landed properly. Core 4Z was cut in

F3. Reentrance of Hole 1193B with ACDB bit, p. 34.

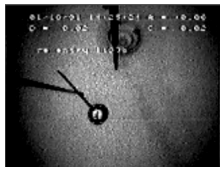

15 min; the driller had a hard time keeping weight on the bit. After a 4.5-m core run, the sinker bars were deployed. The core barrel was jarred up by the wireline jar, but it would not come free. The pumps were turned up in an attempt to see if the barrel could be pushed down with pressure, which sheared off the shear pin in the overshot. Two more jarring attempts would not release the core barrel. The pipe was pulled again to retrieve the barrel, and it was found that the inner tube had collapsed, which distorted the diameter and prevented the section of the inner tube from being pulled through the landing ring. It appears that when the hole collapsed and pump pressures were increased momentarily between 2200 and 2400 psi, the path of least resistance was for the inner tube to collapse before clearing the annulus of the hole.

Hole 1193B was reentered with the ADCB at 0725 hr on 19 January. The bit was advanced to 63.2 mbsf, where ADCB coring was resumed. Total recovery over the interval from 53.8 to 91.0 mbsf yielded 16.4%, compared to 2.6% for the XCB over a similar interval. The bit appeared to have encountered a clay layer with Core 7Z, preventing any advance in 47 min of rotation, despite applying a weight of over 15 kips. The barrel was recovered, and the pump strokes were reduced in an attempt to clean the bit. Apparently, this corrected the problem because penetration and recovery improved on the next core. Drilling parameters were held constant over these cores, with bit weight averaging 5 kips, rotary speed at 40 rpm, and flow rate varying between 6 and 10 strokes/min (30 to 50 gal/min). The other significant difference was that 5 bbl of sepiolite mud was introduced in the pipe before breaking each connection to prevent backflow. After Core 4Z, no other hole problems were experienced.

After cutting Core 11Z, the inner barrel was dropped, but no indications were seen via pump pressure that the barrel had landed properly. Several more unsuccessful attempts were made to deploy the inner barrel. An improvised bit deplugger was run in an attempt to clear the core blockage. Several blows of the wireline jars were necessary to clear the throat. The core barrel subsequently landed correctly, but the low circulation pressure established earlier was lower by over 150 psi. Cores 12Z through 21Z were cut, but core recovery was very poor, and recovered cores were not cut to gauge but only captured by being jammed in the throat of the inner barrel. Average recovery for this portion of the hole dropped to 6.3% with many of the cores being recorded as zero despite the impression from the surface that the bit was encountering material that should have been recovered more easily. Most of the material appeared to be lost because the core was not being trimmed for the catchers. The driller also noted on several occasions that more than 1 m of fill (presumably lost core) was encountered on the bottom of the hole at the beginning of several coring attempts. Drilling parameters were the same for this interval as for the overlying interval that had better recovery.

At this point, the drill string was pulled, and it was found that ~50% of the cast matrix pilot portion of the bit that trims the core was missing. Jarring with the bit deplugger to clear the blockage in the throat had apparently broken it off. The bit looked brand new except for the broken core trimming portion and one lost PDC element. The PDC element was most likely lost from coming into contact with the broken portion of the bit that was lying in the hole after rotation and coring was reinitiated. A properly spaced out and designed bit deplugger is recommended to ensure that this will not occur again. Hole 1193B was officially terminated at 1515 hr on 20 January.

For the second time in 4 days, a medical evacuation by helicopter was required. At 1646 hr on 20 January, a Kawasaki helicopter from Reef Helicopters landed on the vessel. Melchoir Pepito, the roughneck with the kidney stones who was evacuated earlier, returned to the vessel ready for work. A scientist, Brooke Olson, was put on the helicopter in a stretcher, along with her belongings. She was diagnosed with a fractured femur. The helicopter left the vessel at 1657 hr. Olson's diagnosis was confirmed in the Mater Hospital, where she underwent surgery a couple of days later before returning home.

Hole 1193C

As the drilling crew made up the RCB BHA for Hole 1193C, the vessel was offset 20 m northeast of Hole 1193B. Hole 1193C was spudded at 1800 hr on 20 January, with the primary objective of serving as a dedicated logging hole. After drilling through the top pelagic section, the top of the carbonate platform was cored for the third time, from 35 to 70.1 mbsf, with an average recovery of 16.2%. A center bit was deployed, and continuous drilling advanced to 510 mbsf at an average penetration rate of 24 m/hr.

While drilling ahead with the center bit, the float valve is open to allow backflow at the rig floor while making connections. This is necessary because cuttings in the annulus create excess hydrostatic head in the pipe. To counteract the overpressure and ensure the annulus was being circulated clean, 10 bbl of sepiolite was introduced during each connection and then circulated while we drilled the next interval. While making a connection at 156.1 mbsf, the drill string became stuck. Circulation and rotation could only be reestablished after applying 40 kips of overpull and 700 A of rotary current. The string was worked up and down over a 20-m interval until normal torque and pressure values were established. A total of 340 bbl of sepiolite was circulated during this operation.

Four additional cores were taken from 510 to 548.5 mbsf, where basement was penetrated. Mud sweeps were pumped for each cored interval. A 50-bbl sepiolite sweep was circulated, the bit was released on bottom, and the hole was displaced with 172 bbl of sepiolite mud in preparation for logging. The recovery for this portion of the hole was 39.9%, with an average penetration rate of 24.4 m/hr. The total cored interval for Hole 1193C was 73.6 m, with 21.07 m recovered (28.6%). A total interval of 474.9 m was drilled without coring.

The drill string was pulled and had to be worked through a tight spot at 297 mbsf with 80 kips of overpull. After the drill string was freed, excessive backflow propelled mud from the open end of the drill pipe at the rig floor to the monkey board level with one stand of drill pipe pulled above the rotary table. The backflow quickly vented all of the mud from the drill pipe. The top drive was picked up at 297.2 mbsf, but circulation or rotation could not be established. A maximum of 200 kips of overpull was applied in a 3-hr attempt to free the pipe according to shallow-water guidelines. A 50-bbl sweep was pumped while we worked the tight hole. However, no indication was observed that the mud sweep was entering the annulus.

Severing operations commenced with a safety meeting for all personnel involved. The Schlumberger wireline was rigged up and all relevant safety checks were performed. Seventy-two pellets of 1.75-in Goex RDX were loaded for the severing charge. Depth of connection was 433.96 m of drill string length (75.06 mbsf). Prior to severing the drill pipe, the

drill string compensator (DSC) was opened, and 30 kips of overpull was applied. The severing charge was fired, and no indication of free pipe was noted on the weight indicator. The DSC was overpressured to 70 kips, at which point the stuck pipe came free. Circulation and rotation were established. The wireline was retrieved and rigged down. The top drive was used to pull out of the hole, and the fragmented end of pipe was on deck by 2100 hr, ending operations at Site 1193.

As the drill string was being recovered, several attempts to retrieve the beacon failed.

LITHOSTRATIGRAPHY AND SEDIMENTOLOGY

The lithostratigraphy of Site 1193 is divided into seven units (Table T3; Fig. F4). Unit I consists of 3.5 m of uppermost Pleistocene light brown to yellow, planktonic foraminifer-dominated grainstone with underlying mudstone and packstone. Below Unit I is 31 m of unconsolidated Pleistocene to uppermost Miocene hemipelagic foraminiferal packstone (Unit II). Unit II overlies a major hiatus, estimated to have occurred from >12 to 5.6 Ma, at the top of a 194-m-thick unit of coarse bioclastic limestone and subordinate dolostone (Unit III). Unit III corresponds to the upper part of the seismically defined Northern Marion Platform (NMP), which is believed to have prograded southeastward in the early to middle Miocene. The diverse biotic assemblage of bryozoans and larger benthic foraminifers, with subordinate mollusks and red algae but almost no coral, indicates temperate to cool subtropical depositional conditions. Immediately below these high-energy, relatively shallow-water deposits (mainly <100 m water depth) is a clay-rich mudstone interval ~20 m thick (Unit IV). Unit IV grades downward into a 136-m interval of fine-grained bioturbated skeletal packstone (Unit V), believed to represent the progradational platform slope that correlates with clinoforms imaged on seismic data. The base of the sedimentary section consists of 146 m of interbedded grainstone and subordinate quartzose sandstones (Unit VI), deposited in a shallow-water setting. The deepest core at Site 1193 (540–549 mbsf) sampled the top of acoustic basement, consisting of hydrothermally altered volcaniclastic deposits of probable basaltic composition (Unit VII).

T3. Lithologic units, p. 101.

F4. Lithostratigraphic summary, p. 35.

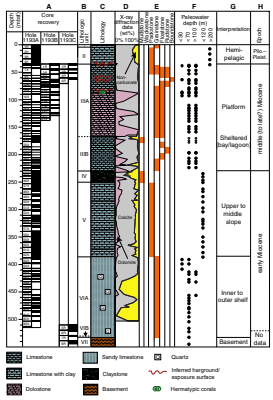

F5. Close-up photograph of grainstone bed, p. 36.

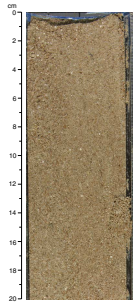

Lithologic Units

Unit I (0–3.5 mbsf; Late Pleistocene)

Unit I consists of light brown to yellow unconsolidated planktonic foraminifer limestone containing subordinate benthic foraminifers and scaphopods (Fig. F4). Also present are rare echinoderm fragments, gastropods, bivalves, ostracods, and arthropod fragments. There is a downward textural change from an upper 2.3-m-thick grainstone interval (Fig. F5) to 0.5 m of mudstone and then a lowermost 0.7-m-thick packstone interval. Bioturbation increases downward from barren at the top to heavy in the packstone. The boundary between Units I and II is marked by a sharp color change from yellow above to light greenish gray below.

Unit II (3.5–35.0 mbsf; Pleistocene to Late Miocene)

This 31.5-m-thick interval of unconsolidated, light olive-gray, skeletal packstone consists of very fine to fine sand–sized planktonic foraminifers in a clay-rich mud matrix (Figs. F4, F6). Bioturbation is heavy, with conspicuous *Chondrites*. Minor components include benthic foraminifers and crustacean fragments. Minor glauconite is present throughout (<1%) the unit.

Unit III (35.0–229.2 mbsf; Late to Middle Miocene)

Based on differences in color, biota, and dolomitization, Unit III is divided into two subunits (Fig. F4). As a whole, however, this unit consists of 194 m of skeletal rudstone and floatstone with subordinate grainstone, packstone, and clay-rich mudstone. Most of the section is white to red-brown and pink limestone. In some places, it is partly to entirely replaced by a light brown to deep orange sucrosic dolomite (Fig. F4). Most intervals are distinctly bedded by size sorting, horizontal orientation of bioclasts, and varying carbonate mud content.

Bryozoans are the main skeletal components of Unit III; larger benthic foraminifers are common. Subordinate components include bivalve, gastropod, and echinoderm fragments and coralline algae. The latter comprise both discrete fragments of branching forms and rhodoliths. A single specimen of branching hermatypic coral was found at 83 mbsf (interval 194-1193B-8Z-1, 2–4 cm).

Micritic matrix varies widely in abundance resulting in marked porosity changes in Unit III (see "Core Physical Properties," p. 24). Porosity has also been reduced by calcite cements.

Subunit IIIA (35.0–167.0 mbsf; Late to Middle Miocene)

Subunit IIIA is mainly composed of bryozoan-rich limestone to dolostone showing a rudstone floatstone fabric with a grainstone/packstone matrix. Above 90 mbsf, the cored intervals are nearly pure limestone, but the lower part of this subunit contains alternating layers composed of ~20% to ~100% dolomite (Fig. F4). The uppermost cores of Subunit IIIA include the following facies (from top to bottom):

1. Foraminifer packstone (Figs. F7, F8) rich in planktonic and subordinate benthic foraminifers, as well as minor echinoderm, bryozoan, and mollusk fragments. The thickness of this bed is uncertain because of low core recovery. It is partly covered by a thin (~0.2–0.5 mm) veneer of dark brown material, interpreted as a phosphatic coating (Fig. F7).
2. Oxidized, tightly cemented bryozoan rudstone (Figs. F7, F9). Minor amounts of planktonic foraminifers are also present at the top of this facies, which was recovered in intervals 194-1193A-6X-CC, 0–50 cm, (37.1 mbsf) and 194-1193B-1R-1, 25–105 cm (35.3 mbsf). A thin surface with a dark phosphate? coating is observed in interval 194-1193A-6X-CC, 21 cm (37.3 mbsf).
3. A thick interval of white bryozoan rudstone (Fig. F9) with moderate to high porosity and layers rich in pebble-sized rhodoliths. Vadose silt is present in vugs near the top of this zone (Fig. F10).

Within the upper part of Subunit IIIA, four distinctive, irregular surfaces are observed (35.9 mbsf [interval 194-1193B-1R-1, 90 cm], 61.9

F6. Close-up photograph of the base of Unit II, p. 37.

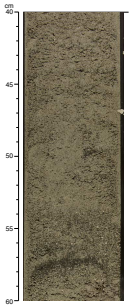

F7. Close-up photograph showing the top of Subunit IIIA, p. 38.

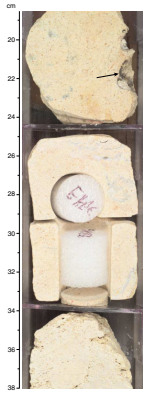

F8. Photomicrograph showing the lithology of Subunit IIIA, p. 39.

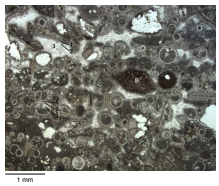

F9. Close-up photograph showing lithologies, Subunit III, p. 40.

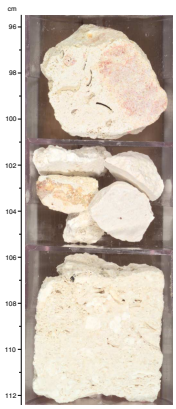

mbsf [interval 194-1193C-4R-1, 30 cm], 68.7 mbsf [interval 194-1193B-6Z-1, 82–89 cm], and 86.5 mbsf [interval 194-1193B-11Z-1, 14–18 cm]) (Fig. F11). Several of these surfaces are underlain by reddened coloring suggesting oxidation. The surfaces at 35.9 and 68.7 mbsf are of special note because they are overlain by centimeter-thick accumulations of skeletal grainstone containing rare to abundant planktonic foraminifers and glauconite pellets, both of which are suggestive of reduced neritic sedimentation.

Also worthy of note is a distinctive rock fabric (present in the intervals 63–64 mbsf and 87–88 mbsf) with millimeter- to centimeter-scale layering defined by size sorting and horizontal orientation of bioclasts (Fig. F12). The lowermost of these two intervals contains multiple zones of thick isopachous cement coatings.

The lower part of Subunit IIIA contains at least three intervals consisting of deep reddish brown to orange dolomitized rudstone to floatstone having a finely crystalline sucrosic dolomite texture that preserves recognizable molds of bryozoan and mollusk fragments (Figs. F13, F14).

Subunit IIIB (167.0–229.2 mbsf; Late to Middle Miocene)

Subunit IIIB is composed mainly of bioclastic rudstone, grainstone, packstone, and floatstone that may contain a certain amount of dolomite. Rock matrix consists of finer-grained grainstone and packstone. The sediments in Subunit IIIB are broadly similar in composition and fabric to those of Subunit IIIA, but the following differences are noted:

1. Color is generally darker than in Subunit IIIA (commonly light greenish gray), suggesting the presence of clay.
2. Thin section data show that Subunit IIIB has a higher content of nonencrusting red algae grains (Fig. F15).
3. No irregular, oxidized surfaces are observed.
4. Completely dolomitized zones are not observed.

Another distinctive feature of Subunit IIIB is the presence of two intervals with mudstone to floatstone fabric having high clay content. The uppermost of these, which is used to define the top of Subunit IIIB, is light greenish gray and at least 9 m thick (167–176 mbsf). It contains layers of largely intact bryozoan fronds 1–3 cm in maximum dimension, together with benthic foraminifers, bivalves, and echinoids. The bryozoans are most abundant in the uppermost 2 m of this interval (Fig. F16), resulting in a coarsening-upward trend. The mud matrix has been entirely replaced by dolomite, whereas the bryozoans are unaltered. The lower clay-rich mudstone bed (interval 194-1193A-41X-1, 0–40 cm; 220 mbsf) occurs at the top of a fining-upward cycle near the base of Subunit IIIB.

The interval from 186 to 210 mbsf, represented by a series of short core segments, shows a large-scale coarsening-upward trend from grainstone through rudstone. The Unit III/IV boundary is inferred to occur between Cores 194-1193A-42X and 43X; therefore, the nature of this boundary could not be determined.

Unit IV (229.2–249.2 mbsf; Late–Middle Miocene)

Unit IV consists of 20 m of greenish gray, clay-rich mudstone containing silt- to very fine sand–sized planktonic and benthic foraminifers and bryozoan fragments, quartz, and glauconite (Figs. F4, F17, F18).

F10. Photomicrograph showing the white, variably porous rudstone to floatstone, p. 41.

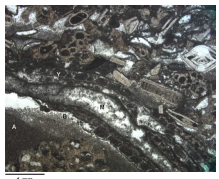

F11. Close-up photograph of a fracture through skeletal packstone, p. 42.

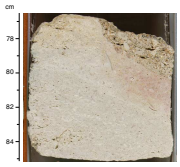

F12. Close-up photograph showing skeletal rudstone, p. 43.

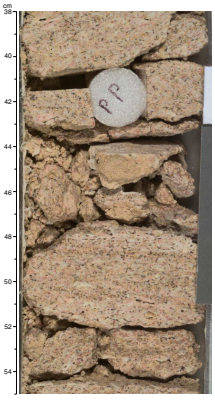

F13. Close-up photograph showing dolomitized rudstone, p. 44.

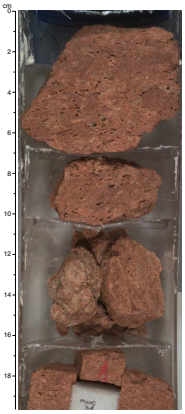

Very rare coccoliths are visible in smear slides. Bioturbation is moderate to heavy throughout Unit IV. The lower boundary of this unit is defined by a sharp color change at the base of Core 194-1193A-46X (249.2 mbsf) from light greenish gray to pale olive. However, the lower boundary of Unit IV is gradational in texture as its basal 4 m show a fining-upward trend from very fine grained packstone through wackestone to mudstone.

Unit V (249.2–385.1 mbsf; Early Miocene)

Unit V is a 135.9-m-thick interval of light olive-gray, skeletal packstone, consisting mainly of fine sand– to silt-sized bioclasts in a clay-rich mud matrix (Fig. F4). Dolomite is common in this unit. Thin section observations indicate that bioclasts are dominantly benthic and planktonic foraminifers with subordinate fragments of echinoderms, bryozoans, red algae, and mollusks (Figs. F19, F20). Quartz sand to silt and glauconite pellets are common. Some intervals are heavily bioturbated. Less bioturbated intervals display current ripples and graded beds up to a few decimeters thick. Concretion-like clusters of coarse celestite crystals with pyrite inclusions are sometimes associated with burrows. The basal contact of Unit V is a surface at interval 194-1193A-62X-5, 77 cm (385.1 mbsf), showing a sharp transition from very fine sand–sized skeletal packstone to underlying coarse-grained skeletal grainstone of Unit VI (Fig. F21).

Unit VI (385.1–531.0 mbsf; Early Miocene)

The 145.9-m-thick Unit VI is coarser than Unit V and is dominated by a grainstone fabric with sandstone beds present in some intervals (Fig. F4). Unit VI is divided into two subunits in order to differentiate a lowermost 2-m-thick interval of conglomerate and sandstone.

Subunit VIA (388.1–529.3 mbsf; Early Miocene)

Subunit VIA consists mainly of fine- to coarse-grained, poorly to well-sorted skeletal grainstone (Figs. F22, F23) with subordinate beds of quartz sandstone (Fig. F24). Color is mostly light to dark greenish gray, with the interval from 426 to 470 mbsf (Cores 194-1193A-69X to 77X) being brown to reddish yellow. Bioclasts in the grainstone are dominantly benthic foraminifers with minor echinoderm, mollusk, bryozoan, and red algae fragments and minor planktonic foraminifers. Common accessories indicate quartz, glauconite, and phosphate sand-sized grains. Sandstones are rich in calcite bioclasts, glauconite, and phosphate grains and are cemented by isopachous coatings of fine-prismatic calcite.

The deepest core in Subunit VIA (194-1193C-6R; 520–522 mbsf) consists mainly of skeletal grainstone to floatstone, characterized by a high glauconite content (up to 50%) and large oyster shells and bryozoans. The middle part of this interval is finely laminated with bidirectional current ripples (Figs. F25, F26).

Subunit VIB (529.3–531.4 mbsf)

Subunit VIB (interval 194-1193C-7R-1, 0 cm, to 7R-2, 54 cm) consists of greenish gray, bioclastic, glauconite-rich, poorly sorted quartz sandstone. Large oyster shells (up to 8 cm long and 2 cm thick) are espe-

F14. Photomicrograph of dolomitized rudstone in Subunit IIIA, p. 45.

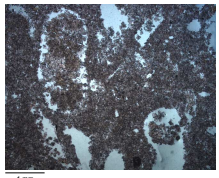

F15. Photomicrograph showing a lithology from Subunit IIIB, p. 46.

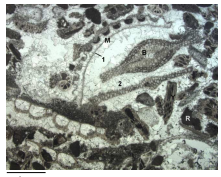

F16. Close-up photograph of floatstone/mudstone interval, p. 47.

F17. Close-up photograph of Unit IV, p. 48.

F18. Photomicrograph showing a lithology from Unit IV, p. 49.

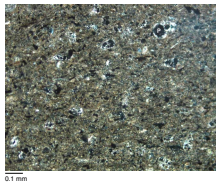

cially abundant in the upper 45 cm (Fig. F27). The basal 60 cm of this subunit consists of interbedded sandstone and conglomerate with pebble-sized carbonate clasts.

Unit VII (531.4–544 mbsf)

Unit VII consists of volcanics believed to represent regional basement (Fig. F4). The top 0.5 m of the basement, recovered in interval 194-1193C-7R-2, 54–104 cm (531.4–531.9 mbsf), is represented by reddish brown to dark green highly altered basaltic flows (Fig. F28). The rock is highly fractured and cut by calcite-filled veins. Slickensides are present on some fracture surfaces. Thin sections reveal a texture dominated by the effects of low-temperature alteration, forming finely crystalline phyllosilicate and possibly zeolite minerals but preserving areas with relict igneous texture (Fig. F29).

Discussion

Unit I, which includes the modern seafloor, has been episodically disturbed allowing for cementation and the development of localized hardgrounds. Both Unit I and the hemipelagic sediments of Unit II formed in an open-ocean setting influenced by distal terrigenous influx.

Unit III was deposited in a carbonate platform setting and affected by moderate to strong current energy, as shown by the coarse bioclastic fraction. Unlike equivalent units in Leg 133 (Sites 815, 816, and 826) no evidence of tropical reefal biota was observed at Site 1193. Warm-temperate to cool subtropical environments are suggested by the predominance of both bryozoans and larger benthic foraminifers and the lack of green algae. The larger benthic foraminifers of Unit III are consistent with water depths in the range of 120 m to <30 m (middle to inner neritic zone), as discussed in "Biostratigraphy and Paleoenvironments," p. 11.

The four irregular surfaces observed in the upper part of Subunit IIIA are interpreted as karst surfaces, recording subaerial exposure. The presence of these surfaces and the greater abundance of red algae and clay in Subunit IIIB suggest a large-scale shoaling-upward trend through Unit III.

Ubiquitous extensive leaching of bioclasts and the presence of vadose silt and possible freshwater cements suggest that Unit III may have experienced meteoric diagenesis throughout the entire interval.

The facies at the top of Subunit IIIA contains a mixture of planktonic foraminifers and biota typical of the underlying shallow-platform carbonates. Therefore, this thin zone may record a transitional final growth stage of the platform. It is uncertain whether the tight cementation of this zone mainly reflects subaerial or submarine exposure. In either case, extended submarine exposure is suggested by the phosphatic coatings on several core pieces (Fig. F5).

In the uppermost mudstone horizon of Subunit IIIB, the benthic foraminiferal assemblage consists exclusively of shallow-water taxa, consistent with a protected setting such as a lagoon or bay. The occurrence of extensively dolomitized horizons in the lower part of Subunit IIIA indicates that this mudstone acted as a laterally extensive aquiclude focusing fluid flow through more permeable layers of the overlying section.

F19. Close-up photograph of Unit V, p. 50.

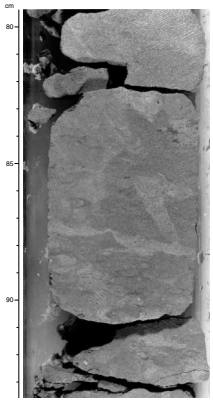

F20. Photomicrograph showing silt- to fine sand–sized packstone, p. 51.

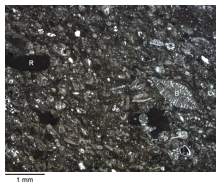

F21. Close-up photograph of contact between Units V and VI, p. 52.

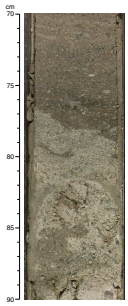

F22. Close-up photograph of skeletal grainstone, p. 53.

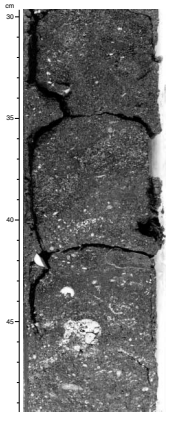

Unit IV contains virtually no micropaleontologic indicators of shallow-water conditions. Its very fine grain size and high clay to silt content are suggestive of distal outer neritic conditions (possibly approaching 200-m water depth) and, thus, are consistent with a location on the seaward slope of a carbonate platform.

Benthic foraminiferal assemblages indicate that Unit V was deposited in outer neritic conditions, but the coarser grain size and lower clay content as compared to Unit IV suggest a more proximal slope setting (>120-m water depth).

Shallow depositional setting is demonstrated for Unit VI by the exclusively shallow-water benthic foraminiferal assemblages (Fig. F4). The frequent occurrences of pelagic foraminifers and glauconite and phosphate grains indicate repeated periods of condensed sedimentation during the depositional history of this unit, possibly corresponding to times of higher relative sea level.

From the interpretations above, a history of geologic events can be proposed for Site 1193:

1. The Marion Plateau basement surface was transgressed and eroded sometime before the early Miocene, possibly beginning in the Eocene according to information from Site 1195, resulting in a mixed grainstone/sandstone unit containing possible hiatuses reflected by abundant glauconite and phosphate grains (Unit VI).
2. After the plateau was submerged, a carbonate platform northwest of Site 1193 supplied neritic carbonate detritus that was mixed with pelagic sediments, resulting in southeastward progradation of the platform slope in the early Miocene (Unit V).
3. The middle Miocene marked a period of lower-energy and more clay-rich sedimentation (Unit IV). This sedimentary response could reflect a rise in relative sea level.
4. In the middle to late Miocene, the platform prograded over the slope sediments previously deposited at Site 1193 (Unit III).
5. Following probable subaerial exposure after the middle Miocene, the platform was transgressed sometime prior to 5.6 Ma, and a marine hardground developed during an extended nondepositional interval. After reflooding, only localized carbonate platform growth initiated on the Marion Plateau, but not at the location of Site 1193.
6. A thin veneer of planktonic foraminiferal ooze accumulated during the latest Miocene to Pleistocene (Units II and I). These sediments have been sorted during redeposition by seafloor currents related to tidal and geostrophic processes.

BIOSTRATIGRAPHY AND PALEOENVIRONMENTS

Biostratigraphic analyses at Site 1193 reveal a Pleistocene to lower Pliocene sequence overlying a lower to middle Miocene carbonate platform and slope succession. Table T4 lists the nannofossil and planktonic foraminifer datums used for age assignments (see "Age Model," p. 20, for age vs. depth and sedimentation rate plots). In addition, larger benthic foraminiferal assemblages and morphologies were evaluated as environmental indicators. Core catcher samples were the basis for the primary analysis, but additional samples from within selected intervals were studied to refine the biostratigraphy. Thin sections were

F23. Photomicrograph showing a typical carbonate lithology, p. 54.

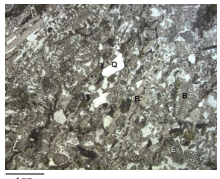

F24. Photomicrograph showing a sandstone from Subunit VIA, p. 55.

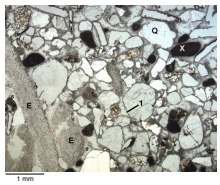

F25. Close-up photograph of the deepest core in Subunit VIA, p. 56.

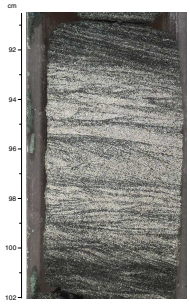

F26. Photomicrograph from the deepest core in Subunit VIA, p. 57.

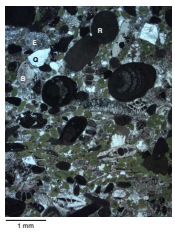

F27. Close-up photograph showing the upper part of Subunit VIB, p. 58.

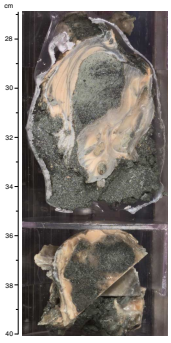

examined to verify selected larger foraminiferal taxa and morphologies. These analyses reveal lower to lower middle Miocene assemblages.

Calcareous Nannofossils

All available core catcher samples from the three holes (1193A through 1193C) plus ~30 samples, mostly from the top three cores in Hole 1193A, were examined for calcareous nannofossils. Pleistocene through lower Miocene nannofossil assemblages were recovered from these samples. Nannofossils are abundant in the top five cores in Hole 1193, virtually absent from Cores 194-1193A-6H through 38X, and generally common to rare from Core 39X to the bottom of the hole (Core 83X). Correspondingly, nannofossil biostratigraphic resolution is relatively good for the top five cores, not available for Cores 194-1193A-6H through 38X, and relatively low for Core 39X to the bottom of the hole. Nannofossils were rare to absent in the core catcher samples from Holes 1193B and 1193C; thus, no useful age information could be produced from these latter samples.

A series of nannofossil datums (last occurrences [LOs] of *Calcidiscus macintyeri, Discoaster brouweri, Discoaster pentaradiatus, Discoaster surculus,* and *Discoaster tamalis*) are apparently truncated between interval 194-1193A-1H-3, 30 cm, and 1H-5, 30 cm, indicating a hiatus at least from 1.7 to 2.8 Ma or at most from 0.9 to 3.7 Ma, as constrained by the presence of *Reticulofenestra asanoi* in samples above and the absence of *Reticulofenestra pseudoumbilica* in samples immediately below.

The nannofossiliferous samples bracketing the carbonate-platform sequence (Cores 194-1193A-6H through 38X) are Samples 194-1193A-5H-CC and 39X-CC. The former contains abundant nannofossils, including *Discoaster quinqueramus* and *D. surculus,* suggesting an age range of 5.6–7.5 Ma. The latter sample contains rare nannofossils, including *Cyclicargolithus floridanus,* which indicates an age older than 11.9 Ma. More precise age information for the carbonate-platform sequence was not possible because the few core catcher samples available from this interval were barren of nannofossils.

Sample 194-1193A-82X-CC contains common and well-preserved nannofossils, including few *Zygrhablithus bijugatus* and *Cylcicargolithus abisectus* and rare specimens that resemble those of *Reticulofenestra bisecta* (except smaller in size than the latter species). As the LO of *Z. bijugatus,* located above Sample 194-1193A-82X-CC, generally occurs only slightly above the last occurrence of *R. bisecta,* which approximates the Oligocene/Miocene boundary, Sample 82X-CC is thus only slightly above the Oligocene/Miocene boundary.

Planktonic Foraminifers

The shipboard planktonic foraminifer biostratigraphy of this site is based on Hole 1193A. Holes 1193B and 1193C were cored to improve NMP recovery in lithified material not suitable for shipboard planktonic foraminiferal analysis.

The sequence overlying the NMP (Samples 194-1193A-1H-CC through 4H-CC) contains lower Pleistocene to lower Miocene assemblages. Within the platform interval (35–229 mbsf), sample lithification and low planktonic foraminiferal abundance hindered analysis. Below the platform interval, limited planktonic biostratigraphy can be provided because the sediments were either barren or showed very low abundance of planktonic foraminifers.

F28. Close-up photograph showing acoustic basement of Unit VII, p. 59.

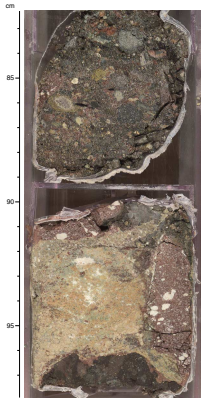

F29. Photomicrograph from Unit VII, p. 60.

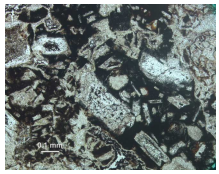

T4. Nannofossil and planktonic foraminifer datums, p. 102.

The uppermost Sample 194-1193A-1H-1, 20 cm, contains *Pulleniatina finalis,* placing the sample between the middle of Zone N22 to the Holocene. This was further confirmed by the absence of *Globorotalia tosaensis* and the presence of *Globorotalia truncatulinoides,* indicating an age of middle to late Pleistocene (Zone N23). In Sample 194-1193A-1H-3, 20 cm, the first occurrence (FO) datum of *G. truncatulinoides* coupled with the absence of *Globigerinoides fistulosus* suggests an age of Zone N22 or younger. The presence of *G. tosaensis* with its LO datum at the Pt 1b/Pt 1a boundary together with the absence of *P. finalis* (FO datum in middle Zone N22) implies a lower to middle Zone N22 age (Pt 1a) for this sample. Sample 194-1193A-1H-5, 18 cm, reveals the absence of *G. truncatulinoides,* whose FO datum defines the base of Zone N22. The first recorded presence of *G. fistulosus* occurs in this sample, and its range defines lower Zone N21 to lower Zone N22; therefore, the overlap with the absence of *G. truncatulinoides* implies an upper Zone N21 age for this sample. *Sphaeroidinellopsis seminulina* is absent in this sample but present in Sample 194-1193A-2H-2, 10 cm, and thus the LO datum (approximating the middle of Zone N21) occurs between the two intervals. This helps to constrain the age of Sample 194-1193A-1H-5, 18 cm, as upper Zone N21 and the age of 194-1193A-2H-2, 10 cm, as Zone N20. An upper age limit in Sample 194-1193A-2H-2, 10 cm, was provided by the absence of *G. fistulosus* as the top of Zone N20. The lower age limit of the sample was defined by the first appearance of *Dentoglobigerina altispira* and its FO datum at the base of Zone N20. This is supported by the absence of *Globorotalia crassaformis,* whose FO datum lies in the lower Zone N20. Sample 194-1193A-2H-5, 20 cm, contains the same assemblage as above but includes the *Neogloboquadrina acostaensis* FO datum, which occurs at the base of Zone N20.

Samples 194-1193A-3H-2, 10 cm, through 4H-5, 100 cm, were dated within Zone N19 (early Pliocene) based on the LO datum of *Globorotalia margaritae* and the presence of *Globorotalia puncticulata*. The LO datum of *Globigerina nepenthes* is close to the top of Zone N19 and occurs between Samples 194-1193A-4H-1, 80 cm, and 4H-2, 10 cm. Based on *G. margaritae,* this datum seems to be lower than the top of Zone N19. Samples 194-1193A-1H-CC through 2H-CC contain no index species for the late Pliocene (i.e., *G. truncatulinoides, G. tosaensis, Globorotalia miocenica,* or *G. fistulosus*). Abundant specimens of *Sphaeroidinella dehiscens,* are just at the base of Zone N18, and their first occurrence juxtaposed with the absence of the listed index species indicates a Zone N18 age for these samples. This is further supported by the presence of *Pulleniatina obliquiloculata* whose FO occurs from Zone N19 to Zone N20 as well as *Globorotalia plesiotumida,* whose LO is at the base to middle of Zone N19. Samples 194-1193A-3H-CC and 4H-CC lack *S. dehiscens* and contain *Globorotalia cibaoensis,* which has its LO in the lower Zone N19 and, therefore, can be placed in Zone N18. The FO of *Globorotalia tumida* is close to the top of Zone N17. This taxon is present in Sample 194-1193A-4H-CC but not in 5H-CC, which implies a N18 zonation for Sample 4H-CC.

Planktonic foraminifers were not of use in establishing the middle to late Miocene biostratigraphy. Samples 194-1193A-45X-CC through 60X-CC usually contained <1% (by volume) planktonic foraminifers and showed high levels of test alteration and overgrowth. In addition, the specimens found were all globigerines (i.e., shallow dwellers common in the photic zone, which broadly equates to the surface mixed layer). This evidence could be loosely construed as a paleodepth indicator. Although the surface mixed layer varies in depth, it averages ~100

m water depth. No deep/subthermocline dwelling Globorotaliid forms are present, which would normally be present with a shallow mixed layer.

Samples 194-1193A-45X-CC through 60X-CC contain many nonindex fossils of extended biostratigraphic range characteristics (e.g., *Globigerina woodi* [Zones P22–N21], *Globigerinoides triloba* [Zones N4b–N22], *Globigerina praebulloides* [Oligocene–Zone N17], and *Globoquadrina dehiscens* [Zones N4b–N18]). Some species such as *Globigerinoides parawoodi* (Zones N4b–N7) and *Globigerina connecta* (Zones N4b–N7) were used in conjunction with the zone fossil *Globigerinoides primordius* (Zones N4a–N5) to tentatively assign a Zone N4–N7 age range to Samples 194-1193A-45X-CC through 60X-CC; however, many of the key defining surface and apertural characters were abraded or overgrown with calcite. Samples 194-1193A-60X-CC through 84X-CC were barren of planktonic foraminifers.

Benthic Foraminifers

Microscopic analysis of biogenic constituents, particularly the diverse and often abundant benthic foraminifers, provide data for paleoenvironmental interpretation of the sediments at Site 1193 (Table T5). Distinctive larger benthic foraminiferal assemblages also provide limited biostratigraphic resolution within intervals lacking diagnostic planktonic foraminifers or nannofossils. Core catcher samples were the basis for primary analysis, supplemented by direct observations of selected cores. Thin sections were examined to verify larger foraminiferal taxa and morphologies.

Biostratigraphy

With the exception of the hemipelagic sediments on top of the NMP (lithologic Unit I), larger benthic foraminiferal associations characteristic of the early to middle Miocene were found in Samples 194-1193A-5H-CC (37 mbsf; lithologic Unit III) through 194-1193C-6X-CC (522 mbsf; lithologic Unit V) just above basement (for lithologic unit descriptions, see "Lithostratigraphy and Sedimentology," p. 6).

The larger benthic foraminiferal assemblage in lithologic Units II–V appears to be consistent with Chaproniere's (1981, 1984) larger foraminiferal associations Zones LF5–LF7, with abundant *Amphistegina* spp. (Fig. F30), *Lepidocyclina (Nephrolepidina) howchini* (Figs. F30, F31, F32), *Cycloclypeus* sp. (Fig. F32), *Operculina complanata* (Fig. F33), and, less commonly, *Miogypsina* spp. (Fig. F34). Chaproniere (1981, 1984) correlated Zones LF5–LF7 biostratigraphically to Neogene planktonic foraminiferal Zones N6 to N9, which are latest early and early middle Miocene in age (~18.8–14.8 Ma). Betzler and Chaproniere (1993) report similar assemblages as ranging from early to early middle Miocene (~24–12 Ma). This age span, which represents all or part of the time of platform buildup, is consistent with the gap in age control from the nannofossil and planktonic foraminiferal data set (Table T4). Detailed biometric analyses of the embryons of specimens of *Lepidocylina* and *Miogypsina* will be necessary to determine the species in lithologic Units II–V to refine the biostratigraphy (e.g., Chaproniere 1981, 1984).

T5. Summary of biostratigraphic and paleoenvironmental interpretations, p. 103.

F30. Vertical sections of *Amphistegina hauerina* and *A. radiata,* p. 61.

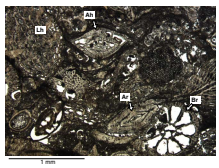

F31. Vertical sections of two *L. howchini* specimens, p. 62.

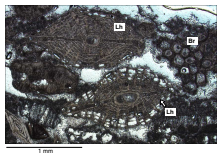

F32. Vertical section of *Cyclocypeus* sp., p. 63.

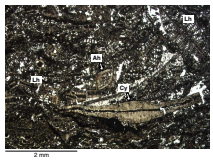

F33. Vertical section of *Operculina complanata,* p. 64.

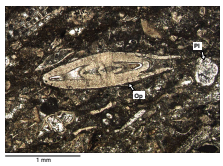

F34. Vertical sections through two *Miogypsina* sp., p. 65.

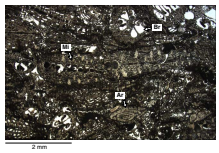

Paleoenvironmental Analysis

Sediments recovered in Samples 194-1193A-1H-CC (6.6 mbsf) through 5H-CC (37 mbsf) are overwhelmingly dominated by well-preserved tests of planktonic foraminifers. Rare benthic foraminifers found in Samples 194-1193A-1H-CC through 3H-CC are characteristic of upper bathyal depths (Table T5). *Laticarinina, Cibicidoides,* and agglutinated foraminifers are conspicuous in this interval. Reworked benthic foraminifers occur in Sample 194-1193A-4H-CC and are abundant in Sample 5H-CC, which is very near the top of the NMP platform (see "Lithostratigraphy and Sedimentology," p. 6). Most notably, specimens of the larger benthic foraminifers, *Amphistegina* and *Lepidocyclina,* range from white and very well preserved to brown and rounded, indicating both reworked material and in situ deposition. These samples are part of lithologic Unit II (see "Lithostratigraphy and Sedimentology," p. 6) and represent hemipelagic sedimentation. Unit I occurs near the top of Core 194-1193A-1H, above the core catcher, and was not sampled for biostratigraphic analysis.

Larger benthic foraminifers are common to abundant throughout lithologic Subunit IIIA, including Samples 194-1193A-5X-CC (37 mbsf) through 30X-CC (171 mbsf), 194-1193B-1X-CC (37.4 mbsf) through 17Z-CC (115 mbsf), and 194-1193C-1X-CC (115 mbsf) through 4X-CC (163 mbsf). Bryozoans are the dominant sediment constituent in these grainstones and packstones; larger benthic foraminifers are locally very abundant. The modern analogs of these foraminifers host algal endosymbionts and live in habitats within the euphotic zone, which is typically <100 m water depth (e.g., Hallock, 1987a, 1999; Hohenegger, 1999). Thus, the larger foraminifer-rich limestones and dolomites of lithologic Subunit IIIA are interpreted to have been deposited at depths of <100 m (inner to middle neritic) in a platform depositional environment. Within this lithologic unit, intervals of very robust and abraded larger foraminifers are found that are indicative of inner neritic (≤30 m, sometimes <10 m) habitat and deposition (Table T5). These foraminifers often occur abundantly immediately below exposure surfaces. Elsewhere in the unit, very large (>2 cm), very flat, well-preserved *Cycloclypeus* and *Lepidocyclina* are observed, indicating untransported assemblages with habitats at paleodepths near the limits of the euphotic zone (likely 60–100 m). More detailed reconstruction of depositional histories and paleodepth estimates for lithologic Subunit IIIA will require detailed analysis of thin sections from this interval.

Sediments in Samples 194-1193A-31X-CC (171 mbsf) through 35X-CC (196 mbsf), from the uppermost part of lithologic Subunit IIIB, have three distinct components that result in a bimodal sediment size distribution. The matrix includes terrigenous clays and silt-sized carbonate debris (see "Lithostratigraphy and Sedimentology," p. 6). Each sample also has a coarse component of relatively well sorted bioclastic material that is rich in larger benthic foraminifers. For example, the coarse fraction of Sample 194-1193A-33X-CC consists of sorted, rounded *Lepidocyclina* tests and strongly resembles the larger foraminiferal beach sands found today at Lizard Island, Australia, Bali, and Okinawa (Lee, 1998). Subsequent samples from lithologic Subunit IIIB (Samples 194-1193A-34X-CC through 42X-CC) generally have a greater coarse bioclast-to-matrix ratio but are similar in their three-component composition that includes terrigenous muds, very fine carbonate debris, and coarse bioclasts. Bryozoan fragments are the dominant constituent, but larger benthic foraminifers are often abundant. Large, flat *Cycloclypeus*

and *Lepidocyclina* morphologies are common in these samples, indicating middle neritic water depths in an outer platform depositional setting (Table T5).

Samples 194-1193A-43X-CC (234 mbsf) through 46X-CC (253 mbsf) (lithologic Unit IV; see "Lithostratigraphy and Sedimentology," p. 6) contain benthic foraminiferal assemblages (*Cibicidoides, Lenticulina, Uvigerina,* etc.) characteristic of outer neritic to upper bathyal depths (>120 m). The muddy sediments are predominantly silt-sized carbonate debris with a significant terrigenous clay fraction (see "Lithostratigraphy and Sedimentology," p. 6, and "Geochemistry," p. 20). These sediments lack coarser shallow-water constituents, including the tests of larger benthic foraminifers, and are interpreted to represent a distal periplatform depositional environment.

Sediments in Samples 194-1193A-47X-CC (263 mbsf) through 61X-CC (378 mbsf) (lithologic Unit V; see "Lithostratigraphy and Sedimentology," p. 6) are intermediate in composition between those of lithologic Subunit IIIB and Unit IV. The dominant constituent of most of these samples is silt and very fine sand–sized carbonate debris, including tiny fragments of bryozoans, red algae, larger benthic foraminifers, echinoids, and worm tubes. Tiny benthic and planktonic foraminiferal tests are also abundant in the fine sediments. Whole juvenile specimens of *Amphistegina, Lepidocyclina,* and *Operculina,* as well as comparable-sized fragments of bryozoans, red algae, and echinoids, are relatively common in thin sections from this unit. However, the presence of outer neritic benthic foraminifers as well as common planktonic foraminifers indicates that debris from shallower-dwelling photosynthetic organisms, particularly red algae and larger foraminifers, were transported into deeper water. These sediments are interpreted as having been deposited in a proximal periplatform depositional environment.

Samples 194-1193A-62X-CC (388 mbsf) through 83X-CC (513 mbsf), which correspond to lithologic Unit VI (see "Lithostratigraphy and Sedimentology," p. 6), include both coarse bioclastic and terrigenous clastic sediments. Packstones dominated by *Lepidocyclina* and other larger benthic foraminifers (Figs. F30, F31, F32, F34) are found at the top of Unit VI. Terrigenous constituents generally increase downsection. The presence of larger benthic foraminifers indicates inner to middle neritic water depths for most of this section. The presence of large, flat, well-preserved *Cycloclypeus* in Sample 194-1193A-70X-CC (431 mbsf) in very coarse terrigenous and bioclastic sediments indicates that the sediments were neither transported during the lives of these delicate foraminifers, nor abraded prior to their burial. The flat shape of these foraminifers indicates low light conditions characteristic of middle neritic depths (Table T5).

Interpretation

Most of the neritic carbonate sediments and rocks encountered at Site 1193 represent sedimentation by a diverse bryozoan community in which larger benthic foraminifers were an important component. Bryozoans are commonly associated with cool-water carbonates, often at subeuphotic depths (e.g., James, 1997). However, the abundant larger foraminifers found in lithologic Units III and VI indicate at least a cool subtropical (e.g., 17°–23°C) climate and paleodepths within the euphotic zone (<120 m), which is the depositional environment of mod-

ern bryozoan-coralline algal-larger foraminiferal sediments found on the southwest Australian shelf (James et al., 1999).

The larger foraminifers found in lithologic Units III, V, and VI between 37 and 520 mbsf represent a reduced Australian lower to middle Miocene assemblage (e.g., Chaproniere, 1981, 1984; Betzler and Chaproniere, 1993; Chaproniere and Betzler, 1993). The Site 1193 assemblages are characterized by having only rotaline, low-Mg calcite taxa including at least two species each of *Lepidocyclina, Amphistegina, Miogypsina,* and *Cycloclypeus,* as well as *Operculina complanata*. *Lepidocyclina howchini* is the most consistently abundant species and is the dominant constituent of packstones in the upper portion of Unit VI (Figs. **F30, F31, F32, F34**). Porcellaneous, high-Mg calcite larger foraminifers such as *Marginopora* and *Flosculinella* are strikingly rare in these units, as are zooxanthellate coral and *Halimeda,* which may be a geochemical indication of carbonate saturation state below the threshold for coral-reef constructions (e.g., Hallock, 1987b; Kleypas et al., 1999).

The sedimentology and larger benthic foraminifers both indicate that lithologic Unit VI was deposited at inner to middle neritic water depths (Table **T5**). This unit likely represents initial flooding of terrigenous basement at this location (see **"Lithostratigraphy and Sedimentology,"** p. 6). Paleoenvironmental data indicate deepening to upper bathyal depths in lithologic Unit V, as indicated by the presence of planktonic and benthic foraminiferal assemblages. This unit is dominantly composed of very fine bioclastic sediments, possibly deposited by contour currents. Pulses of coarser bioclastic sediments from inner and middle neritic settings, which are common in this interval, were likely transported directly downslope to this proximal periplatform setting. Lithologic Unit IV has the same outer neritic/upper bathyal benthic foraminiferal assemblage in fine bioclastic sediments of neritic origin as are found in Unit V, but lacks pulses of coarser, distinctively shallow-water bioclastics, possibly indicative of a distal periplatform setting. However, Unit IV also contains significantly more fine terrigenous clays and organic matter, suggesting an environmental mechanism that increased terrigenous input to the coastal system. Terrigenous siliciclastic sediments, accompanied by dissolved nutrients and organic matter, may have reduced carbonate production by inner and middle neritic benthic communities, resulting in reduced downslope transport of coarser bioclastic sediments.

Subunit IIIA sediments, which are bryozoan-dominated boundstones and coarse bioclastics with common to abundant larger foraminifers, appear to represent platform sedimentation at inner to middle neritic depths (Table **T5**). The depositional environment of sediments deposited in lithologic Subunit IIIB appears to be middle neritic and intermediate between the inner to middle neritic platform of lithologic Subunit IIIA and the outer neritic to upper bathyal setting of lithologic Unit V. The sediments of lithologic Unit IV, although occurring between Subunit IIIB and Unit V, indicate the least shallow neritic influence.

PALEOMAGNETISM

The natural remanent magnetization (NRM) of archive sections from Site 1193 was measured at 5-cm intervals using the pass-through cryogenic magnetometer. An alternating-field demagnetization with a maximum intensity of 30 mT was used. The large diameter of the ADCB cores prevented the use of standard measurement procedures. There-

fore, we readjusted core fragments that appeared to have retained their orientation in the liner by reorienting them with their downcore axis in the +y direction of the archive coordinate convention. In this way, core pieces up to 7 cm in length, which can pass through the magnetometer aperture, were run in the cryogenic magnetometer.

Discrete samples were collected from Holes 1193A, 1193B, and 1193C at a general sample rate of 2 per core. However, the special nature of the platform material required modifications in our sampling technique. Discrete samples were used to aid the interpretation of the long-core record of magnetization by providing additional measurements of polarity and basic magnetic characterization. Most of these samples were demagnetized at 5, 10, 15, 20, 40, 60, and 80 mT to permit principal component analysis. For rock magnetic properties, anhysteretic remanent magnetization (ARM) was generated using 0.2-mT DC and 200-mT AC fields and isothermal remanent magnetization (IRM) in a DC field of 1 T. Samples were also progressively magnetized in fields up to 1.0 T to study the acquisition of the IRM. In addition, a number of thermal demagnetizations were done using the Schonstedt Model TSD-1 oven. These measurements included demagnetization of NRM to help interpret the nature of the NRM magnetization, and saturation of the IRM to help identify the magnetic carriers.

Results

Natural Remanent Magnetization

The NRM intensity generally varies between 10^{-2} and 10^{-5}A/m with some values decreasing to 10^{-6} A/m downcore (Fig. F35) with some occasional discrete peaks exceeding these bounds. When all NRM measurements are plotted in stereographic projection, the data indicate that nearly the entire data set has a downward magnetic inclination (Fig. F36A). Under normal circumstances all types of rocks have a viscous remanent magnetization (VRM) overprint due to the modern-day Earth's magnetic field. This would result in an upward inclination of the majority of NRM measurements. The downward overprint imparted by the drilling effect overwhelms the VRM signal resulting in movement of the data points toward the center of the stereonet and down (Fig. F36A). Demagnetization to 30 mT effectively cleans this downward overprint (Fig. F36B). The distribution of data points after this demagnetization becomes more random. However, full cleaning of the VRM has still not been attained in the long-core sample measurements.

Magnetostratigraphy

Declination, inclination, and intensity were routinely measured for all cores recovered. Results for the first 35 mbsf in Hole 1193A showed a clear sequence of magnetic reversals (Fig. F36A). Based on the preliminary age estimates (Pliocene–Pleistocene) (see "Biostratigraphy and Paleoenvironments," p. 11), the identified sequence appears to match well with the Gilbert Chron to the top of C3r on the recent geomagnetic polarity time scale (GPTS) (Fig. F35A; Table T6). The short-term events on the C3n (Cochiti, Nunivak, Sidufjall, and Thvera) are very distinctive in this correlation. The top normal polarity interval observed above the Gilbert Chron, however, does not seem to match with the bottom of the Gauss Chron (C3n4n) when compared with biostratigraphic data. Instead, either it was remagnetized or must have been de-

F35. Long-core measurements of intensity and inclination, p. 66.

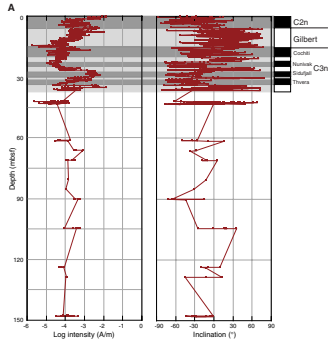

F36. Stereographic plot of directions of magnetization, p. 73.

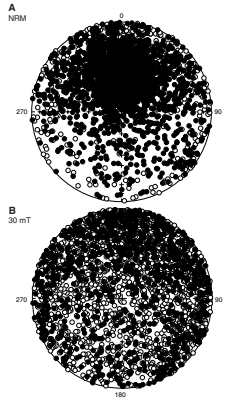

T6. Magnetic polarity transitions, p. 105.

posited after a hiatus in the late Pliocene, in which case it should match with the Olduvai (C2n) Subchron. Between 35 and 220 mbsf, the depth interval of the carbonate platform (see **"Lithostratigraphy and Sedimentology,"** p. 6), the recovery was low and long core measurements did not give useful results. Despite a number of data gaps, between 225 and 375 mbsf, an attempt was made to correlate some of the observed magnetic polarity zones with the GPTS. For example, between 230 and 250 mbsf the normal-reversed-normal-reversed-normal (N-R-N-R-N) polarity sequence identified was tentatively assigned to Chron C5Cn (Fig. **F35B**). In addition, the relatively long normal polarity interval found between 340 and 365 mbsf is likely to represent the C6N Chron (Fig. **F35C**) (early Miocene). The sequence of reversals observed between 380 and 500 mbsf in Hole 1193A is difficult to match with the GPTS (Fig. **F35D**).

Rock Magnetism

Twelve samples from the depth interval 140–384 mbsf (in Hole 1193A) were thermally demagnetized through a stepwise heating to a temperature of 680°C. Three components of magnetization have been identified. The first one, often removed by heating to 100°C, is most likely related to recent remagnetization. The second and third components have an antiparallel direction (segments A and B on the Zijderveld diagrams of Fig. **F37**). The second component has a blocking temperature between 100° and 200°C, whereas the third component starts to demagnetize between 600° and 680°C (Fig. **F37**). The magnetic moment decay curve increases, and the magnetic vector does not intersect the origin in the Zijderveld diagram (Fig. **F37**) for elevated temperatures. To identify the magnetic minerals carrying this remanence, ARM, IRM and IRM thermal demagnetizations were carried out on an unheated, new set of 16 selected samples in two batches. The first batch was collected from Hole 1193A, corresponding to the same interval as the one above, and the second batch was collected from 35 to 74 mbsf in Hole 1193B (four samples) and Hole 1193C (four samples).

ARM experiments performed on these samples showed straightforward demagnetization results for most samples analyzed (Fig. **F38A**). However, some samples showed a slope break in the magnetic moment decay curve (Fig. **F38B**), which is well-reflected on the Zijderveld plot as opposing components. The IRM acquisition curve (Fig. **F39**) demonstrates a rapid initial increase and a gradual acquisition at stronger fields (above 300 mT), indicating the presence of both low coercive (soft) and high coercive (harder) material.

After thermal demagnetization of acquired IRM, samples of the first batch showed two components with antiparallel directions (segments A and B on the Zijderveld diagrams in Fig. **F40**), indicating two different Curie temperatures (normalized magnetic moment decay curve in Fig. **F40**). The first component, characterized by a low blocking temperature of ~150° to 200°C, might be due to goethite, whereas the second component has a Curie temperature of ~600°C, indicating that it might be due to titanomagnetite or magnetite. The antiparallel nature of the two components that were magnetized in the same laboratory magnetic field can be best explained by a self reversal of the low Curie temperature mineral (goethite). Other samples showed two phases having similar directions: one Curie temperature of ~350°C, suggestive of pyrrhotite, and a gradual decay to zero at ~350°–680°C suggests the presence of titanomagnetite and small amounts of hematite (Fig. **F41**).

F37. Examples of Zijderveld diagrams, p. 74.

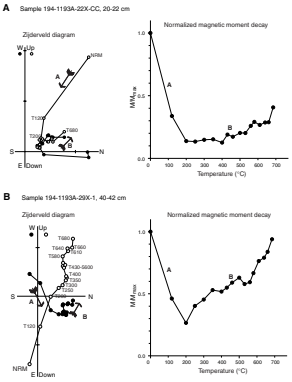

F38. ARM results, p. 75.

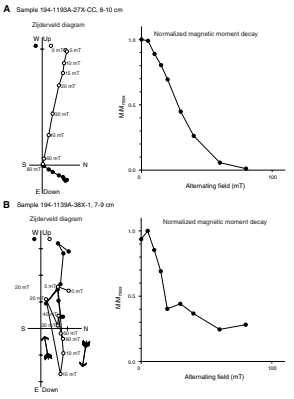

F39. IRM acquisition results, p. 76.

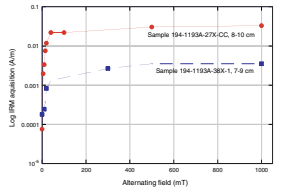

F40. Thermal demagnetization results of IRM showing two antiparallel directions, p. 77.

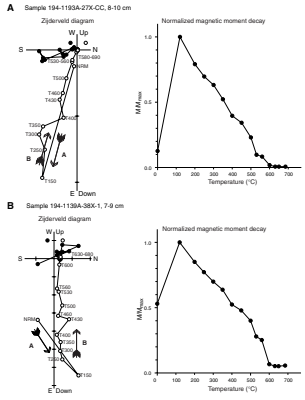

AGE MODEL

The age model for the 549-m-thick lower Miocene to Pleistocene sequence cored at Site 1193 is well dated above 35 mbsf, poorly dated in the carbonate platform interval (35–229 mbsf), and moderately well dated below 229 mbsf (Table T7; Fig. F42) (see "Biostratigraphy and Paleoenvironments," p. 11). In the uppermost 35 mbsf, the hemipelagic Pliocene–Pleistocene Megasequence D, 11 calcareous nannofossils and four planktonic foraminifer datums provide a rather detailed biostratigraphy. Below 229 mbsf, the lower part of Megasequence B and Megasequence A, four calcareous nannofossil datums and two planktonic foraminifer datums offer low-resolution, early Miocene biostratigraphic control. The carbonate platform, from 35 mbsf to 229 mbsf, was barren of age-diagnostic planktonic microfossils. However, larger benthic foraminiferal assemblages in the entire sequence below 35 mbsf indicate an age of 12–24 Ma, constraining the time of platform buildup to 12–16 Ma (Fig. F42) (see "Biostratigraphy and Paleoenvironments," p. 11). This age range does not necessarily exclude younger platform growth that could have been eroded.

A sequence of magnetostratigraphic reversals in the sediments above the platform (0–35 mbsf) is interpreted so that it matches the biostratigraphic results in this interval. Below that depth, recovery was insufficient to allow development of a magnetostratigraphy. Because of the difficulties with the magnetostratigraphic record, the biostratigraphic control points are used to construct the shipboard age model for Site 1193 (Fig. F42).

Interval sedimentation rates range from 0 (hiatus) to almost 160 m/m.y. in the lower Miocene periplatform deposits. The most significant increase (one order of magnitude) in sedimentation rate occurs in the upper lower Miocene in lithologic Subunit VIA and can be interpreted as the onset of shedding from the prograding carbonate platform, augmented by clay from the continent and modified by current activity (see "Lithostratigraphy and Sedimentology," p. 6). In the latest Miocene, several million years after the demise of the carbonate platform, hemipelagic sedimentation began at Site 1193 and continued through the Pleistocene at interval rates of 0–25 m/m.y. The postplatform sequence shows one distinct hiatus in the interval of 3.3–6.3 mbsf depth that is constrained by nannofossil datums to at least 2.8–1.7 Ma, and possibly up to 3.7–0.9 Ma in age. Peaks in the natural gamma radiation and magnetic susceptibility data at 5.7 ± 0.2 mbsf (see "Core Physical Properties," p. 24), and iron-stained sediment observed in Section 194-1193A-1H-4 (see "Site 1193 Visual Core Descriptions," p. 1) are the sedimentary expression of a hiatus and confine the depth interval of the hiatus further.

Age picks for lithologic and seismic unit boundaries are well defined except for the lithologic Subunit IIIA/IIIB boundary within the carbonate platform and the boundaries below 500 mbsf (Fig. F42; Table T8).

GEOCHEMISTRY

Volatile Hydrocarbons

Concentrations of volatile hydrocarbon gases were measured from every core using the standard ODP headspace sampling technique and gas chromatographic analysis. Methane only occurred in very minor

F41. Thermal demagnetization results of IRM showing two components with similar directions, p. 78.

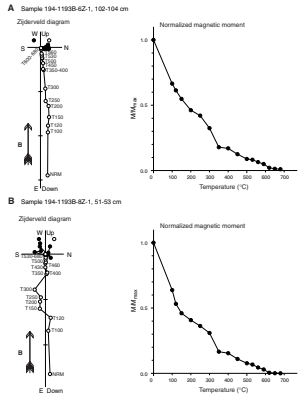

T7. Age-depth control points, p. 106.

F42. Age-depth model and sedimentation rates, p. 79.

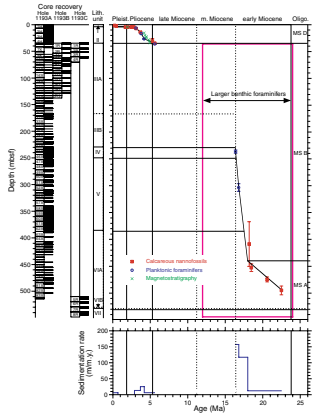

T8. Age picks, p. 107.

concentrations (1–3 ppmv); the highest value obtained was ~7 ppmv at ~485.6 mbsf (Table T9).

The low gas content at Site 1193, as at Site 1192, is likely a function of low total organic carbon (TOC) content of the sediments that prevents sulfate reduction from going to completion, low pore water SO_4^{2-} concentrations that limit bacterial methanogenesis, and the immaturity of organic matter present in the sediments relative to hydrocarbon expulsion and petroleum generation.

T9. Headspace gas composition, p. 108.

Interstitial Water Chemistry

Thick sequences of cemented shallow-water carbonates at Site 1193 limited pore water sampling to finer-grained, more clastic-rich sediments above, below, or within these carbonates. Some of the sediments were extremely well compacted or cemented, making it impossible to extract sufficient water for all shipboard chemical analyses from every sample. However, it was still possible to obtain a good picture of the pore water chemistry.

Chloride concentrations are ~565 mM in the upper 40 mbsf at Site 1193 (Table T10; Fig. F43A) within the hemipelagic sediments of lithologic Units I and II (see "Lithostratigraphy and Sedimentology," p. 6). Within the lower part of the carbonate platform sediments of lithologic Unit III, the chloride concentrations increase slightly to 567 mM. Just below the thickest section of shallow-water carbonates at ~240 mbsf, a rapid decrease in chloride is observed with values as low as 552 mM. The observed decrease is about 2%–3% of the total ion concentration and, therefore, is difficult to detect in other dissolved constituents but is probably expressed as small decreases observed in potassium and magnesium over the same depth interval (Fig. F43C, F43D). The origin of the rapid decline in chloride is not certain. Below 250 mbsf, chloride concentration generally increases downhole, with a value of 566 mM at the base of the hole.

T10. Interstitial water chemistry, p. 109.

F43. Dissolved constituents vs. depth, p. 80.

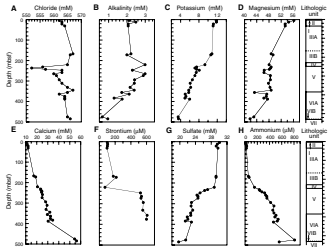

Alkalinity is near typical bottom-water values (2.1 mM) at the top of the hole. Values vary only slightly to 300 mbsf then decrease to <1 mM at the base of the cored interval (Fig. F43B). In all likelihood, alkalinity is removed from the pore waters by calcium carbonate precipitation.

Potassium concentration changes little from near the sediment surface to ~200 mbsf, with values between 11 and 12 mM (Fig. F43C). Below 200 mbsf, the concentration decreases to below 4 mM at the bottom of the cored interval.

Dissolved magnesium decreases slightly downhole in the upper 40 mbsf from 56 to 53 mM and decreases further to 48 mM just below lithologic Unit III (Fig. F43D). Thereafter, the concentration remains nearly constant to the base of the hole.

Calcium concentrations increase almost linearly from the seafloor to the base of the sediment column. Just above basement, the concentration is 56.25 mM, approximately three times the seawater concentration (Fig. F43E). The linear profile suggests a simple diffusion gradient between the basement and seawater, with low-temperature alteration of the mafic basement rocks supplying calcium to the pore waters.

Strontium concentration remains low, below 200 µM, from the shallowest sample at 4.4 mbsf through the base of lithologic Unit III at 220 mbsf (Fig. F43F). Below this interval, strontium increases sharply to over 500 µM and then increases gradually to over 600 µM at 375 mbsf. This increase is likely to be caused by the steady release of strontium during calcite recrystallization. As at Site 1192, high strontium and sul-

fate concentrations result in celestite precipitation, as confirmed by X-ray diffraction.

Sulfate and ammonium profiles are essentially mirror images of one another (Fig. F43G, F43H). The concentrations remain near seawater values until a depth of 220 mbsf below the carbonate platform sediments of lithologic Unit III. Below this interval, sulfate reduction begins. Sulfate values decrease to 22 mM at 300 mbsf then decrease more slowly to below 20 mM at the base of the hole. Ammonium values increase in antipathetic fashion over the same interval. Ammonium concentration is 419 µM at 300 mbsf and further increases to 559 µM at 485 mbsf. The single ammonium value above 800 µM could be an artifact.

Iron and manganese were measured on most samples from Site 1193, but all values were within the measurement error. Small clots of black iron sulfide staining occur over large parts of the more hemipelagic sediments. The Fe sulfides attest to release of iron during sediment diagenesis, with the iron rapidly removed in the zone of sulfate reduction.

Overall, the pore water geochemistry from Site 1193 indicates that fluids within lithologic Units I–III are little evolved from seawater. Although pore water samples could not be taken from within the shallow-water facies of the platform, the highly permeable lithologies suggest that similar values found above and below this interval can be extrapolated to provide an estimate of the values within it. Even the strontium concentrations, which might be expected to increase because of ongoing carbonate recrystallization, show no increase until below the platform. The best explanation for the lack of change in fluid chemistry is that fluids are moving through the sediments.

X-Ray Diffraction and Carbonate Mineralogy

The percentages of carbonate minerals were determined on 147 samples (Table T9; Fig. F44). Lithostratigraphic Unit I is entirely calcitic in mineralogy, whereas the percentages of dolomite and calcite vary greatly through the rest of the sedimentary section (Table T11). Lithostratigraphic Subunit IIA contains the highest concentration of dolomite that exists in the alternating 20- to 30-m-thick layers that are either 80–90 wt% dolomite or 80–90 wt% calcite (Table T11). These variations are observed in both Holes 1193A and 1193B (Fig. F44). Dolomite content decreases in lithologic Subunit IIB and in lithologic Unit III, averaging ~30 wt%, although several ~5-m-thick layers seem to contain up to 50 wt% dolomite. The dolomite content decreases further in lithologic Unit IV to 10–20 wt% (Table T11). In lithologic Unit V, total carbonate decreases greatly and the sediments are primarily calcite with only a few layers containing up to 10 wt% dolomite.

Sedimentary Geochemistry Results

Calcium carbonate ($CaCO_3$) content at Site 1193 ranges from ~5 to >100 wt% (Fig. F45; Table T12). Measurements are calibrated for calcite; thus, the presence of dolomite can result in calcium carbonate values >100 wt%. The TOC content of all measured samples at Site 1193 is <0.5 wt%, with the exception of an interval at 366 mbsf where 0.96 wt% TOC was measured. Note that percent TOC values from Rock-Eval pyrolysis and carbon-nitrogen-sulfur (CNS) analyses provide similar profiles with differences in absolute values (Fig. F45; Tables T12, T13) and that TOC values covary inversely with percent $CaCO_3$ (Fig. F45).

F44. Dolomite, calcite, and noncarbonate mineral percentages, p. 81.

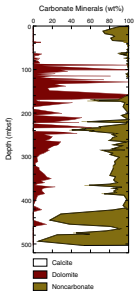

T11. Aragonite, calcite, dolomite, and noncarbonate mineral percentages, p. 110.

F45. Carbon, HI, and sulfur plots, p. 82.

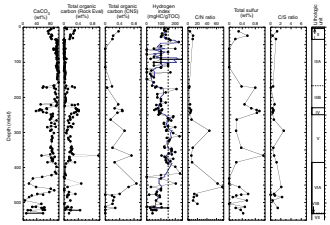

T12. Carbon, nitrogen, sulfur, and hydrogen results, p. 112.

T13. Rock-Eval analyses results, p. 115.

Hydrogen index (HI) values range from 0 to 233 mg HC/g TOC at Site 1193 (Fig. F45; Table T13). Oxygen index (OI) values vary from 0 to 925 mg CO_2/g TOC (Table T13). The low percent TOC limits the reliability of some HI and OI values. To ensure they are reproducible, duplicate and triplicate analyses were performed on these samples. T_{max} values range from 311° to 435°C (Table T12), although the most reliable T_{max} values cluster between 400° and 420°C below ~200 mbsf.

Total sulfur (S) content in Site 1193 sediments ranges from 0 to >1.05 wt% (Fig. F45; Table T12) and displays a similar distribution to percent TOC.

Discussion

Variations in the generally high calcium carbonate content (average = ~82 wt%) (Fig. F45) of sediments at Site 1193 mostly reflect fluctuations in the ratio of biogenic carbonate to terrigenous sediment input through time. Carbonate contents exhibit a decrease from ~89 wt% at ~2.25 mbsf to ~72 wt% at 11.85 mbsf followed by an increase to 83 wt% at 33.85 mbsf. These sediments contain well-preserved foraminifers with lesser amounts of calcareous nannofossils (see "Biostratigraphy and Paleoenvironments," p. 11) and correspond to lithologic Unit II (see "Lithostratigraphy and Sedimentology," p. 6). The slightly elevated TOC content with mostly low HI values in this interval indicates the presence of terrigenous or reworked refractory organic matter and/or oxic seafloor conditions. The abrupt change in calcium carbonate content at the lithologic Unit II/III boundary coincides with a major exposure surface. In the underlying carbonate platform from ~35 to 167 mbsf (lithologic Subunit IIIA [see "Lithostratigraphy and Sedimentology," p. 6]), calcium carbonate content is effectively 100 wt%. A slight decrease in $CaCO_3$ concentration at ~61 mbsf appears to coincide with the presence of two exposure surfaces between ~60 and 67 mbsf (see "Lithostratigraphy and Sedimentology," p. 6). The carbonate platform interval contains effectively no organic matter, as is common in these types of sediments.

Within the interval from ~167 to 245 mbsf, at least three horizons are well defined by decreased $CaCO_3$ content, increased percent TOC values, low HI values, and relatively elevated S concentrations. The uppermost horizon (~167–172 mbsf) correlates to the top of lithologic Subunit IIIB and is described as mudstone with large shallow-water benthic foraminifers that appear to have undergone transport (see "Biostratigraphy and Paleoenvironments," p. 11). Two additional horizons occur at ~215 and 245 mbsf within lithologic Unit IV. Unit IV is a mudstone with fine sand–sized bryozoan and benthic foraminifer fragments and few associated worn planktonic foraminifers, suggestive of transport (see "Biostratigraphy and Paleoenvironments," p. 11). The combination of geochemical, paleontological, and lithological characteristics is compatible with an interpretation of the horizons as basinward facies shifts. In this conceptual sequence stratigraphic model, increased terrigenous input may have caused carbonate dilution, whereas increased sulfur content may be attributable to pyrite formation due to iron associated with the terrigenous influx. Therefore, these horizons may represent relative sea-level lowstands.

Between ~245 and 365 mbsf, $CaCO_3$ contents are generally >80 wt%, TOC values are ~0.2 wt%, and HI values are relatively high, suggesting that organic matter preservation occurred on the most distal open-

marine, deepest, or dysoxic seafloor recorded at the site. Therefore, the overall downsection trend from Subunit IIIB to Unit V may represent an overall landward facies shift or deepening.

Other conspicuous horizons exist at ~365 ($CaCO_3$ = ~54 wt%) and ~385 mbsf ($CaCO_3$ = ~72 wt%), below which a zone of bioclastic material (see "Biostratigraphy and Paleoenvironments," p. 11) displays slightly elevated $CaCO_3$ content and low TOC values reminiscent of lithologic Subunit IIIB. The highest TOC content measured at this site (0.96 wt%) occurs at ~365 mbsf. This organic matter is most likely terrigenous in origin.

The widest range in carbonate values (~5–92 wt%) at Site 1193 is observed from ~420 mbsf to the base of the drilled section, including two horizons with the lowest $CaCO_3$ contents observed (5 and 9 wt%) (Fig. F45). TOC (up to ~0.5%) and total S concentrations are relatively elevated through this interval. Generally low carbonate and high TOC contents above basement suggests that this basal unit was deposited in a setting most affected by terrigenous inputs.

CORE PHYSICAL PROPERTIES

Evaluation of core physical properties at Site 1193 included nondestructive measurements of bulk density, bulk magnetic susceptibility (MS), natural gamma radiation (NGR), and *P*-wave velocity on whole cores using the multisensor track (MST). *P*-wave velocity (x-, y-, and z-direction) and moisture and density (MAD) were measured on split cores and on core samples. Low recovery in Cores 194-1193A-6X through 40X, 194-1193A-63X through 83X, and throughout Hole 1193C limited the use of the MST. The large diameter of cores recovered with the ADCB (Cores 194-1193B-3Z through 21Z) prohibited MST analysis. Thermal conductivity was measured on whole cores and on semilithified and lithified core samples.

Density and Porosity

Bulk density at Site 1193 was computed from gamma ray attenuation (GRA) measurements conducted on unsplit cores and from MAD measurements conducted on samples from split cores. The two independently derived bulk density data sets indicate the same general trend over most intervals (Fig. F46A). The similarity is best displayed in the interval from 0 to 35 mbsf, recovered using the APC. Samples from cores recovered with the XCB and the RCB and ADCB data (35–540 mbsf) have MAD density values that are on average 0.1 to 0.2 g/cm³ higher than the GRA values. The largest bulk density difference occurs between 340 and 360 mbsf, where the MAD density is 0.4 g/cm³ higher than the GRA density. Most likely, this is the result of reduced core diameter and a decrease in sample integrity that results from XCB and RCB core disturbance affecting GRA measurements.

Overall, bulk density ranges between 1.5 and 2.6 g/cm³ (Fig. F46A). The data show a general increasing trend downhole to a depth of 540 mbsf. Bulk density averages 1.67 g/cm³ in the upper 35 m at Hole 1193A, the interval corresponding to lithologic Units I and II (Fig. F46A). At 35 mbsf, the top of the carbonate platform, density increases to 1.75 g/cm³. The lithified platform sediments of Unit III (35–229 mbsf) (see "Lithostratigraphy and Sedimentology," p. 6) are excep-

F46. GRA and MAD bulk density, grain density, and porosity, p. 83.

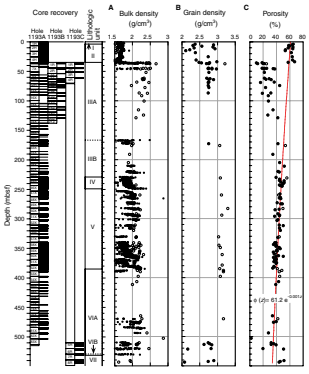

tions to the general downhole trend and have density values between 1.95 and 2.65 g/cm³ with a slightly decreasing trend with depth. Below 35 mbsf, local maxima can be observed at 220, 249, 365, and 385 mbsf (Fig. F46A). The maxima at 249 and 385 correspond to the top and bottom of lithologic Unit V.

Grain density averages 2.77 g/cm³ and shows broad scatter throughout most of Site 1193 (Fig. F46B). Approximately constant values of grain density exist between 35 and 130 mbsf, where the average grain density is 2.73 g/cm³. This interval corresponds to the upper part of the carbonate platform (lithologic Subunit IIIA) (see "Lithostratigraphy and Sedimentology," p. 6). Values increase slightly with depth from 2.5 g/cm³ at 50 mbsf to 2.9 g/cm³ at 505 mbsf. Below that interval, a slight decrease occurs to ~2.65 g/cm³. Suspect grain density values >3.0 g/cm³, possibly due to grain volume measurement error, have been identified in Figure F46B.

The porosity profile mirrors the bulk density profile, with minor differences caused by variations in grain density, indicating that bulk density variations are consistently controlled by porosity (Fig. F46C). Porosity at Site 1193 shows a general decrease with depth, except within the platform sediments (35–229 mbsf). Porosity is relatively low at the seafloor (55% to 70%) and decreases gradually to 30%– 40% at a depth of 500 mbsf (Fig. F46C). The platform interval shows the most scatter with values ranging from 10% to 45%, reflecting the various degrees of cementation in the carbonate rocks. In general, porosity increases slightly downhole within the platform interval. Porosity (ϕ) of the nonplatform sediments of Site 1193 can be related to depth (z) using an exponential function

$$\phi(z) = \phi_o e^{-kz},$$

where ϕ_o is the seafloor porosity, and k describes the rate of porosity decay with depth (Athy, 1930). A least-squares fit to this equation yields ϕ_0 = 61.2% and k = 0.001 m^{-1} (correlation coefficient = 0.60) (Fig. F46C).

P-Wave Velocity

P-wave velocity was measured with the PWS3 contact probe system on split cores (within the core liner) and ~10 cm³ samples of semilithified and lithified sediments. The *P*-wave logger was not used at Site 1193. From Cores 194-1193A-1H through 4H, velocity measurements were only taken in the x-direction. From Cores 194-1193A-6X through 79X and for Holes 1193B and 1193C, x-, y-, and z-direction velocity was routinely measured using sample cubes prepared from indurated sediment.

Velocity averages ~1600 m/s from 0 to 35 mbsf (lithologic Units I and II) (Fig. F47). From 35 to 165 mbsf (lithologic Subunit IIIA), velocity values are scattered from 1600 to 5200 m/s without a clear trend. In a third interval, from 229 to 415 mbsf, a distinct downhole-increasing velocity trend is visible. Velocity values in this interval start at 1600–1700 m/s and increase downhole to nearly 2700 m/s. Velocity in the top of the acoustic basement is low (1960 m/s at 540 mbsf).

A crossplot of velocity vs. porosity for Site 1193 shows a distinct inverse trend (Fig. F48). The measured velocities can be compared with the time-average equation of Wyllie et al. (1956):

F47. *P*-wave velocity, p. 84.

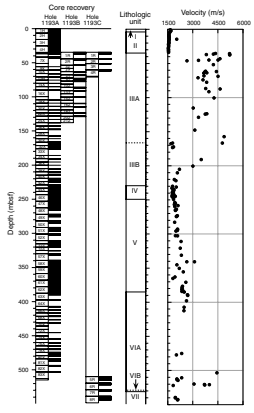

F48. Crossplot of velocity vs. porosity, p. 85.

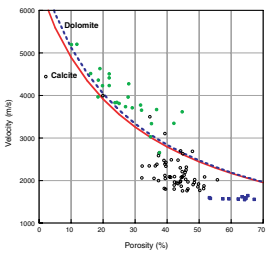

$$1/V_{rock} = (1 - \phi)/V_{matrix} + \phi/V_{fluid}.$$

This empirical equation states that the traveltime of an acoustic signal through rock is the sum of the traveltime through the solid and the fluid phases. For Site 1193, the matrix was assumed to be calcite (V_{matrix} = 6530 m/s), and the pore fluid was assumed to be seawater (V_{fluid} = 1500 m/s). Often, the time-average equation provides a lower envelope for carbonate sediments. Deviations from the time-average equation are explained by different kinds of pore types (Anselmetti and Eberli, 1993). Moldic porosity shows a positive deviation from the time-average equation because the pores are integrated in a rigid framework. This type of porosity is common in the platform carbonates of Site 1193 (see **"Lithostratigraphy and Sedimentology,"** p. 6). Platform velocity values plot almost entirely above the time-average equation (Fig. **F48**). The time-average equation for dolomite (V_{matrix} = 7000 m/s) shows that the positive deviation cannot uniquely be explained by mineralogy (Fig. **F48**). Three velocity clusters can be clearly separated from each other in terms of lithology:

1. Hemipelagic sediments (lithologic Units I and II) (see **"Lithostratigraphy and Sedimentology,"** p. 6);
2. Platform sediments (lithologic Unit III); and
3. Upper-slope sediments (lithologic Units IV and V).

The negative deviations of upper-slope sediments from the time-average equation range from 600 to 1000 m/s, which is high for these types of rocks and might be explained by interparticle porosity and micrite cement.

Thermal Conductivity

Thermal conductivity values of the carbonate platform rocks at Site 1193 differ greatly from those of the remainder of the section (Fig. **F49**). From 40 to 130 mbsf, platform values decrease from 2.7 to 1.6 W/(m·K). Below 230 mbsf, in lithologic Units IV–VI, thermal conductivity increases with depth, ranging from ~1.1–2.0 W/(m·K). Variations in thermal conductivity are consistent with those in bulk density and porosity. A direct inverse relationship should exist between porosity (ϕ) and thermal conductivity because of the power law dependence of bulk thermal conductivity (K_{bulk}) on the solid matrix grain thermal conductivity (K_{grain}) and the thermal conductivity of the interstitial fluid (K_w) (Keen and Beaumont, 1990). This equation can be expressed as

$$K_{bulk} = K_w^{\phi} \cdot K_{grain}^{(1-\phi)}.$$

The observed relationship between the thermal conductivity and porosity can be compared with calculated bulk thermal conductivity using the measured porosity values and grain thermal conductivity values summarized in Table **T6,** p. 56, in the "Explanatory Notes" chapter (Keen and Beaumont, 1990). The majority of the measured thermal conductivity values lie between the theoretical shale and sandstone curves, giving confidence in the measured thermal conductivity (Fig. **F50**). Given the predominance of carbonate through the various sections, the observed thermal conductivity is consistent with mixed siliciclastic/carbonate and clay/carbonate sediments.

F49. Average thermal conductivity, p. 86.

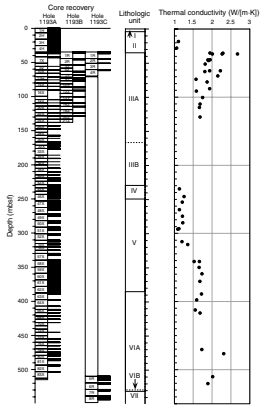

F50. Crossplot of thermal conductivity vs. porosity, p. 87.

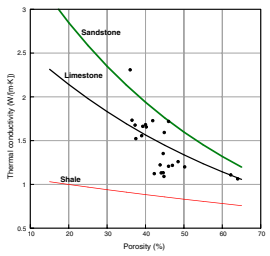

Magnetic Susceptibility and Natural Gamma Ray

The quality of the MS and NGR data at Site 1193 is degraded in XCB sections where the core is undersized with respect to the liner inner diameter and/or is disturbed (Fig. F51).

Downhole trends for MS and NGR are similar to that of the GRA bulk density in the first 35 mbsf (Fig. F52). All three data sets show a transition at 5.5 mbsf, which is best detected in the NGR with a downhole decrease from 50 to 5 cps (Fig. F52C). The MS data displays a positive spike at 5.5 mbsf, which is likely explained by the presence of framboidal pyrite found at this level (see "Site 1193 Visual Core Descriptions"). This transition coincides with a change in texture from grainstone to packstone and correlates with a hiatus (see "Age Model," p. 20). Below, the data show two distinct intervals with downhole-increasing NGR with a length of ~13 m (Fig. F52C). At 35 mbsf, the values of all three data sets increase sharply in response to the hardground at the top of the carbonate platform (lithologic Unit III) (see "Lithostratigraphy and Sedimentology," p. 6). Below the hardground, NGR values range from 0 to 35 cps. However, from 35 to 540 mbsf, low recovery prevented observations of cyclicity in NGR. An MS spike of 1500 × 10^{-6} SI occurs at the top of acoustic basement, which is likely caused by the presence of volcaniclastics (see "Lithostratigraphy and Sedimentology," p. 6).

SEISMIC STRATIGRAPHY

Introduction

Site 1193 penetrated 538.9 m of sediment and 5.45 m of acoustic basement through seismic Megasequences D, B, and A, (Fig. F53). Megasequence C is not present at this site as it onlaps the adjacent slope sediments of the NMP farther to the east (Fig. F2, p. 62, in the "Leg 194 Summary" chapter). The site is located at the intersection of multichannel seismic lines MAR13 (shotpoint 4755; Fig. F53) and MAR34 (shotpoint 2241). Site 1193 was chosen to sample the sediments of the NMP. This site is located ~31 km east of Site 1194 (Fig. F2, p. 62, in the "Leg 194 Summary" chapter).

Time-Depth Conversion

Because of deteriorating hole conditions that developed during retrieval of the drill string, the pipe became stuck in the drill hole and, as a result, needed to be severed with explosives; thus, Site 1193 was not logged and no check shot information is available to accurately tie the seismic record to the sedimentary section. The time-to-depth conversion used here is calculated by integrating shipboard velocity measurements collected with the *P*-wave sensor (PWS) (Figure F54) (see "Core Physical Properties," p. 24). Velocity values for the platform section were overestimated by the shipboard data so that lower values were used. To constrain the resulting time-to-depth function, two tie points, one at the basement-sediment contact (909 ms two-way traveltime [TWT] and 531 m) and one at the top of the NMP (510 ms TWT and 35 m) were used for calculation of this synthetic seismogram. Both horizons are recognized in the seismic data by unique and strong reflections, so they can be used as accurate ties.

F51. Magnetic susceptibility, and natural gamma radiation as a function of depth, p. 88.

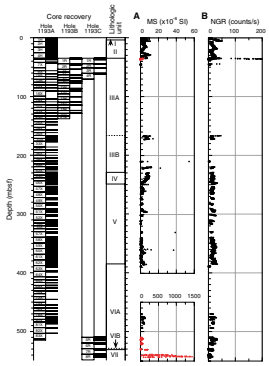

F52. Bulk density, magnetic susceptibility, and natural gamma radiation, 0 to 35 mbsf, p. 89.

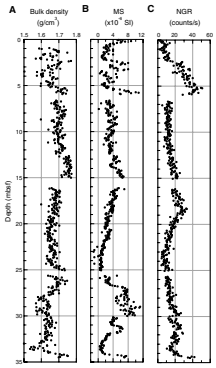

F53. Multichannel line MAR13, p. 90.

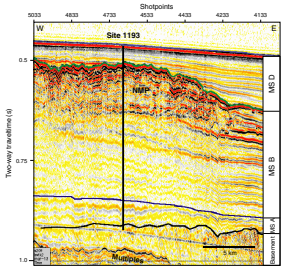

F54. Synthetic seismogram plotted on line MAR13 and core-to-seismic correlation, p. 91.

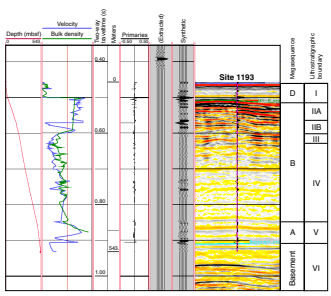

The PWS velocity, together with GRA bulk density, was also used for the calculation of a synthetic seismogram. A normal polarity, zero-phase wavelet of 80-ms length was statistically extracted from the seismic data of line MAR13. The result is superimposed onto line MAR13 and displayed at left on Figure F54. Because of the limited data set and the lack of check shot information, both the time-depth conversion and the synthetic seismogram carry considerable uncertainty.

Megasequence D

Seismic Facies and Geometries

The seismic facies of Megasequence D (Fig. F53) is characterized by laterally continuous reflections that dip gently eastward. The top portion of this onlapping package has a wedge-shaped geometry that appears to be truncated by erosion. This conclusion is supported by paleontological evidence indicating that sediments at 2.1 mbsf are 0.33 Ma in age and that a major hiatus occurs at 5.5 mbsf, lasting at least from 1.7 to 2.8 Ma (see "Age Model," p. 20).

At Site 1193, Megasequence D is thin (48 ms TWT) and is seen to infill the erosional surface on top of the middle Miocene NMP. Reflection amplitudes are generally low, with the most prominent intramegasequence high-amplitude reflection directly overlying the top of the NMP at 504 ms TWT. Megasequence D thickens to the east as sediments onlap the paleotopographic surface of the NMP. The lower Megasequence D sequence boundary directly overlies the upper boundary of Megasequence B, which at Site 1193 coincides with the top of the NMP, resulting in a large hiatus that spans the entire Megasequence B.

Correlation with Cores

Megasequence D is a thin, ~40-m-thick layer of hemipelagic sediment that overlies the NMP. Seismic Megasequence D incorporates lithologic Unit I, which is composed of a foraminiferal nannofossil ooze deposited in water depths >200 m (see "Lithostratigraphy and Sedimentology," p. 6). Paleontological evidence indicates that the sediments of Megasequence D are Pliocene–Pleistocene in age (see "Biostratigraphy and Paleoenvironments," p. 11). As with Site 1192, Holocene sediments were absent at this site, confirming that modern sedimentation is strongly reduced or nonexistent and that the seafloor represents an unconformity.

The exact magnitude of the hiatus is unknown but has been estimated by tracing the first reflection on top of the NMP platform to Site 1192, where sediments of Megasequence D were thicker and exhibited a more complete biostratigraphic succession. The initial sediments overlying the NMP that correspond to this reflection provide an age of ~5 Ma. Because the reflection traced did not lie directly on the platform surface but slightly above, this reflection is likely to provide an age for initial sedimentation on top of the NMP that is younger than the true age of the flooding. Biostratigraphically the base of the sediments overlying the NMP are dated as 5.6 Ma (see "Biostratigraphy and Paleoenvironments," p. 8, in the "Site 1192" chapter). The top of the underlying NMP is biostratigraphically not well constrained, but benthic foraminifer assemblages give an age of >12 Ma. Thus, the hiatus is at least 5.6 to 10.5 Ma in age or as much as 5.6 to >12 Ma.

Megasequence B

Seismic Facies and Geometries

The top of Megasequence B is characterized by a high-amplitude unconformity at 508 ms TWT that marks the top of the NMP. The upper portion of this platform (508–610 ms) is characterized by a seismically transparent to chaotic carbonate platform section with hummocky reflections (Fig. F53). The B/D boundary forms the top of the NMP. The top of Megasequence B was traced into the basin to Site 1192, where it could be assigned an age of 10.5 Ma (see "Age Model," p. 13, in the "Site 1192" chapter). The time-depth correlation used at this site places the seismic sequence boundary on top of the platform at 37 mbsf (Fig. F54). Below the platform interval is a sequence of moderately continuous reflections dipping to the east, indicating an eastward progradation of the platform slope (610–830 ms TWT) (Fig. F53). The seismic character of reflections within this portion of Megasequence B is disturbed by the overlying platform facies. Despite this, it is clear that these sediments grade eastward into a prograding sequence with more continuous reflections that can be consistently traced through the study area. The basinward transition of the upper "reefal" NMP facies is not as continuous as it is for the lower prograding slope sediments and, in many instances, shows evidence of erosional channels adjacent to the platform margin, indicating subaerial exposure and possibly current reworking after flooding (Figs. F53 and F7, p. 67, in the "Leg 194 Summary" chapter). The time-depth correlation used at this site places the lower boundary of Megasequence B at 440 mbsf (Fig. F54).

Correlation with Cores

Megasequence B incorporates lithologic Units II through IV, all of which are Miocene in age. The upper carbonate platform facies observed on the seismic data correlates well with lithologic Unit II, which is composed of skeletal rudstones and floatstones with lesser amounts of packstone and clay-rich mudstone (see "Lithostratigraphy and Sedimentology," p. 6). This section has been interpreted as a shallowing-upward interval of subtropical carbonate platform deposition dominated by benthic foraminifers and bryozoans. Physical properties data of this interval are characterized by highly varying *P*-wave velocity (2.7–5.2 km/s) and porosity (10%–45%) (see "Core Physical Properties," p. 24). Several irregular surfaces were observed in the cores, indicating subaerial and submarine erosion and reworking. The lack of regular bedding, together with the large range of physical properties values, explains the hummocky, chaotic seismic facies.

The sequence of dipping reflections below the platform interval correlates with lithologic Units III and IV, representing a deepening-upward sequence of platform-derived slope sediments (see "Biostratigraphy and Paleoenvironments," p. 11) characterized by bioclastic packstones to mudstones that are dominated by benthic foraminifers and bryozoans.

Megasequence A

Seismic Facies and Geometries

At the location of Site 1193, Megasequence A is difficult to characterize as a result of the seismic interference from the overlying NMP. Mega-

sequence A is characterized by a nearly horizontal series of reflections of varying amplitudes that can be traced laterally underneath sediments of Megasequence B. Megasequence A overlies and infills basement irregularities resulting in an overall variability in thickness. The time-depth correlation used at this site places the lower boundary of Megasequence A at 531 mbsf (Fig. **F54**).

Correlation with Cores

The sediments of Megasequence A were deposited in a shallow-water inner-shelf setting and consist of a series of grainstones with quartz sand, bryozoans, and benthic foraminifers (see **"Biostratigraphy and Paleoenvironments,"** p. 11).

Basement

Seismic Facies and Geometries

Acoustic basement at Site 1193 is difficult to characterize as a result of the interference of the overlying carbonate platform sediments and the seafloor multiple (Fig. **F53**). Despite this interference, the basement top surface is recognized as a high-amplitude reflection at the interface with overlying sediments and numerous diffractions caused by the irregular bedrock surface.

Correlation with Cores

Approximately 5 m of acoustic basement was recovered at Site 1193 (Fig. **F53**). These rocks consisted of volcaniclastic red breccia with fine-grained layers (see **"Lithostratigraphy and Sedimentology,"** p. 6).

REFERENCES

Anselmetti, F.S., and Eberli, G.P., 1993. Controls on sonic velocity in carbonates. *Pure Appl. Geophys.,* 141:287–323.

Athy, L.F., 1930. Density, porosity, and compaction of sedimentary rocks. *AAPG Bull.,* 14:1–24.

Betzler, C., and Chaproniere, G.C.H., 1993. Paleogene and Neogene larger foraminifers from the Queensland Plateau: biostratigraphy and environmental significance. *In* McKenzie, J.A., Davies, P.J., Palmer-Julson, A., et al., *Proc. ODP, Sci. Results,* 133: College Station, TX (Ocean Drilling Program), 51–66.

Chaproniere, G.C.H., 1981. Australasian mid-Tertiary larger foraminiferal associations and their bearing on the East Indian Letter Classification. *BMR J. Aust. Geol. Geophys.,* 6:145–151.

Chaproniere, G.C.H., 1984. Oligocene and Miocene larger foraminiferida from Australia and New Zealand. *Bull.—Bur. Miner. Resour., Geol. Geophys. (Aust.),* 188:1–98.

Chaproniere, G.C.H., and Betzler, C., 1993. Larger foramineral biostratigraphy of Sites 815, 816, and 826, Leg 133, northeastern Australia. *In* McKenzie, J.A., Davies, P.J., Palmer-Julson, A., et al., *Proc. ODP, Sci. Results,* 133: College Station, TX (Ocean Drilling Program), 39–49.

Davies, P.J., McKenzie, J.A., Palmer-Julson, A., et al., 1991. *Proc. ODP, Init. Repts.,* 133 (Pts. 1, 2): College Station, TX (Ocean Drilling Program).

Hallock, P., 1987a. Fluctuations in the trophic resource continuum: a factor in global diversity cycles? *Paleoceanography,* 2:457–471.

Hallock, P., 1987b. Reefs and reef limestones in Earth history. *In* Birkeland, C. (Ed.), *Life and Death of Coral Reefs:* New York (Chapman and Hall), 13–42.

Hallock, P., 1999. Symbiont-bearing foraminifera. *In* Sen Gupta, B.K., *Modern Foraminifera:* Amsterdam (Kluwer), 123–149.

Hohenegger, J., 1999. Larger foraminifera—microscopical greenhouses indicating shallow-water tropical and subtropical environments in the present and past. *Occasional Papers*. Kagoshima Univ. Res. Central Pacific Islands, 32:19–45.

James, N.P., 1997. The cool water carbonate depositional realm. *In* James, N.P. and Clarke, J.A.D (Eds.), *Cool Water Carbonates*. Spec. Publ.—Soc. Econ. Paleontol. Mineral., 56:1–20.

James, N.P., Collins, L.B., Bone, Y., and Hallock, P., 1999. Subtropical carbonates in a temperate realm: modern sediments on the southwest Australian shelf. *J. Sediment. Res.,* 69:1297–1321.

Keen, C., and Beaumont, C., 1990. Geodynamics of rifted continental margins. *In* Keen, M.J., and Williams, G.L. (Eds.), *Geology of the Continental Margin of Eastern Canada,* Geol. Soc. Am., 1:391–472.

Kleypas, J.A., Buddemeier, R.W., Archer, D., et al., 1999. Geochemical consequences of increased atmospheric carbon dioxide on coral reefs. *Science,* 284:118–120.

Lee, J.J., 1998. Living sands: larger foraminifera and their endosymbotic algae. *Symbiosis,* 25:71–100.

Pigram, C.J., Davies, P.J., Feary, D.A., and Symonds, P.A., 1992. Absolute magnitude of the second-order middle to late Miocene sea-level fall, Marion Plateau, Northeast Australia. *Geology,* 20:858–862.

Wyllie, M.R.J., Gregory, A.R., and Gardner, L.W., 1956. Elastic wave velocities in heterogeneous and porous media. *Geophysics,* 21:41–70.

Figure F1. Bathymetry map showing locations of Leg 194 sites.

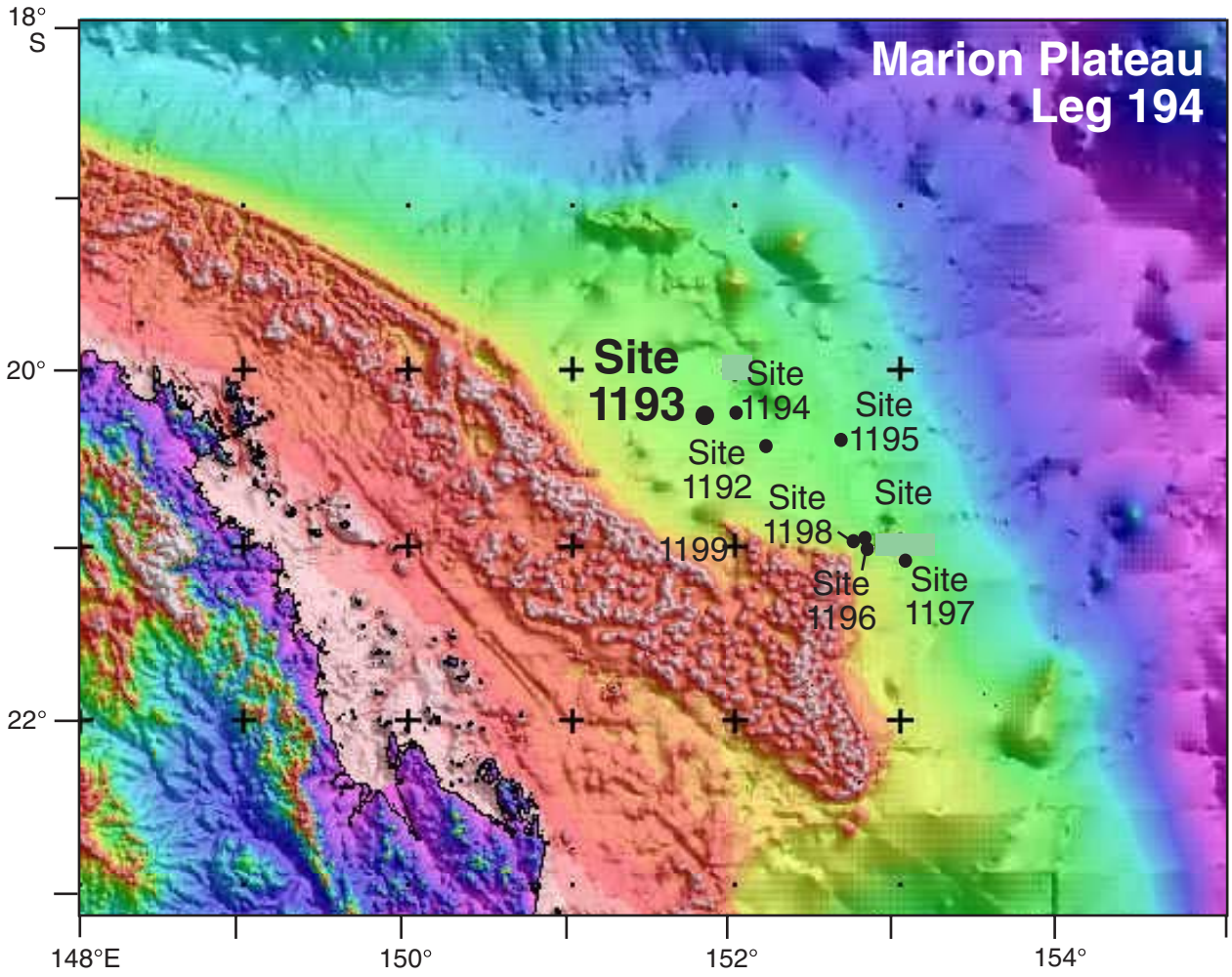

Figure F2. Seismic line MAR13 showing locations of Sites 1193 and 1194. Site 1193 is positioned on top of the Northern Marion Platform (NMP). MS = Megasequence.

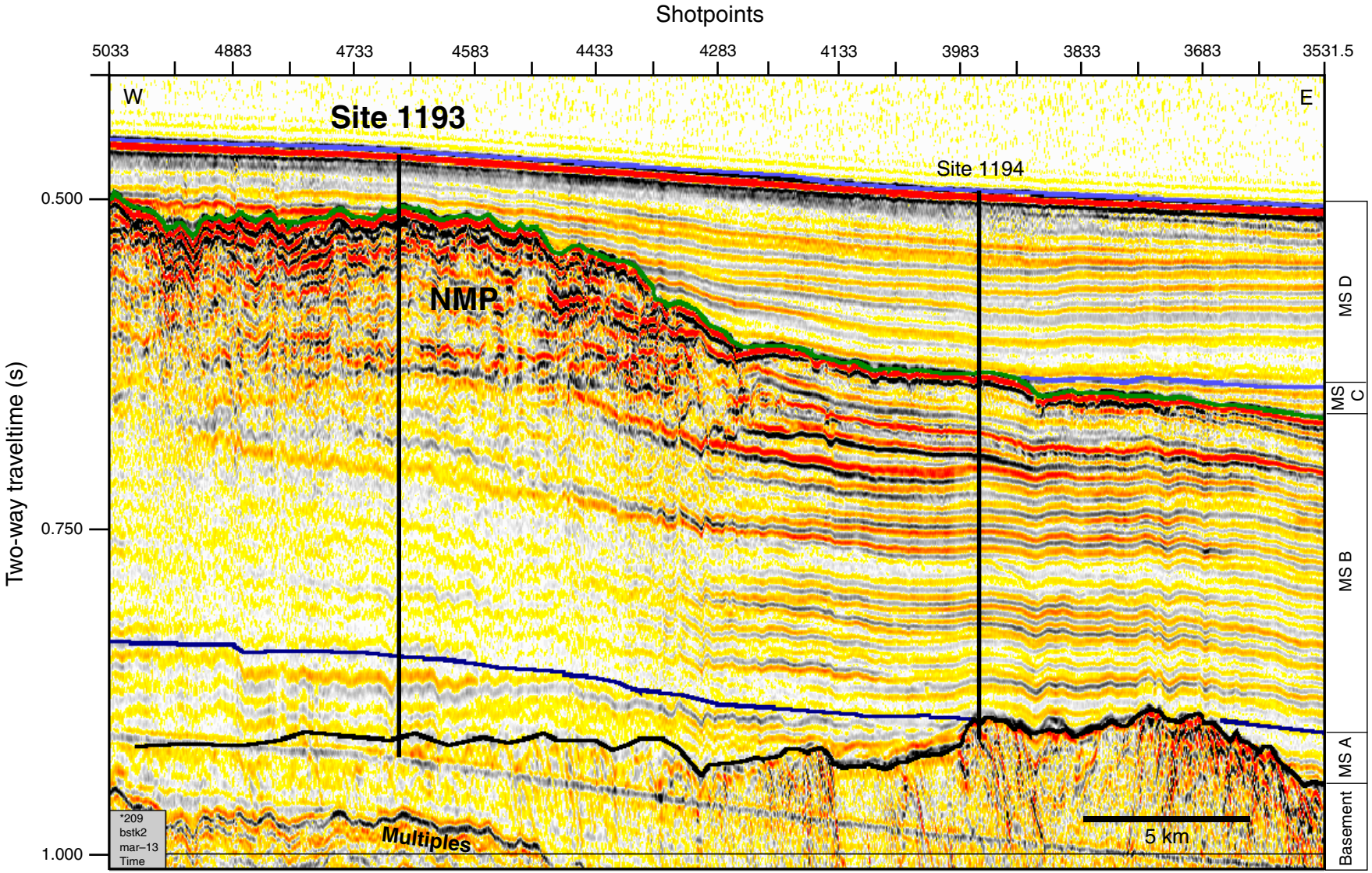

Figure F3. Video sequence of reentrance of Hole 1193B with an ADCB bit through a previously deployed FFF. The small dial with the arrow attached to the drill string indicates north. The diameter of the FFF is 2.4 m; the outer diameter of the ADCB bit is 18.5 cm (7.25 in). (QuickTime software is available for the Macintosh and Windows platforms only. Please see **"QuickTime Movies"** in 194IR.PDF for further information. Click the image to play the movie.)

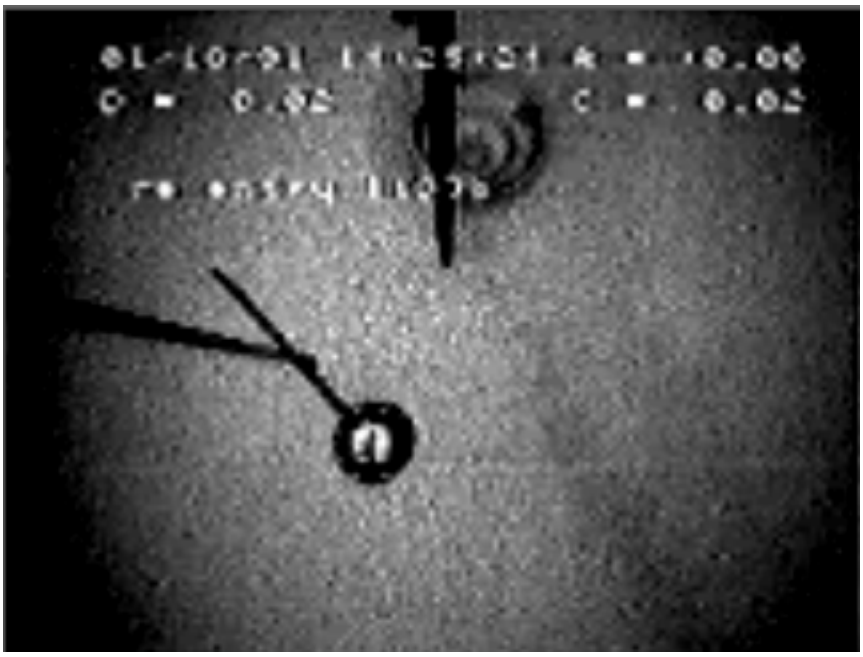

Figure F4. Lithostratigraphic summary for Site 1193. Information columns are identified by letter. **A.** Core recovery for Holes 1193A, 1193B, and 1193C. Black = recovered, white = gap. **B.** Lithologic units. **C.** Lithology. **D.** Percentages of dolomite and non-carbonate minerals determined by x-ray diffraction. **E.** Limestone textural classification. **F.** Water depths estimated from benthic foraminiferal assemblages (see "Biostratigraphy and Paleoenvironments," p. 11). **G.** Ages derived from biostratigraphy (see "Biostratigraphy and Paleoenvironments," p. 11). **H.** Interpretation of depositional environments.

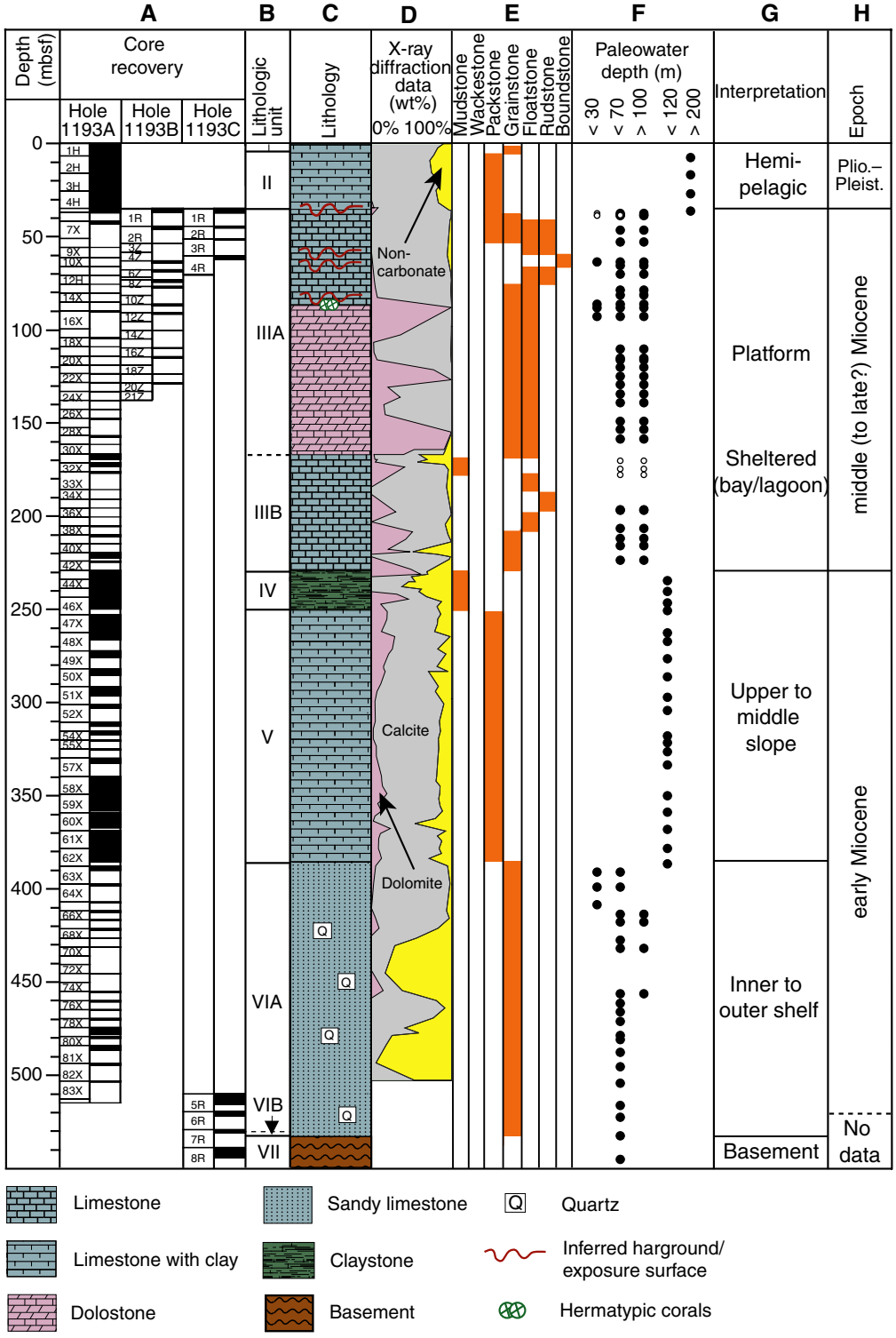

Figure F5. Close-up photograph of the grainstone bed at the top of Unit I (1.0 mbsf) (interval 194-1193A-1H-1, 0–20 cm).

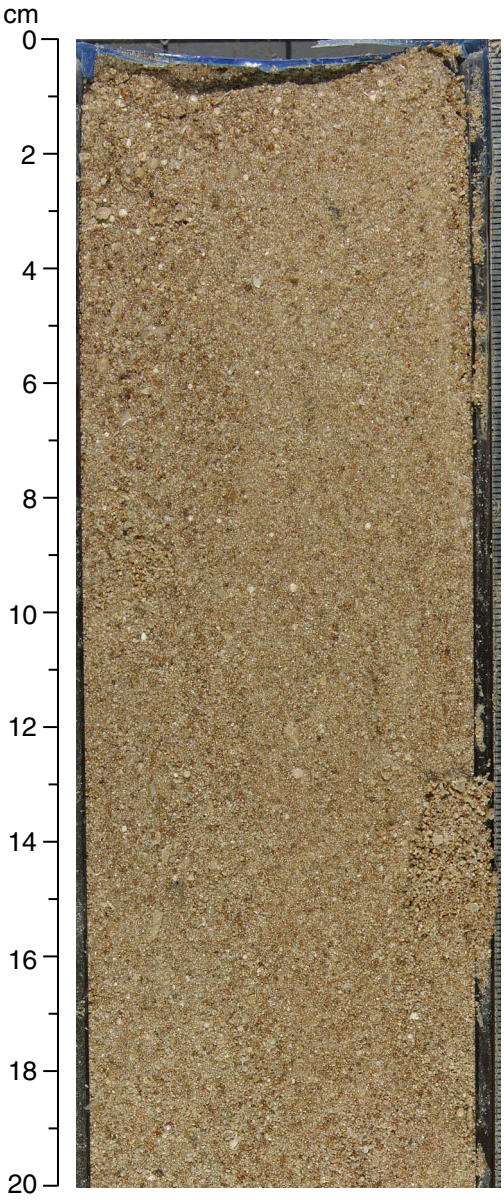

Figure F6. Close-up photograph of the base of Unit II (35.2 mbsf) (interval 194-1193A-4H-7, 40–60 cm).

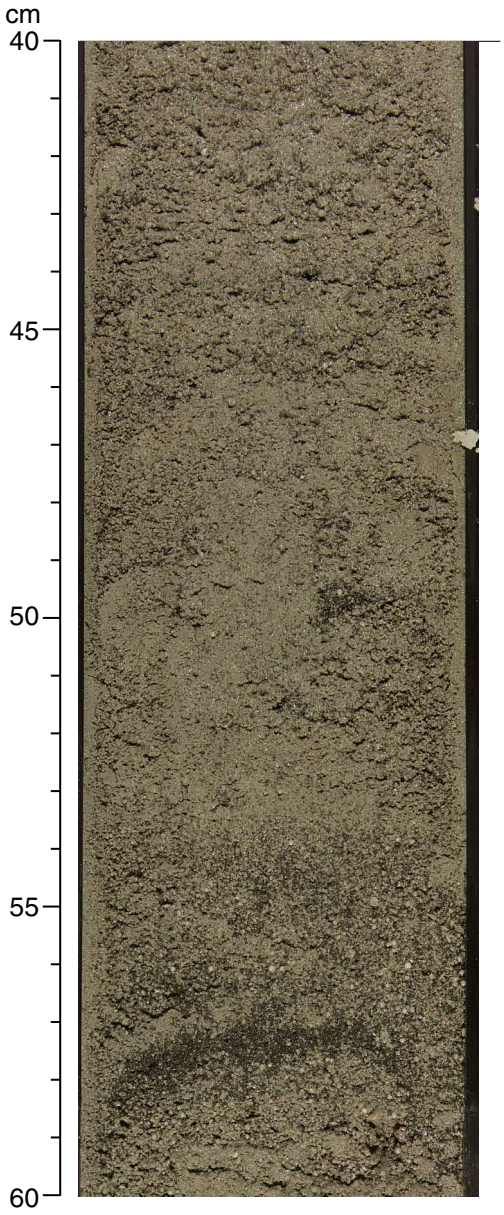

Figure F7. Close-up photograph showing the top of Subunit IIIA (interval 194-1193B-1R-1, 19–38 cm; 35.2 mbsf). The uppermost core piece consists of skeletal packstone rich in planktonic foraminifers. Part of one surface is coated with dark brown to black material that may be phosphate (arrow). The underlying core pieces consist of tightly cemented skeletal packstone with reddish brown coloring.

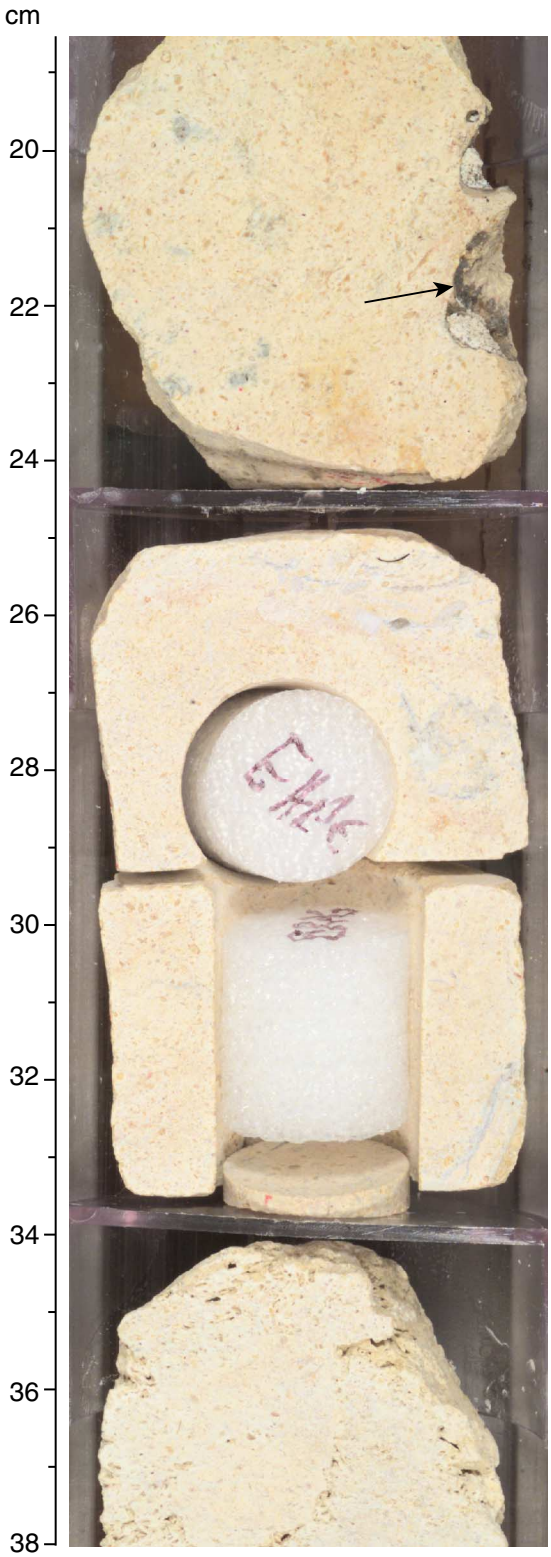

Figure F8. Photomicrograph showing the lithology of the topmost several centimeters of Subunit IIIA (Sample **194-1193A-5H-1, 143 cm;** 36.5 mbsf). This skeletal packstone contains planktonic (P) and benthic foraminifers (B). Three stages of cementation are visible in mud-free interparticle spaces and within the upper portions of the partly mud-filled planktonic foraminifer tests: (1) a thin coating (~10 µm) of finely fibrous, inclusion-rich calcite; (2) a thick syntaxial overgrowth of acicular calcite; and (3) infilling of remaining space by blocky calcite. Blocky calcite also infills all interparticle spaces that are not mud filled. Some grains, such as the benthic foraminifer, have limonitic oxidized coloring.

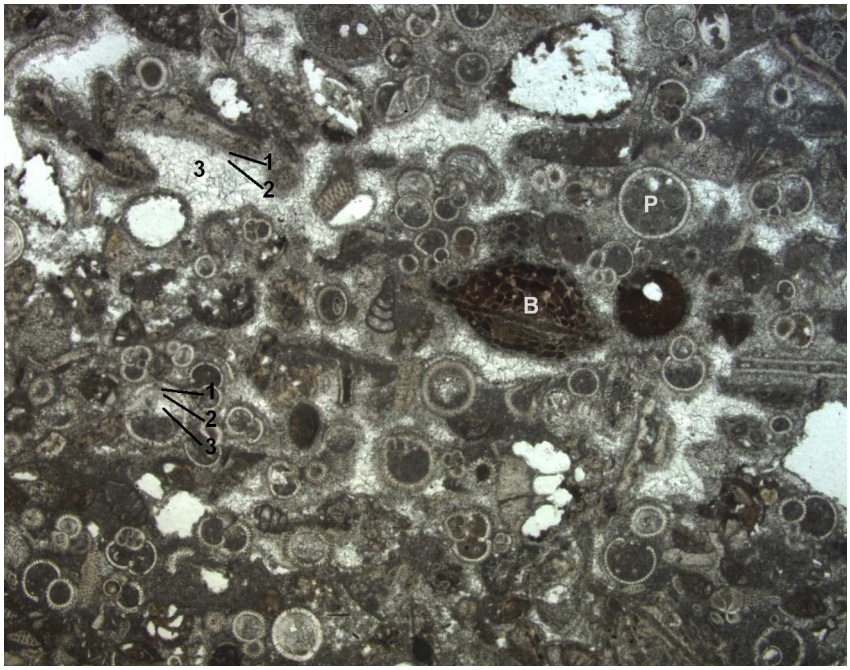

Figure F9. Close-up photograph showing representative lithologies from below the top of Subunit III (interval 194-1193B-1R-1, 96–112 cm; 36.0 mbsf). The uppermost core pieces consist of tightly cemented skeletal floatstone having reddish brown coloring. The lower core piece consists of white, highly porous, skeletal floatstone.

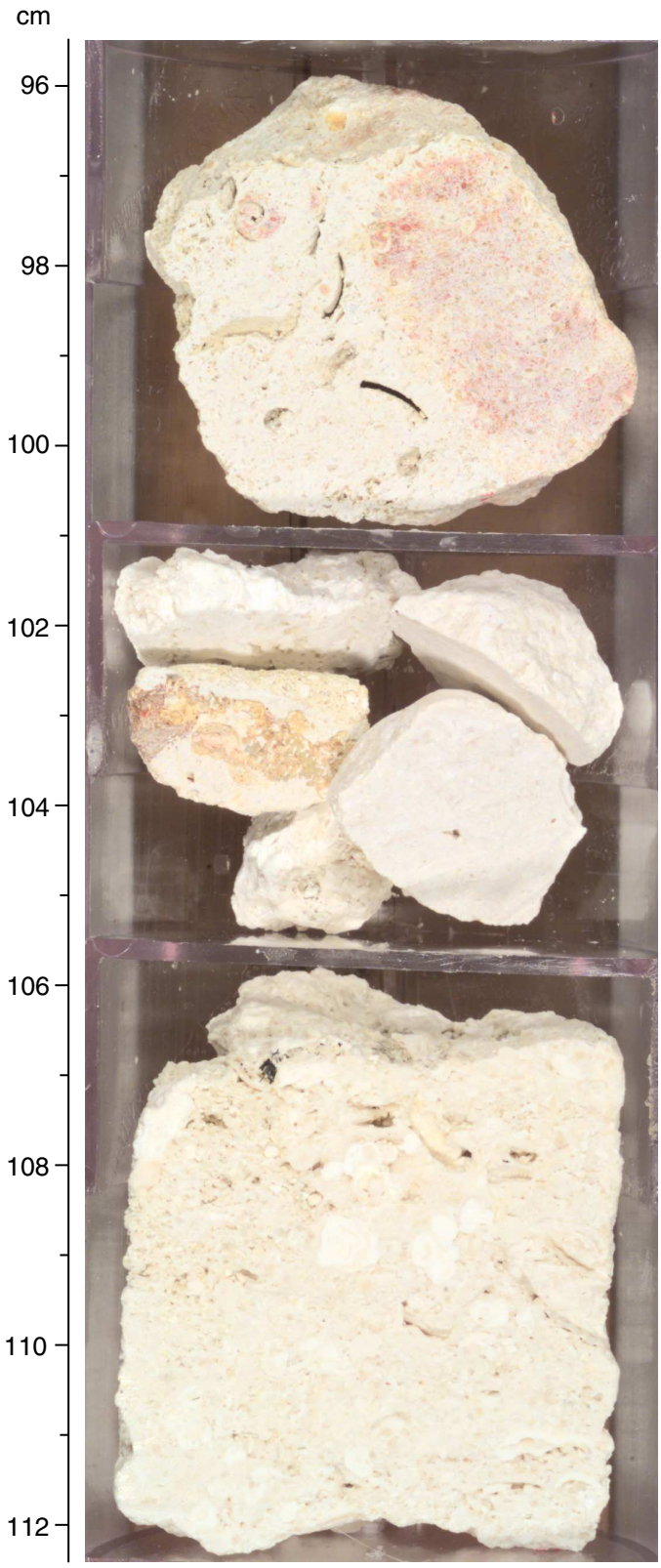

Figure F10. Photomicrograph showing the lithology of white, variably porous rudstone to floatstone just below the tightly cemented uppermost zone of Subunit IIIA (Sample **194-1193A-6X-CC, 46 cm;** 37.6 mbsf). A partly dissolved bivalve shell fragment (M) is encrusted by bryozoans (Y) and underlain by a shelter pore that shows geopetal fabric with partial filling by micritic mud (A) followed by coarser-grained material (B) interpreted as crystal silt. The latter feature is evidence for vadose diagenetic conditions.

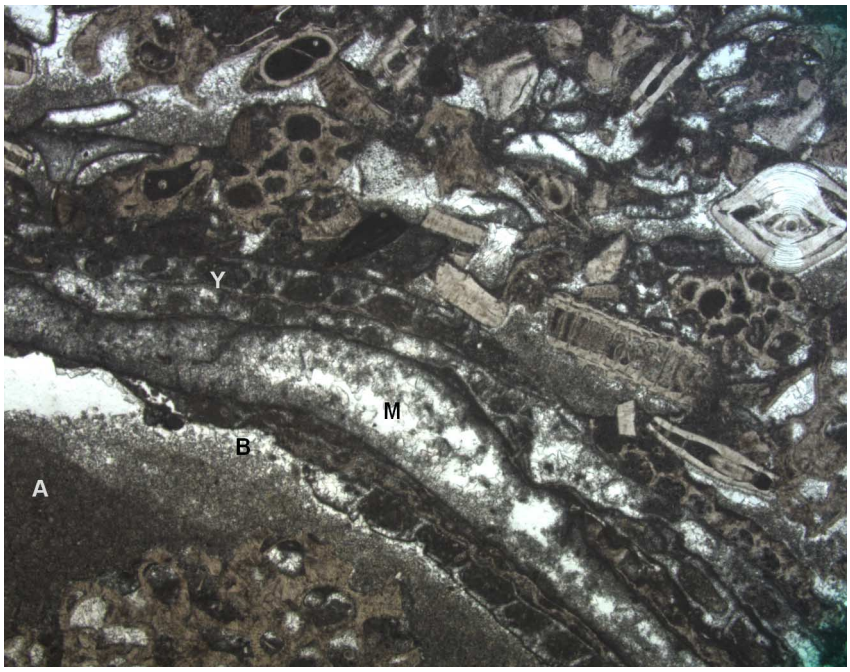

Figure F11. Close-up photograph of a fracture through a bryozoan-dominated skeletal packstone in the upper part of Subunit IIIA (69.7 mbsf). The fracture is infilled by darker grainstone rich in glauconite pellets and quartz sand. Based partly on its reddish (oxidized) lower surface, this feature is interpreted as a karstic exposure surface (interval 194-1193B-6Z-1, 77–85 cm).

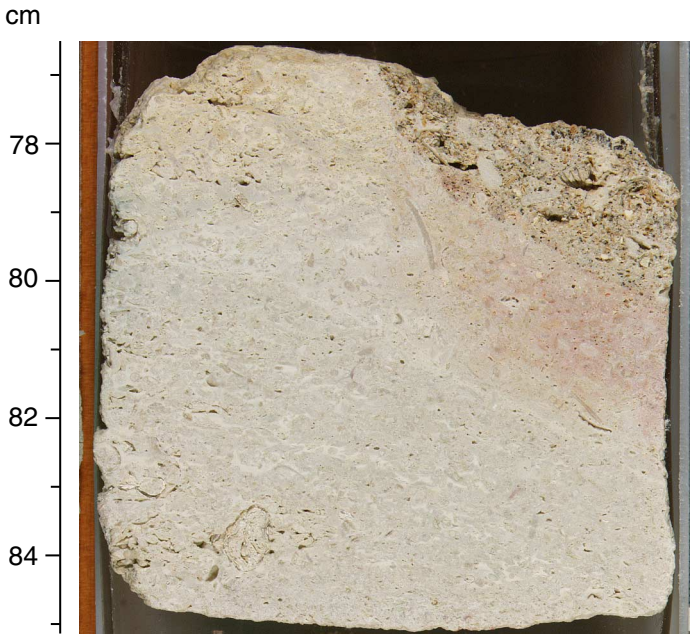

Figure F12. Close-up photograph showing a skeletal rudstone consisting mainly of bryozoan fragments and larger benthic foraminifers from Subunit IIIA (interval 194-1193B-5Z-1, 38–55 cm; 63.6 mbsf). This lithology has fine-scale layering defined by size sorting and horizontal orientation of bioclasts.

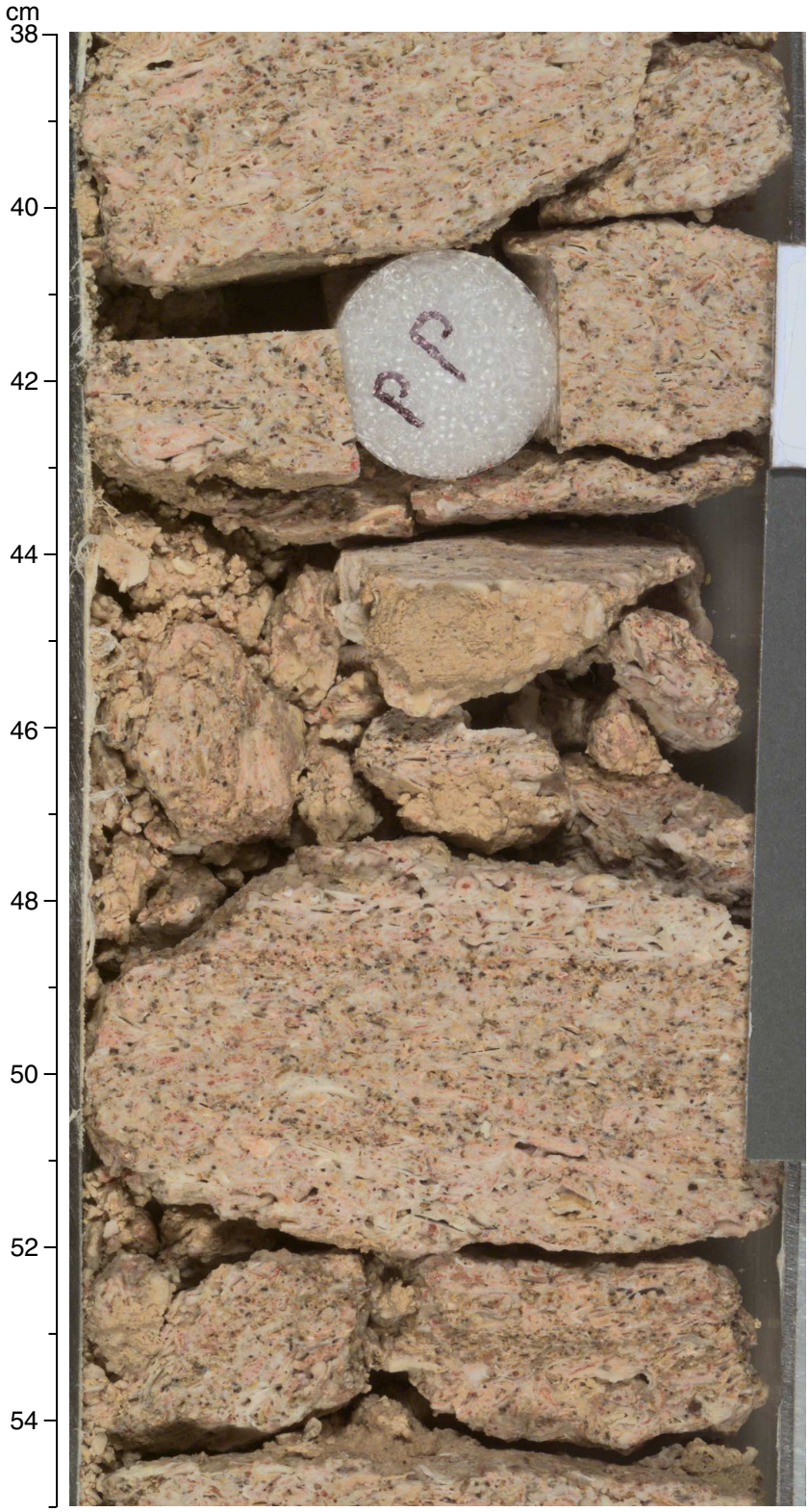

Figure F13. Close-up photograph showing a dolomitized rudstone from Subunit IIIA (interval 194-1193B-14Z-1, 0–19 cm; 100.4 mbsf). This lithology consists of finely crystalline sucrosic dolostone with abundant molds of bioclasts.

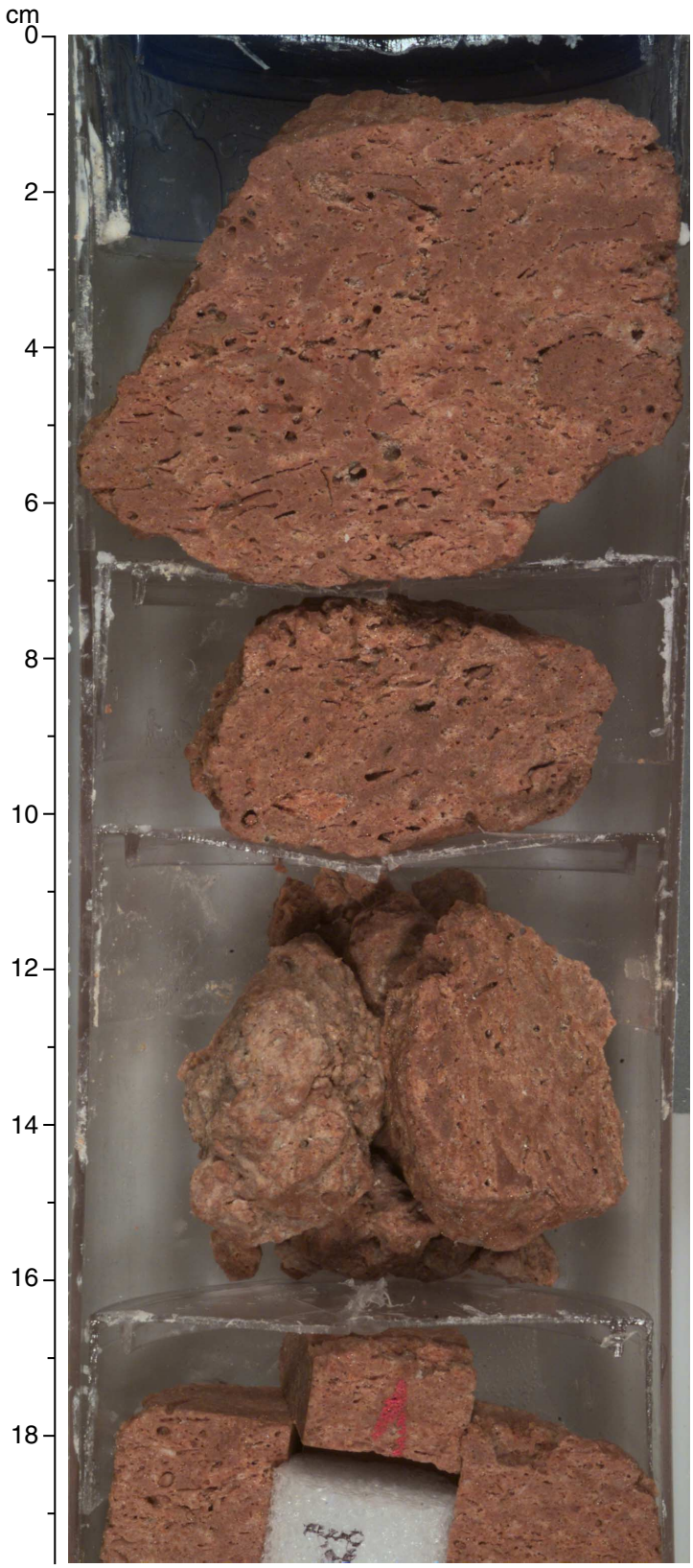

Figure F14. Photomicrograph of a dolomitized rudstone from Subunit IIIA (Sample 194-1193B-14Z-1, 18 cm; 100.6 mbsf). Molds of bioclasts are surrounded by fine crystalline, sucrosic dolomite.

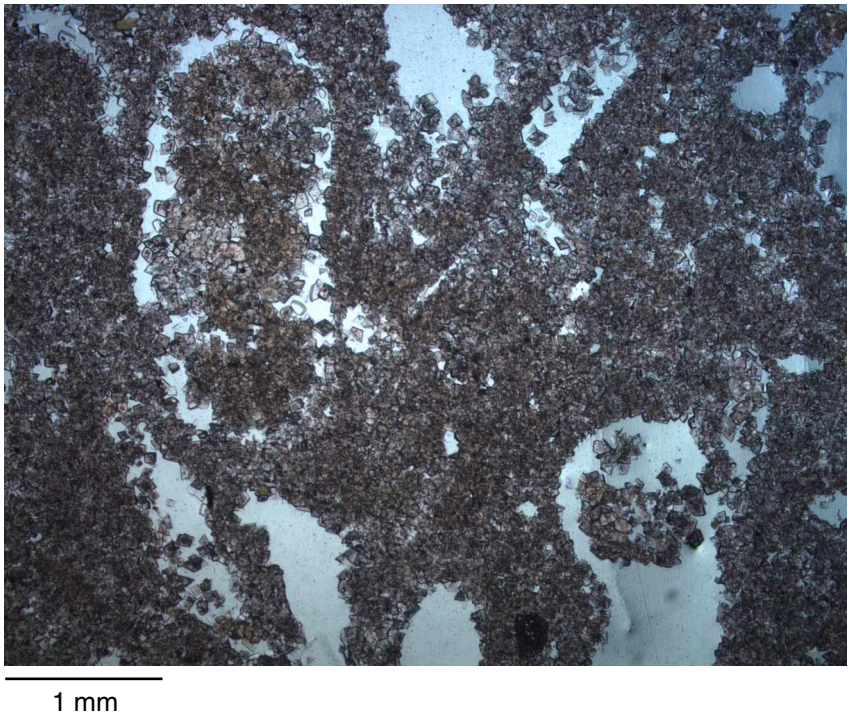

Figure F15. Photomicrograph showing a lithology from Subunit IIIB (Sample **194-1193A-40X-1, 2 cm;** 214.8 mbsf). This skeletal grainstone consists mainly of bryozoan fragments and subordinate benthic foraminifers (B), red algae (R), and bivalves (M). Bioclasts are fringed by isopachous fine prismatic calcite cement (1), and interparticle space is mostly infilled by later fine blocky calcite spar (2).

Figure F16. Close-up photograph of the clay-rich floatstone/mudstone interval at the top of Subunit IIIB (168.7 mbsf) (interval 194-1193A-31X-2, 15–35 cm).

Figure F17. Close-up photograph of ~3 m above the base of Unit IV (245.3 mbsf) (Section 194-1193A-46X-2, 22–60 cm).

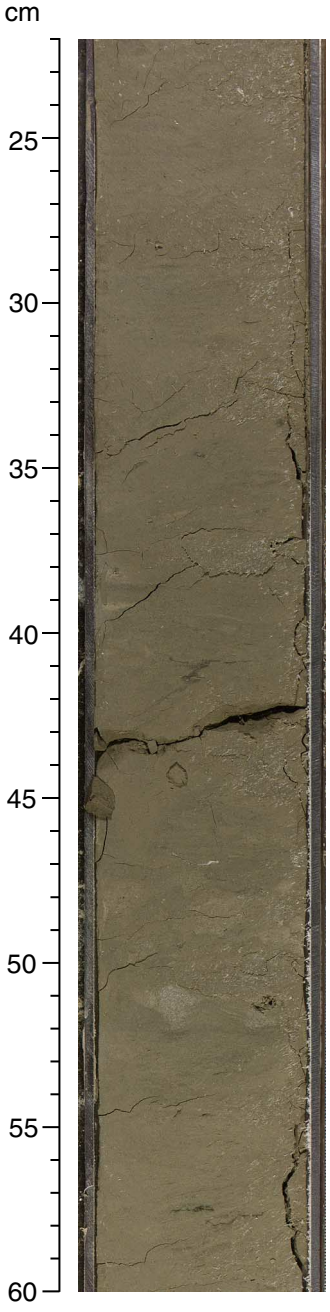

Figure F18. Photomicrograph showing a lithology from the upper part of Unit IV (Sample **194-1193A-43X-CC, 39 cm;** 233.7 mbsf). This lithology is intermediate between carbonate mudstone and claystone. It consists of recrystallized carbonate mud and clay matrix, containing abundant pyrite, planktonic foraminifers (P), and fine skeletal debris.

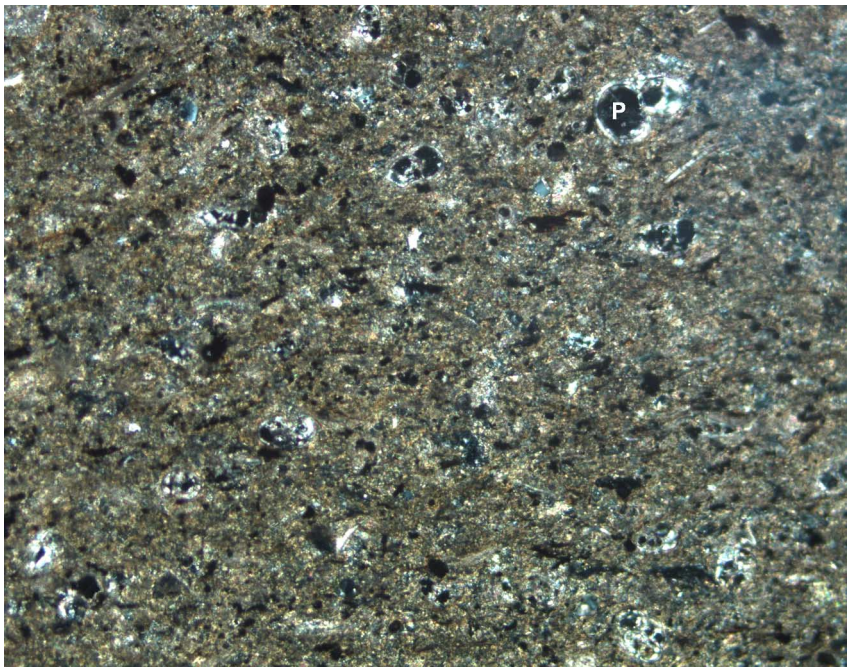

Figure F19. Close-up photograph of the central portion of Unit V (331.0 mbsf) (interval 194-1193A-57X-1, 80–93 cm).

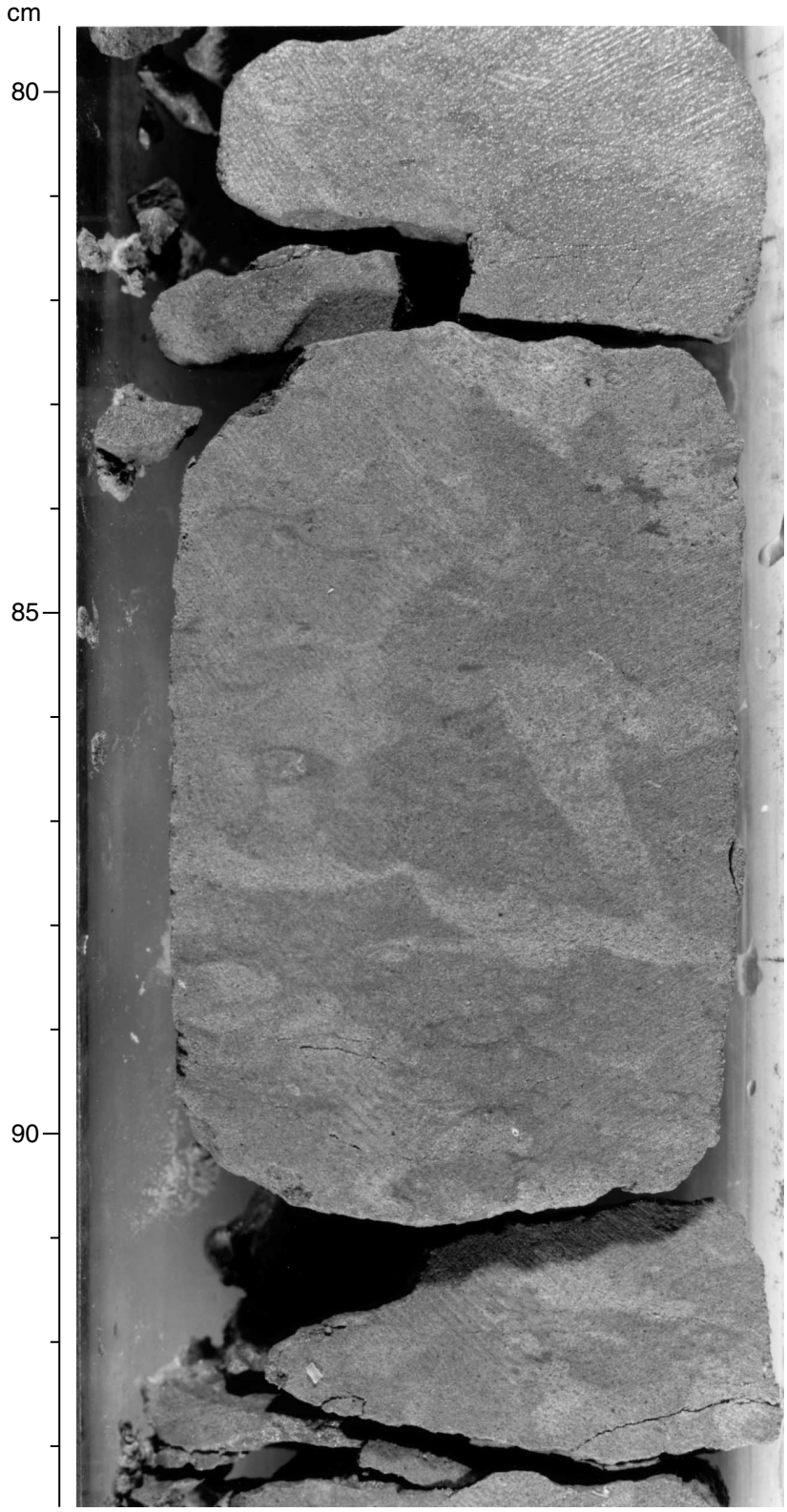

Figure F20. Photomicrograph showing silt- to fine sand–sized packstone from Unit V (Sample **194-1193A-52X-2, 25 cm;** 302.9 mbsf). It contains benthic (B) and planktonic (P) foraminifers and fragments of bryozoans and red algae (R) in a clay-rich mud matrix with minor quartz silt and glauconite.

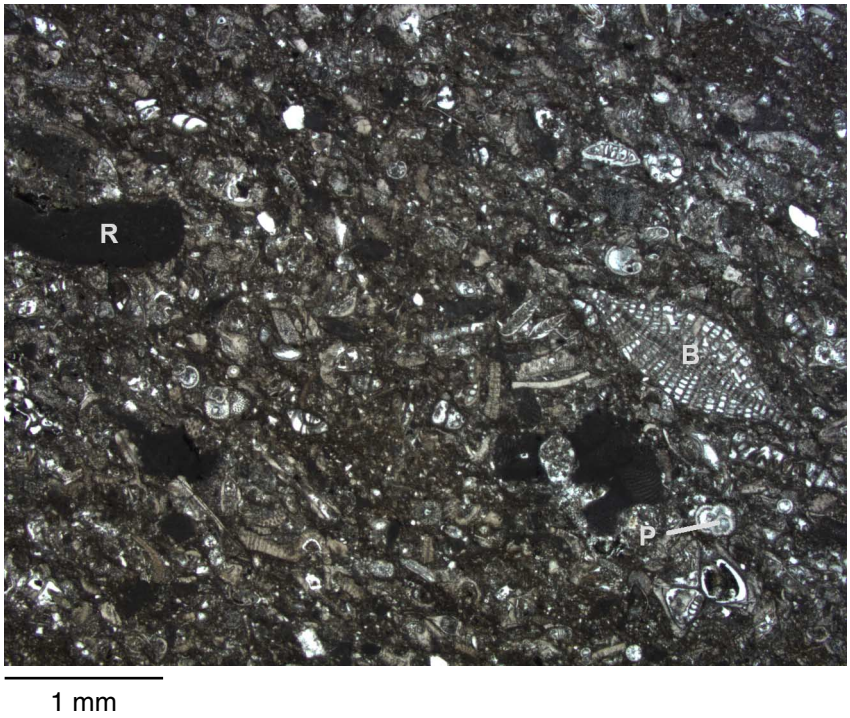

Figure F21. Close-up photograph of the contact between Units V and VI (385.1 mbsf) (interval 194-1193A-62X-5, 70–90 cm).

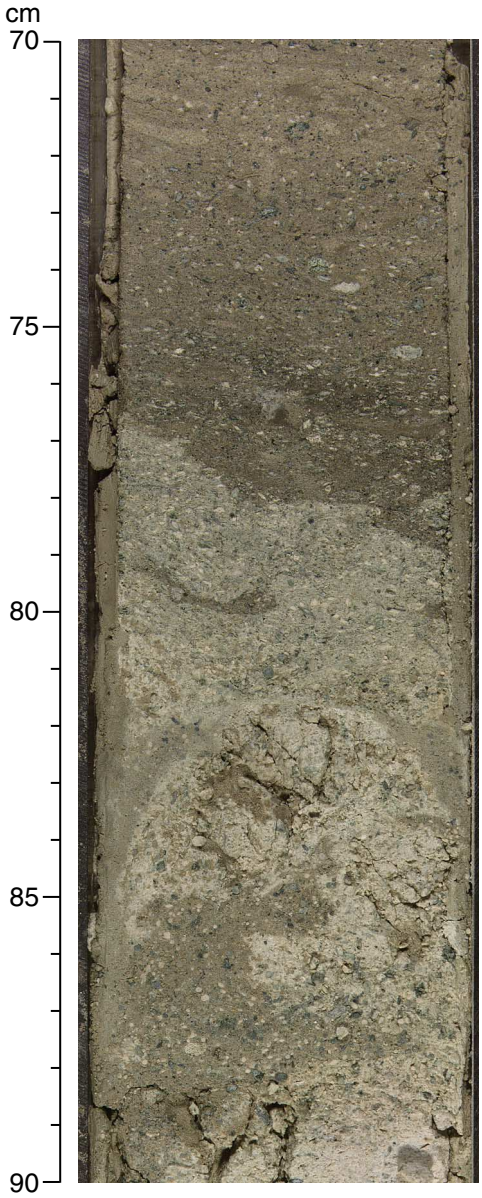

Figure F22. Close-up photograph of skeletal grainstone lithology in the central part of Unit VI (479.7 mbsf) (interval 194-1193A-80X-1, 30–49 cm).

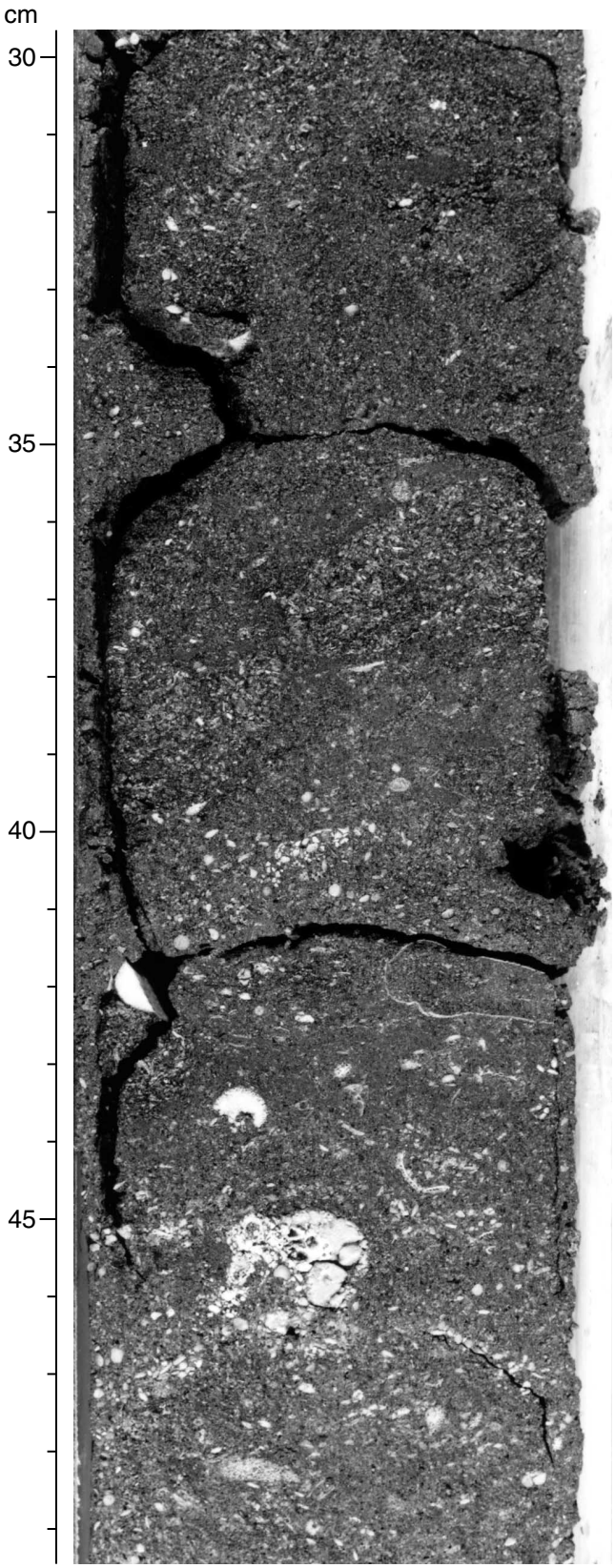

Figure F23. Photomicrograph showing a typical carbonate lithology from Subunit VIA (Sample 194-1193A-65X-CC, 13 cm; 407.3 mbsf). This grainstone contains benthic (B) and rare planktonic foraminifers and subordinate fragments of bryozoans and echinoderms (E). Minor quartz sand (Q) and glauconite are also present. Most interparticle pore space has been lost through compaction.

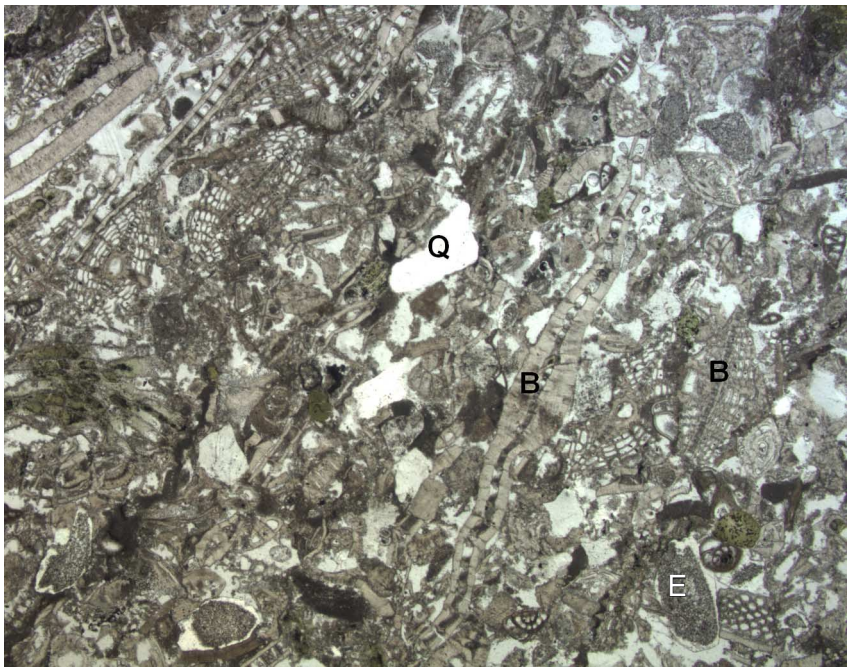

Figure F24. Photomicrograph showing a sandstone from Subunit VIA (Sample **194-1193A-70X-CC, 4 cm;** 431.2 mbsf). Poorly sorted quartz grains (Q) are accompanied by subordinate bioclasts (mainly echinoderm (E) and bryozoan fragments) and dark grains of phosphate (X) and oxidized glauconite. The grains have an isopachous coating of very fine crystalline, equant calcite (1), which coarsens outward from the grain surface. Echinoderm fragments are enclosed in syntaxial calcite cement overgrowths (S).

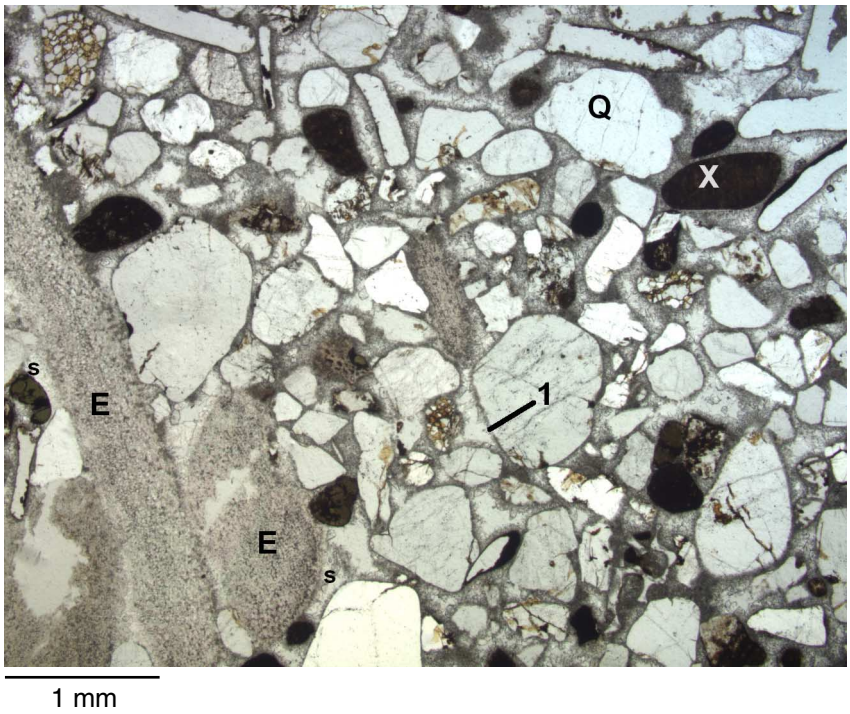

Figure F25. Close-up photograph showing part of the deepest core in Subunit VIA (interval 194-1193C-6R-1, 91–102 cm; 520.5 mbsf). This finely laminated grainstone shows bidirectional current ripples with hydrodynamic segregation of white bioclasts and dark green glauconite pellets.

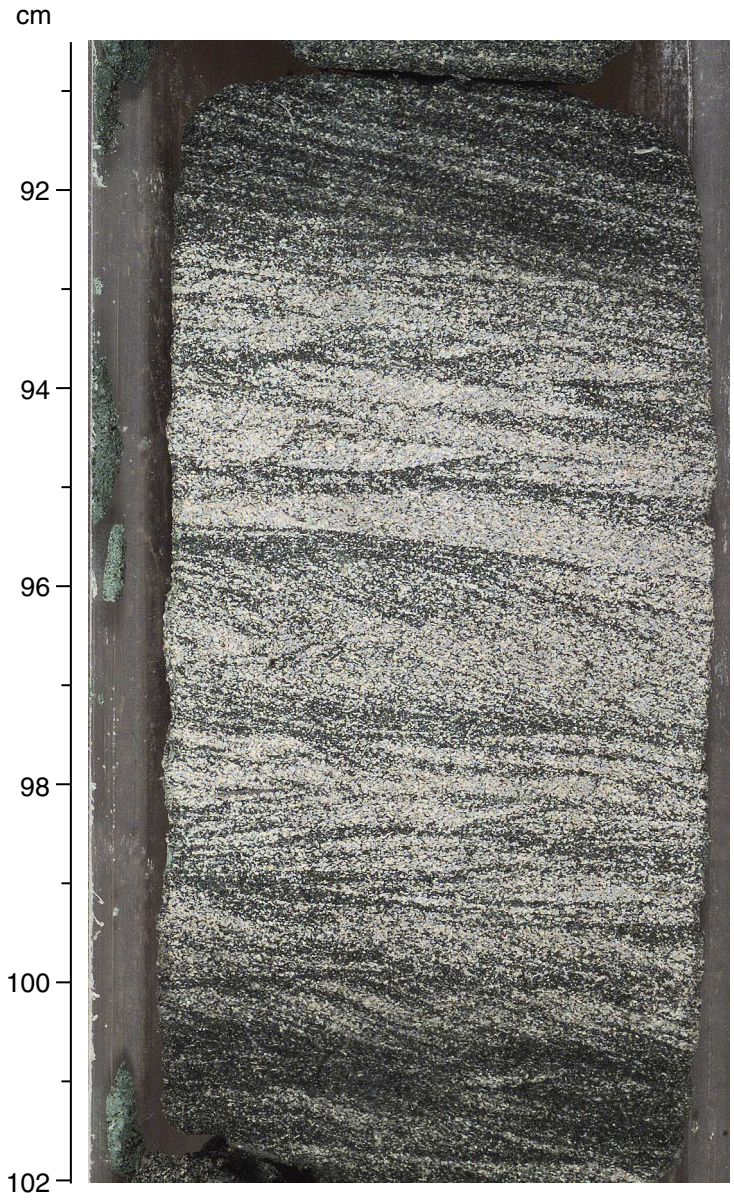

Figure F26. Photomicrograph from the deepest core in Subunit VIA (Sample **194-1193C-6R-1, 30 cm;** 519.9 mbsf). This laminated grainstone contains roughly equal proportions of well-sorted glauconite pellets (green) and coarser bioclasts of red algae (R), benthic foraminifers (B), and echinoderm fragments (E), along with minor quartz grains (Q).

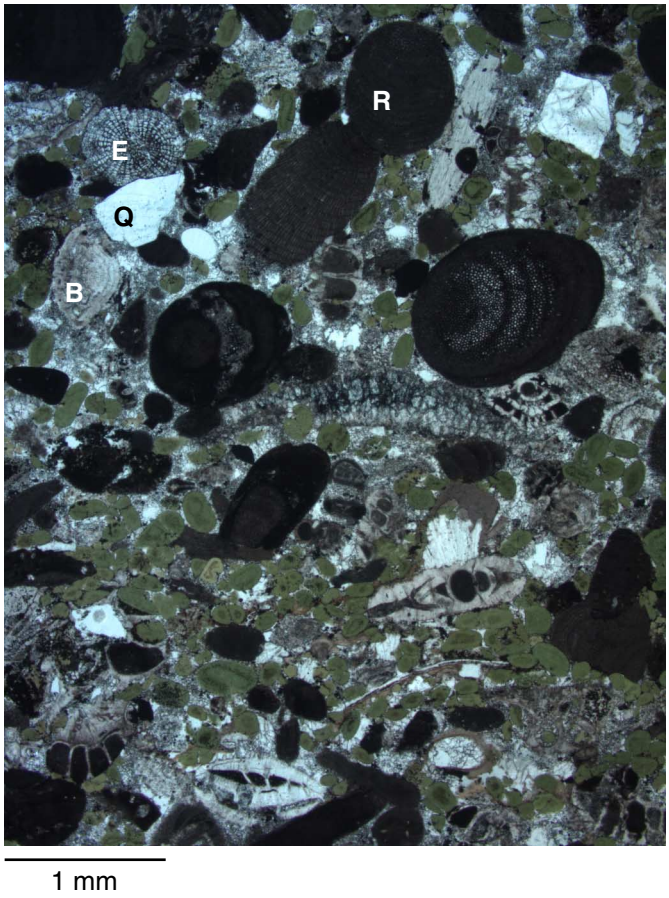

Figure F27. Close-up photograph showing the upper part of Subunit VIB (interval 194-1193C-7R-1, 27–40 cm; 529.6 mbsf). Large articulated oyster shells are enclosed in poorly sorted clay-rich sandstone.

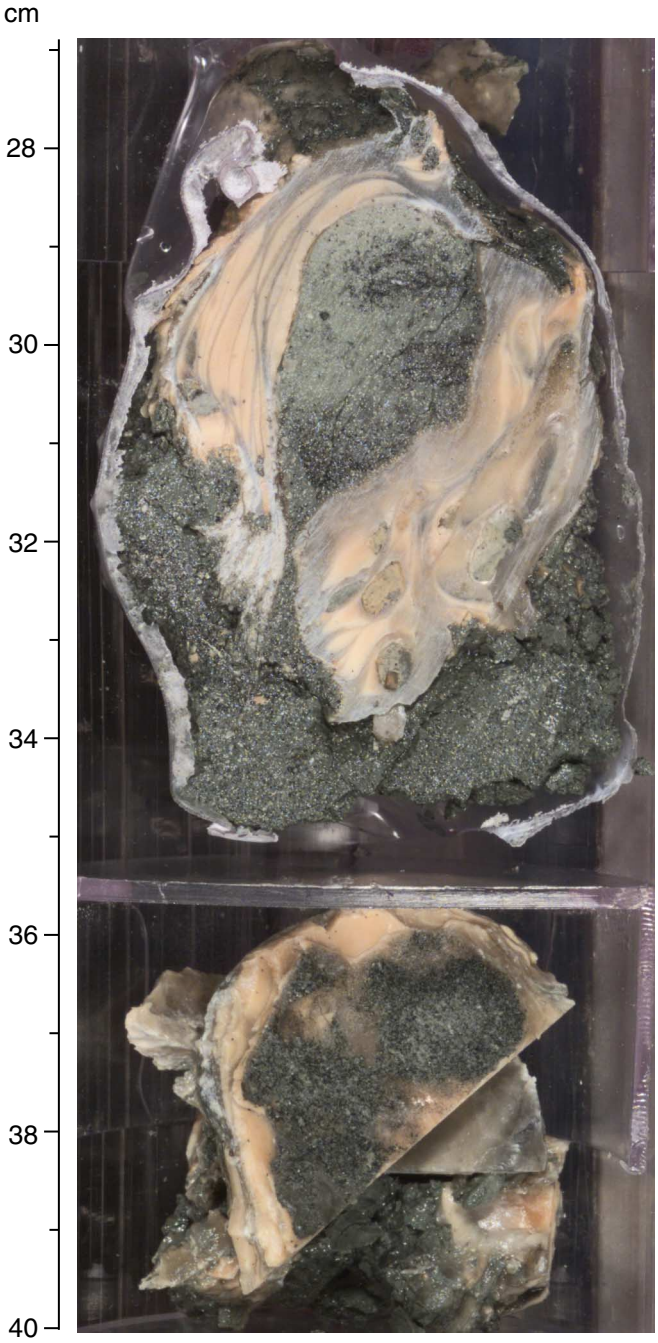

Figure F28. Close-up photograph showing the top part of the acoustic basement of Unit VII (interval 194-1193C-7R-2, 83–98 cm; 531.0 mbsf).

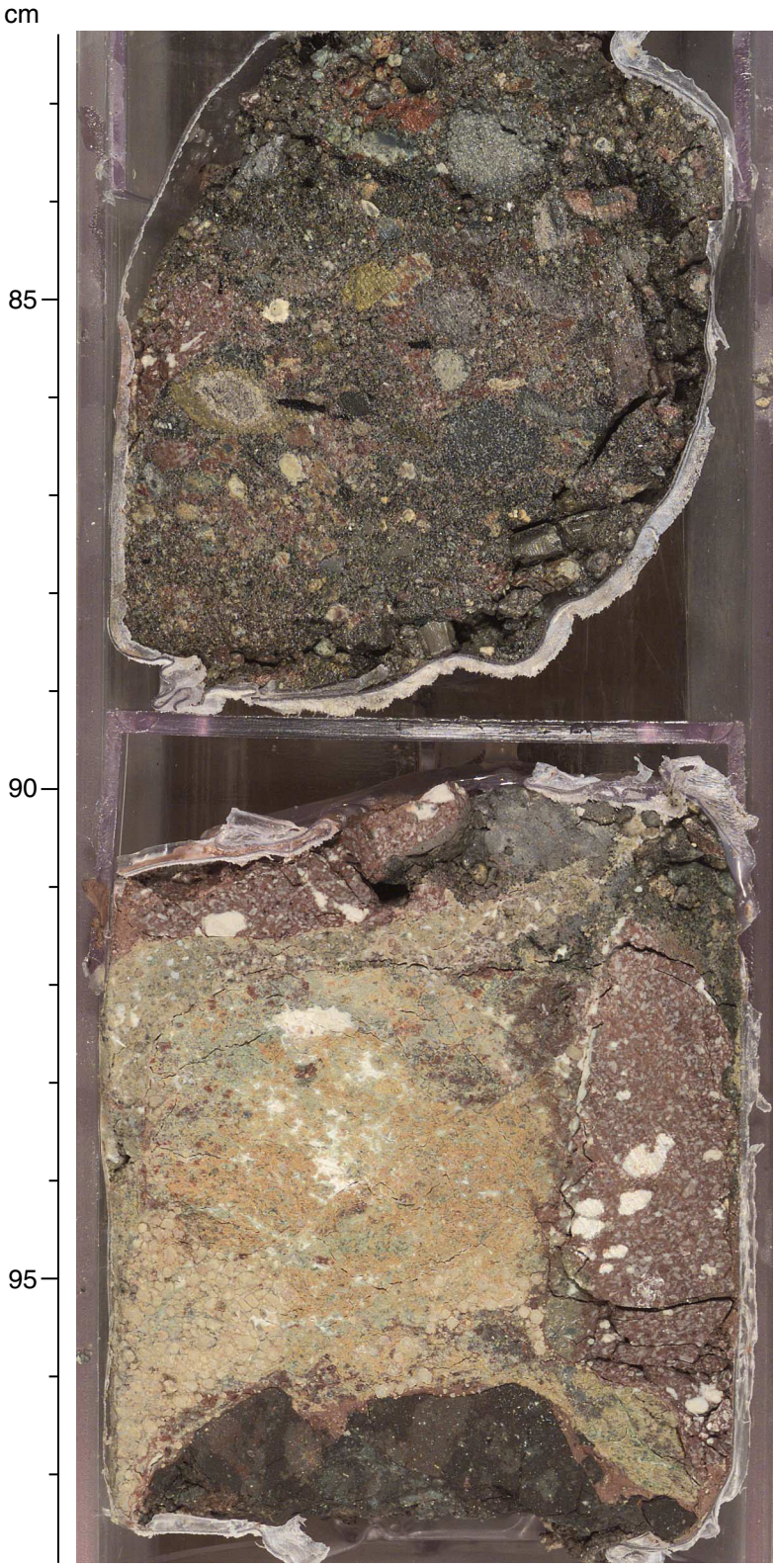

Figure F29. Photomicrograph from Unit VII (Sample **194-1193C-8R-3, 123 cm;** 542.8 mbsf). This hydrothermally altered basaltic rock consists of a patchwork of areas composed mostly of very fine crystalline alteration products. Enclosing areas have a partly altered igneous texture, such as in the view shown here. Plagioclase phenocrysts of varying size and degree of alteration are surrounded by dark areas representing former groundmass or glass.

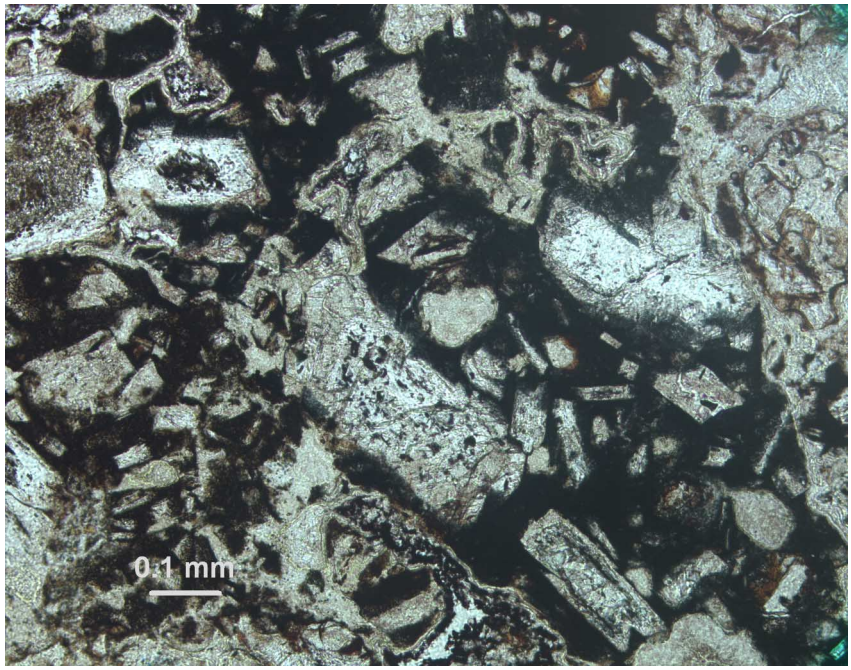

Figure F30. Vertical sections of *Amphistegina hauerina* (Ah) and *Amphistegina radiata* (Ar) in a *Lepidocyclina* (Lh) packstone from Sample **194-1193A-63X-1, 31–34 cm.** A cross section of a bryozoan branch (Br) is also noted.

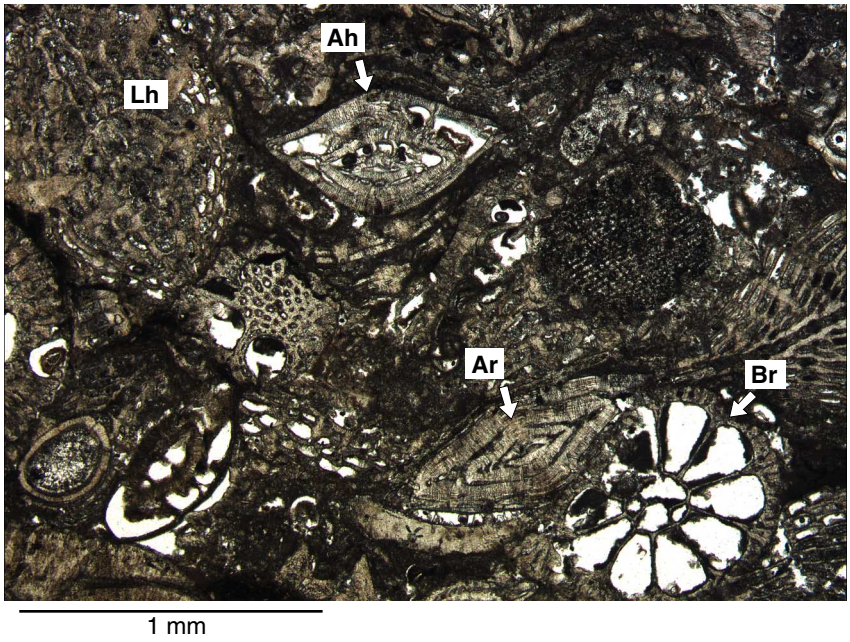

Figure F31. Vertical sections of two *Lepidocyclina howchini* (Lh) specimens from Sample **194-1193A-61X-1, 7 cm.** A portion of a bryozoan colony (Br) is also noted.

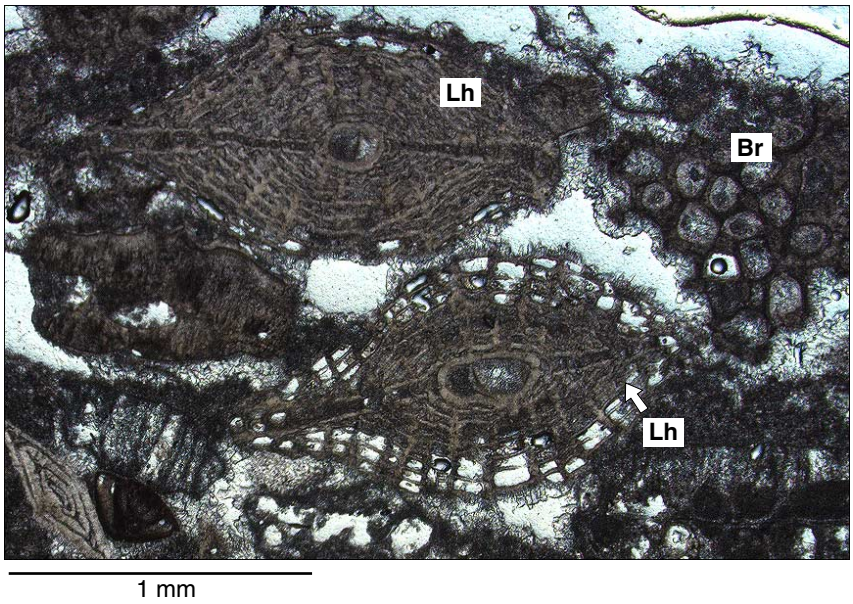

Figure F32. Vertical section of *Cycloclypeus* sp. (Cy) in a *Lepidocyclina* (Lh) packstone from Sample **194-1193A-63X-1, 31–34 cm.** An oblique section through an *Amphistegina hauerina* (Ah) can also be seen.

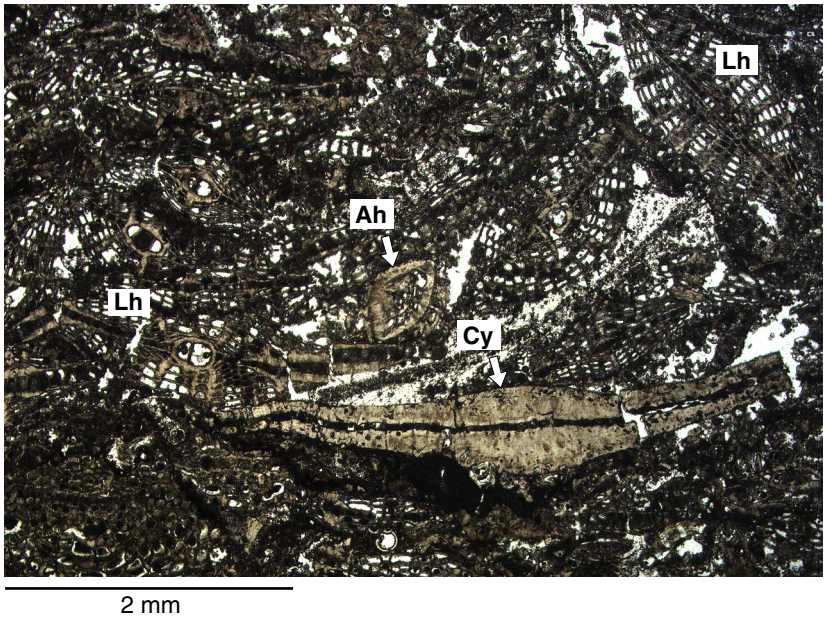

Figure F33. Vertical section of *Operculina complanata* (Op) from Sample **194-1193A-62X-2, 110–113 cm.** A planktonic foraminifer (Pl) can also be seen.

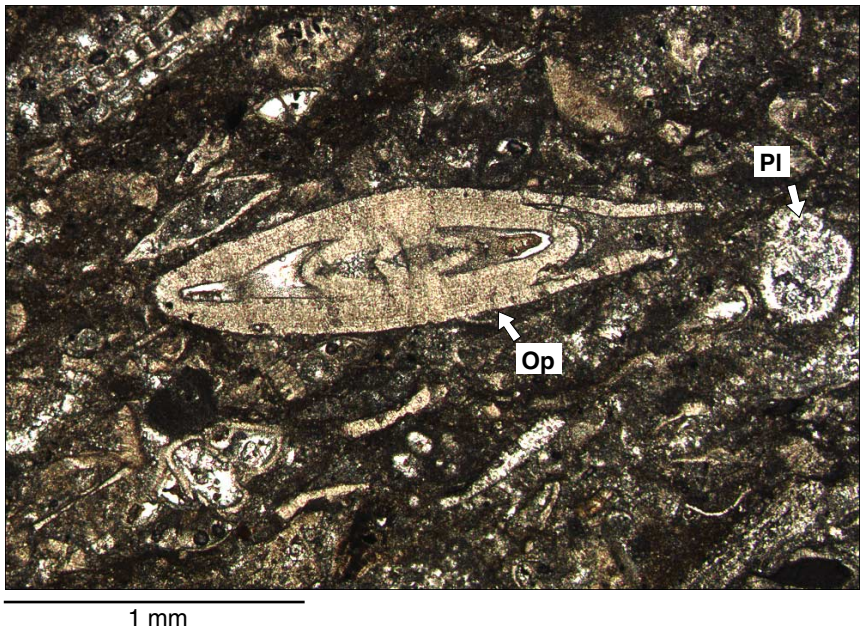

Figure F34. Vertical sections through two *Miogypsina* sp. (Mi) in a *Lepidocyclina* packstone from Sample **194-1193A-63X-1, 31–34 cm.** A vertical section through an *Amphistegina radiata* (Ar) and a portion of a bryozoan branch (Br) are also noted.

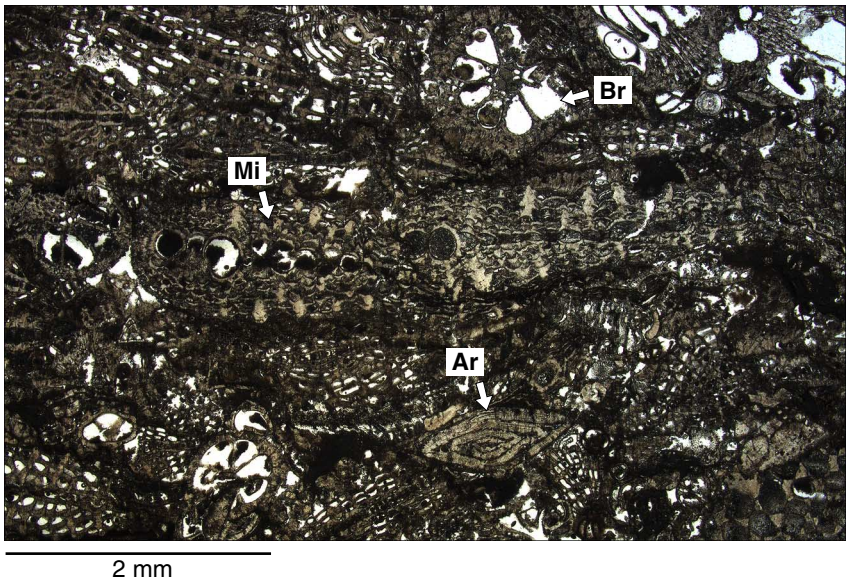

Figure F35. Long-core measurements from Holes 1193A, 1193B, and 1193C, showing intensity and inclination as a function of depth. **A.** Hole 1193A, 0–150 mbsf. (Continued on next six pages.)

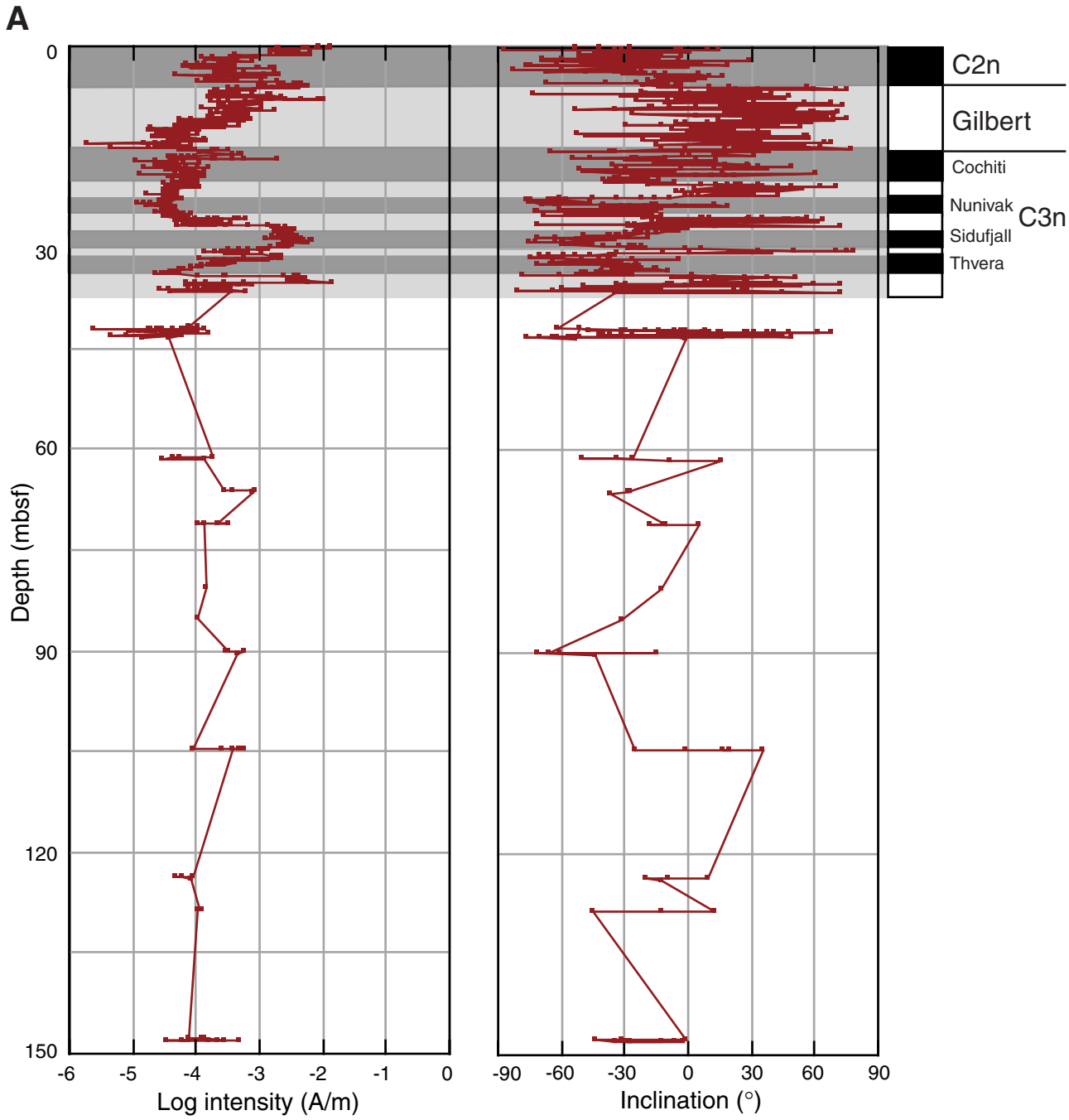

Figure F35 (continued). B. Hole 1193A, 175–300 mbsf.

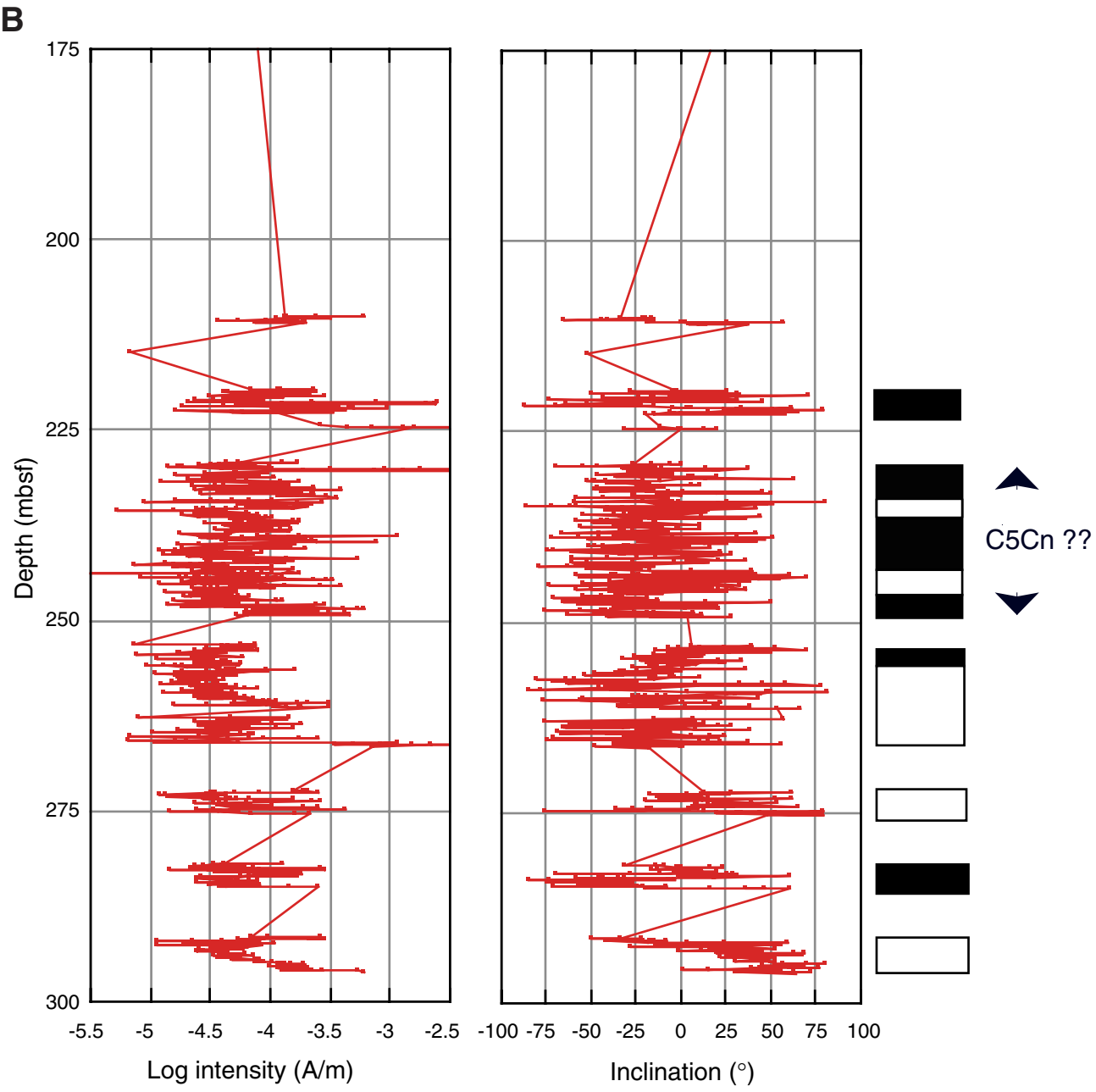

Figure F35 (continued). C. Hole 1193A, 300–400 mbsf.

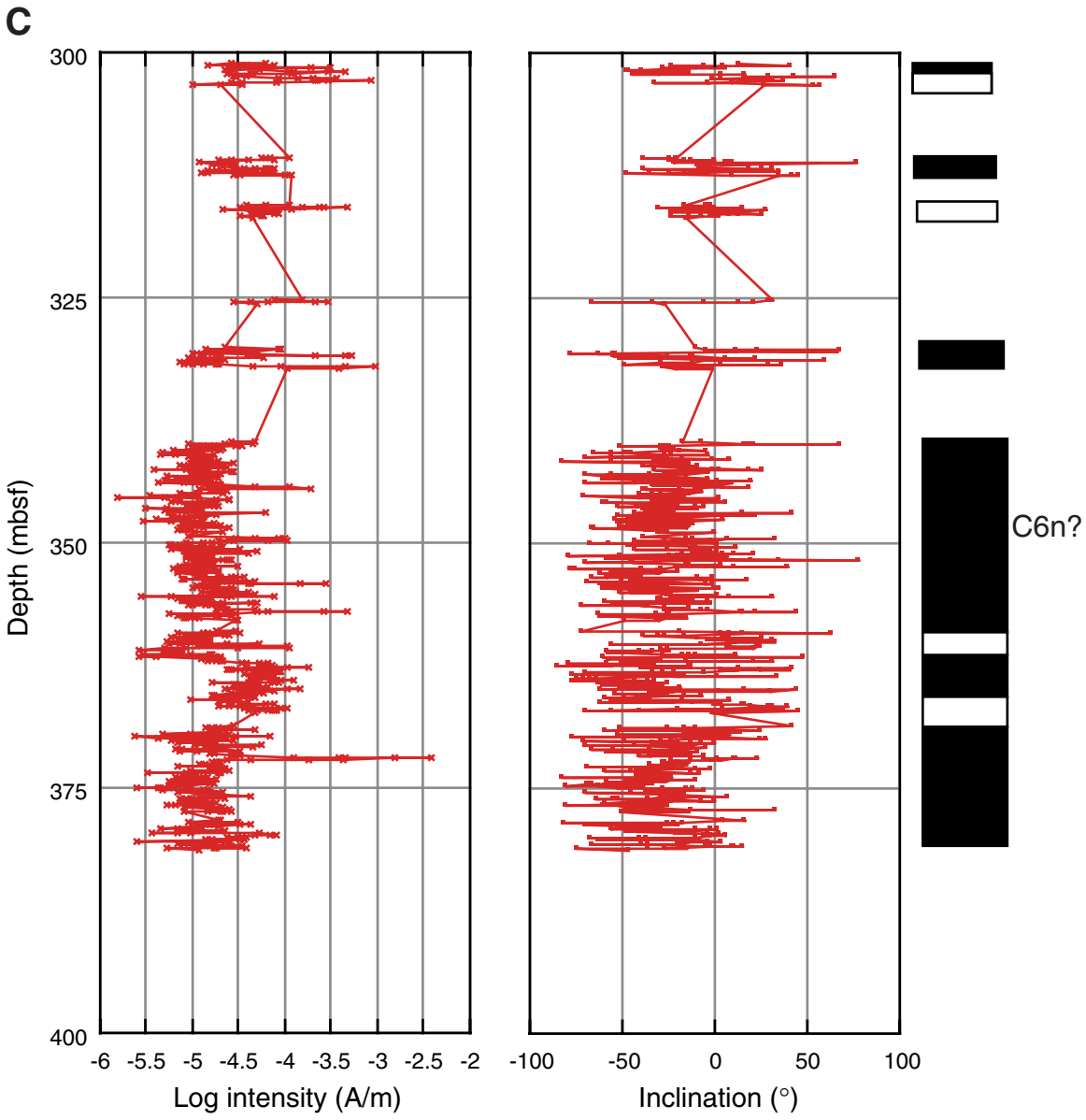

Figure F35 (continued). D. Hole 1193A, 380–500 mbsf.

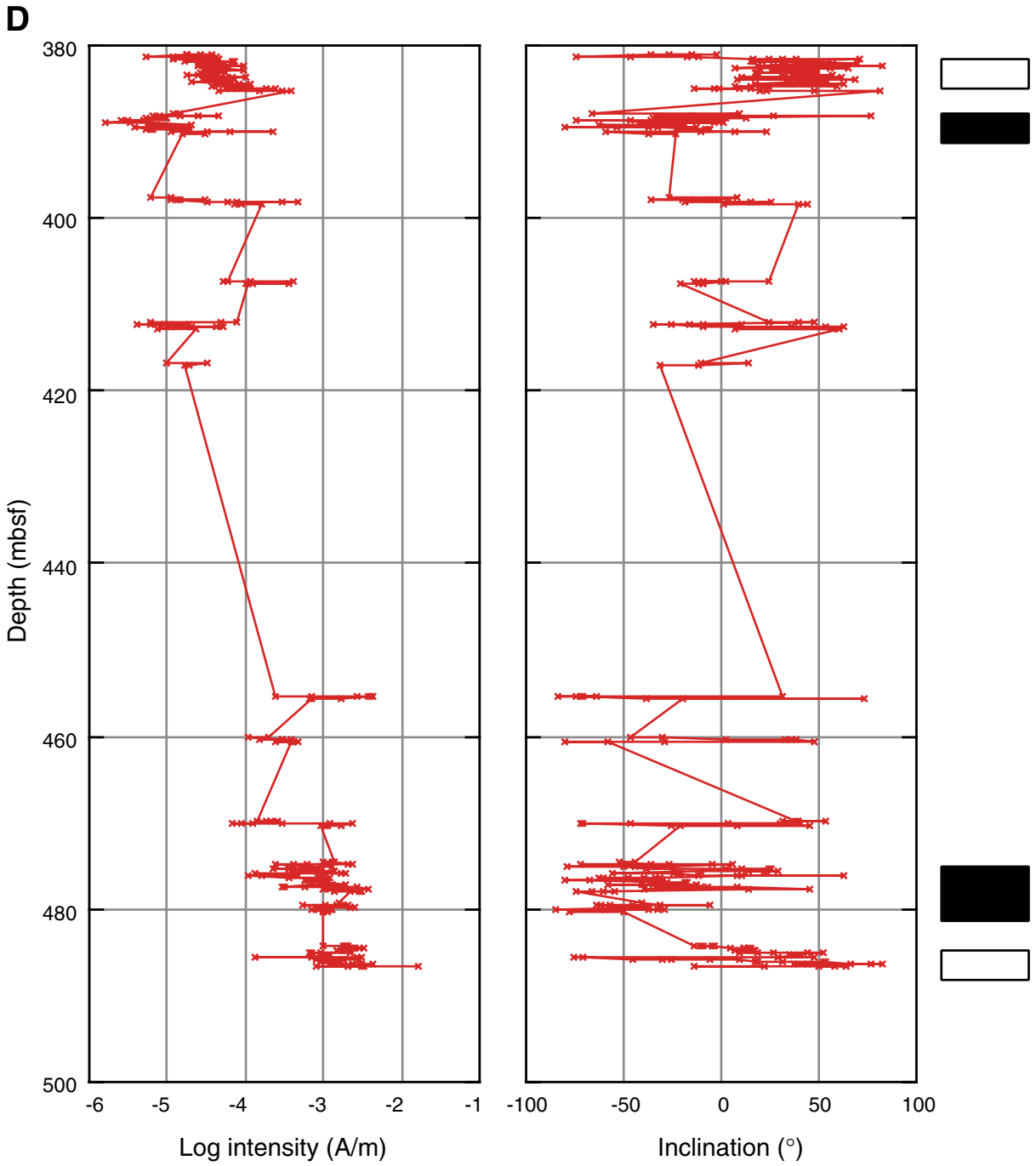

Figure F35 (continued). E. Hole 1193B, 20–120 mbsf.

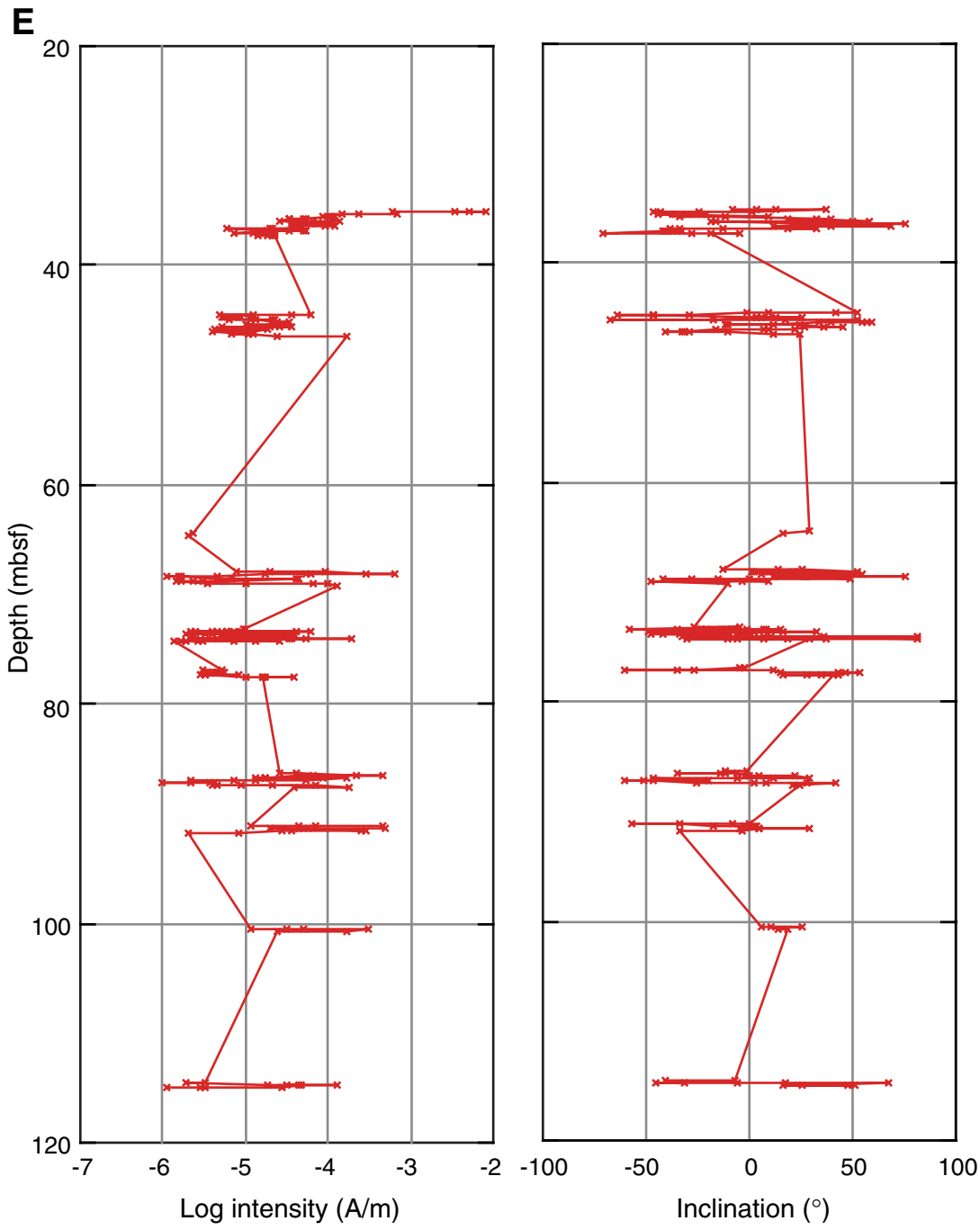

Figure F35 (continued). F. Hole 1193C, 35–65 mbsf.

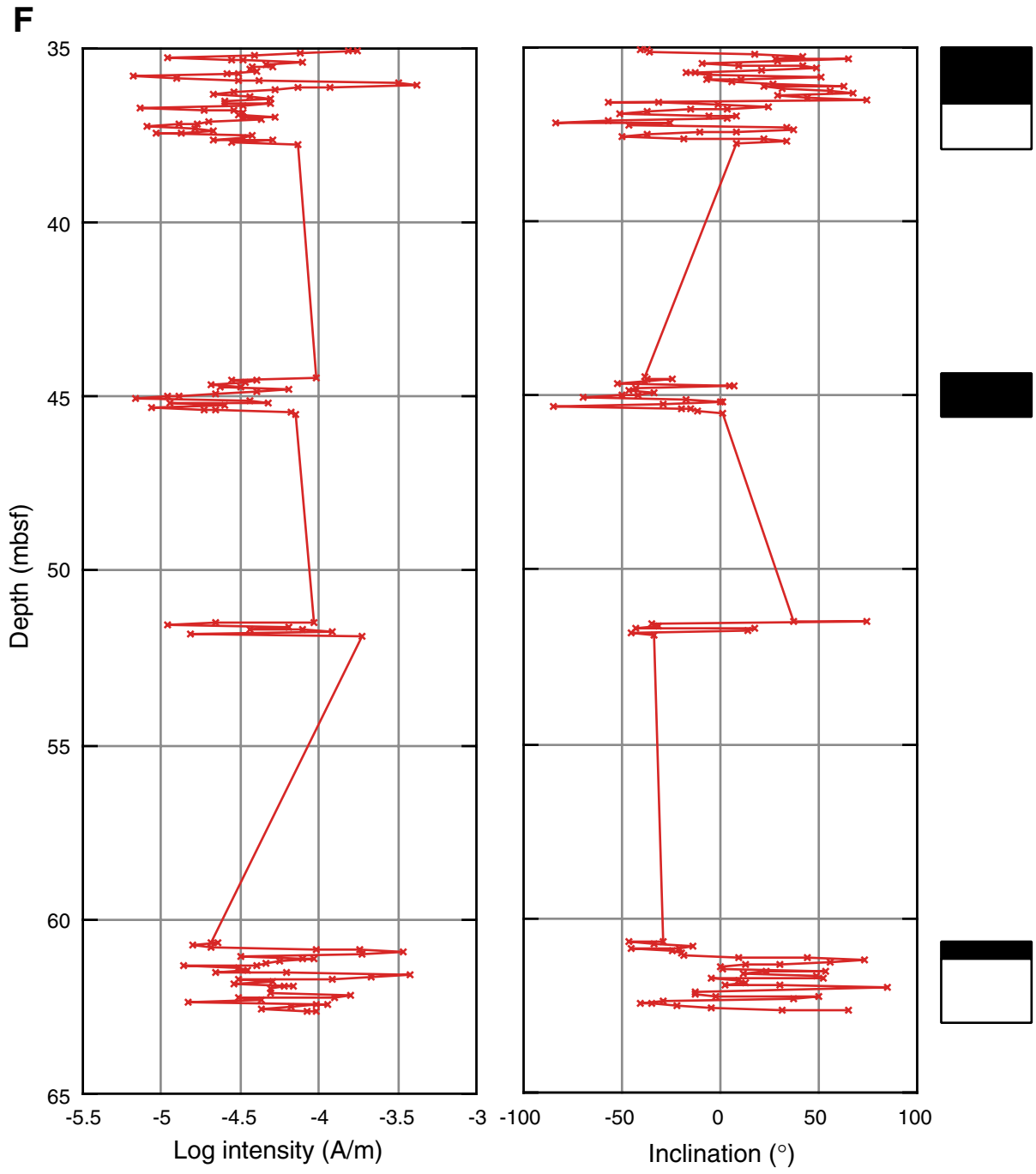

Figure F35 (continued). G. Hole 1193C, 510–545 mbsf.

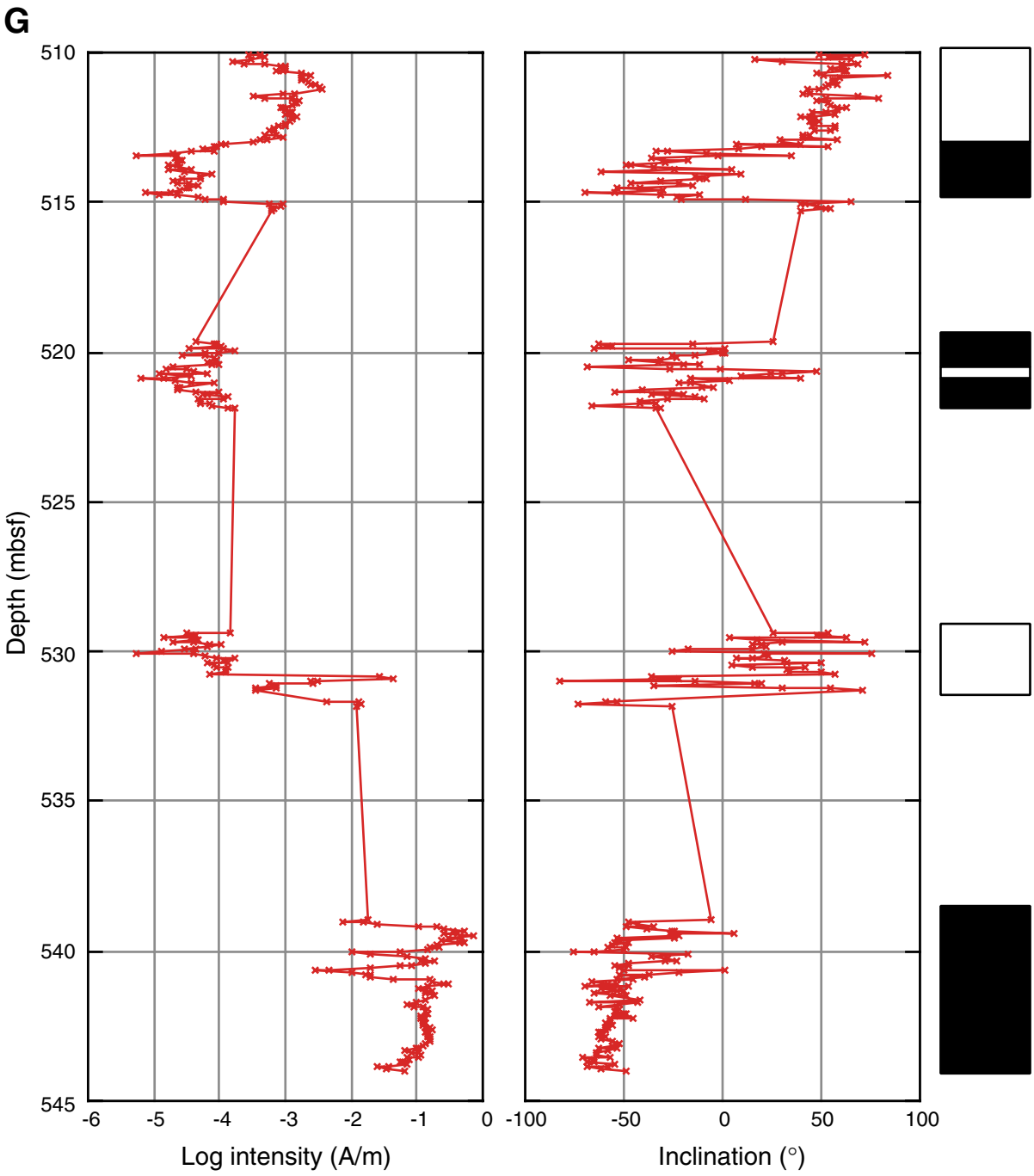

Figure F36. Stereographic plot of directions of magnetization in ODP coordinates (i.e., +x down and +x in the direction of the double line on the working half of core liners). **A.** Natural remanent magnetization (NRM). **B.** After 30-mT demagnetization.

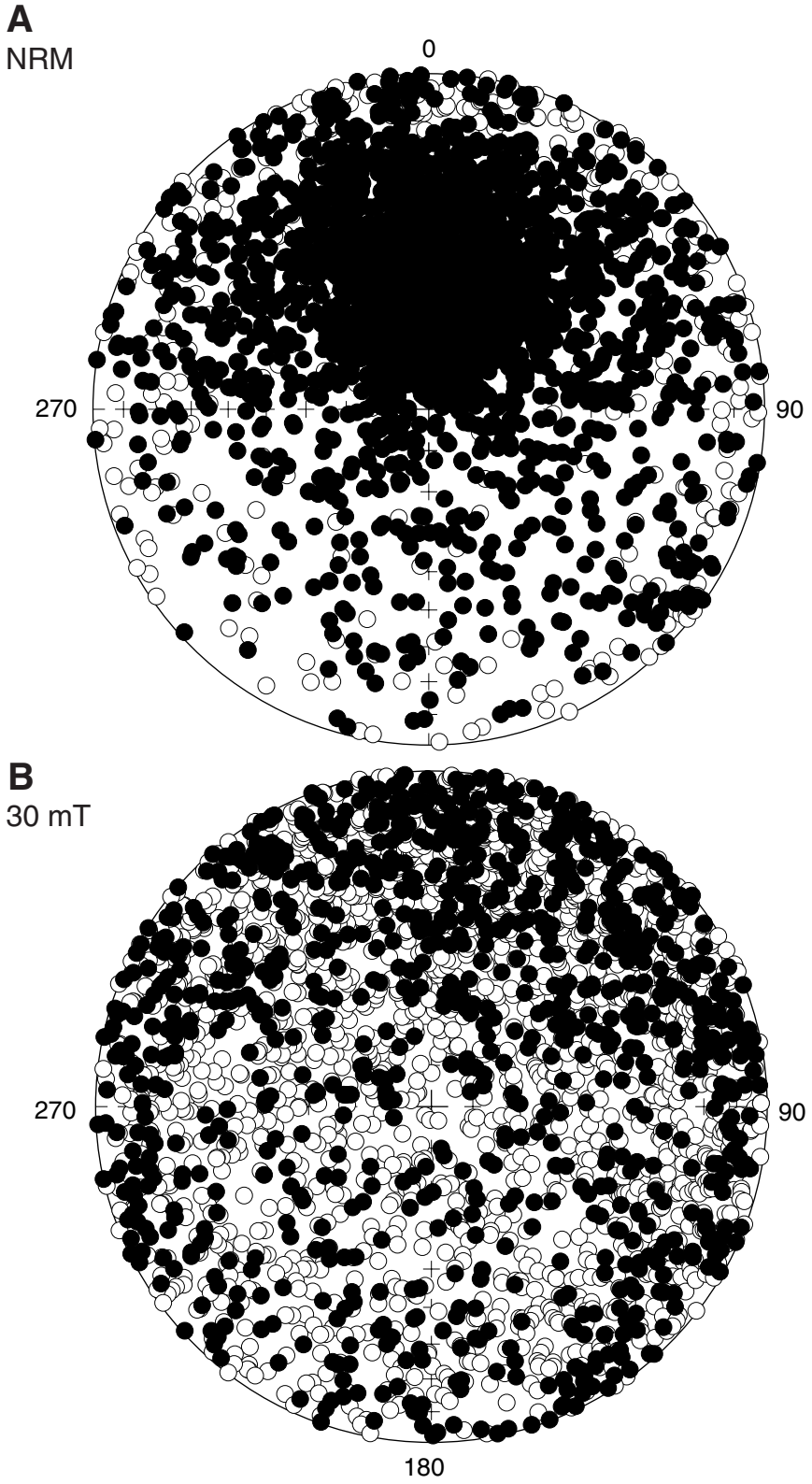

Figure F37. Examples of Zijderveld diagrams of the thermally demagnetized samples and their normalized magnetic moment decay curve equivalent. **A.** Sample 194-1193A-22X-CC, 20–22 cm. **B.** Sample 194-1193A-29X-1, 40–42 cm. NRM = natural remanent magnetization.

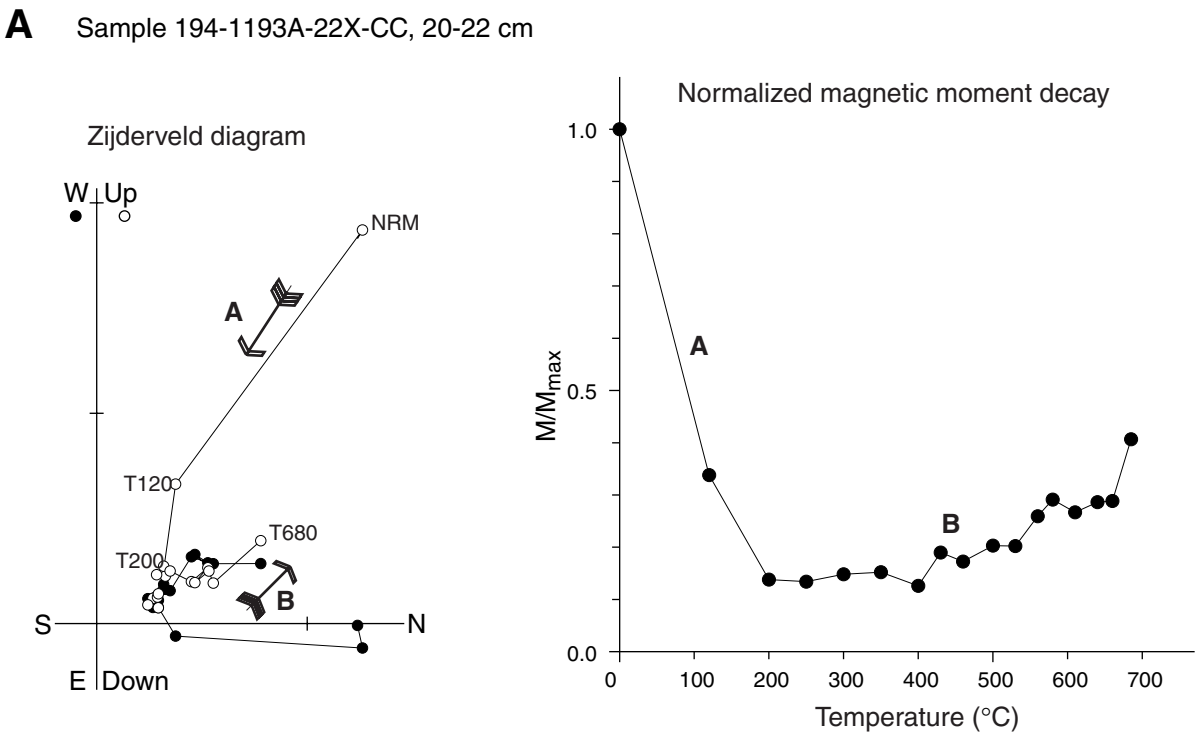

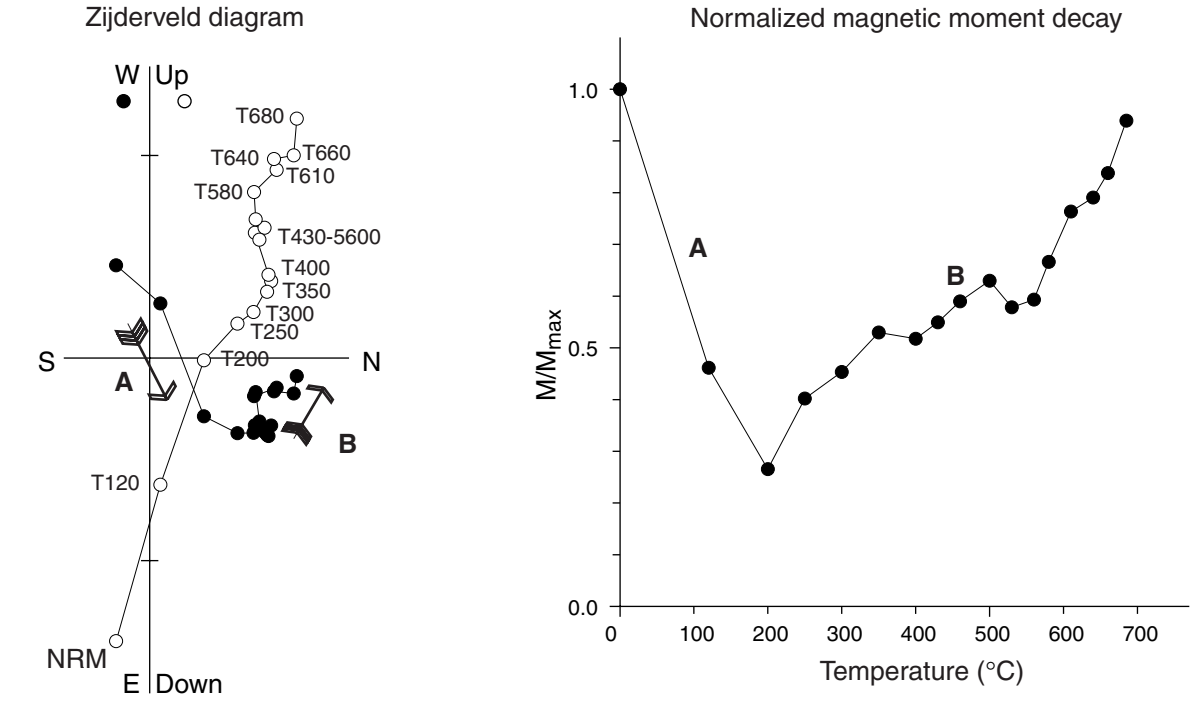

Figure F38. ARM results for two representative samples. For the artificial remanence process with a single direction of magnetization, as in (**A**), ARM is typical behavior; however, (**B**) is anomalous, showing a break in the slope, indicating two remanence components with two opposed directions, as shown by the arrow.

A Sample 194-1193A-27X-CC, 8-10 cm

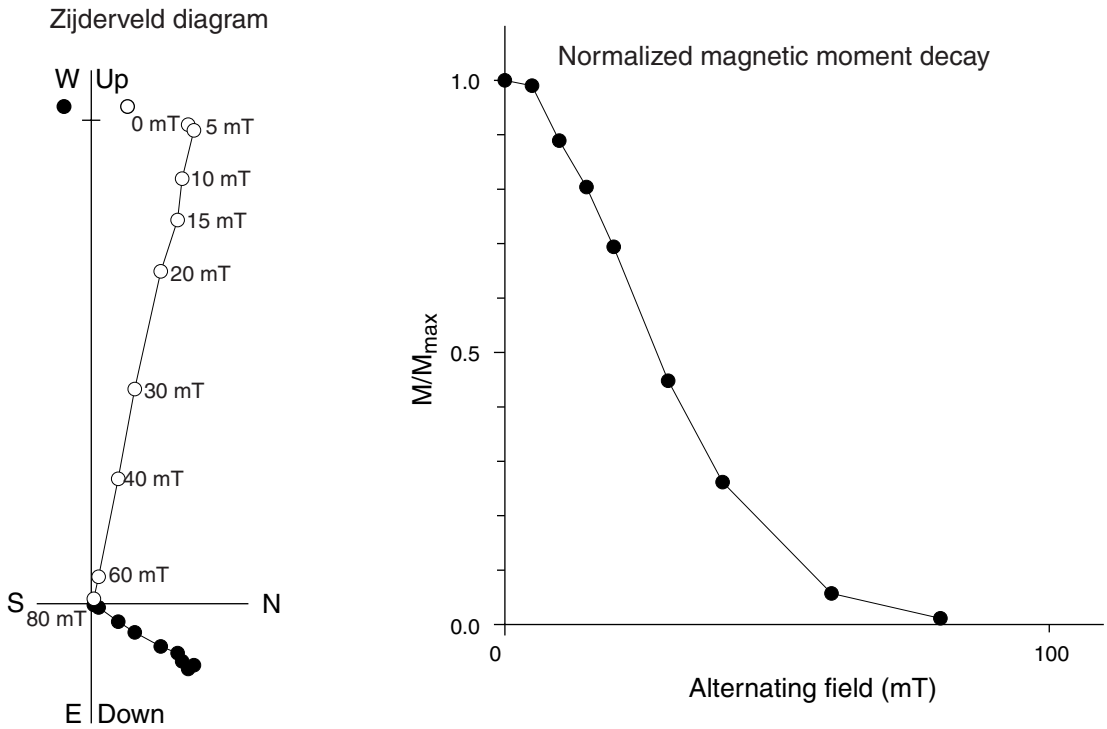

B Sample 194-1139A-38X-1, 7-9 cm

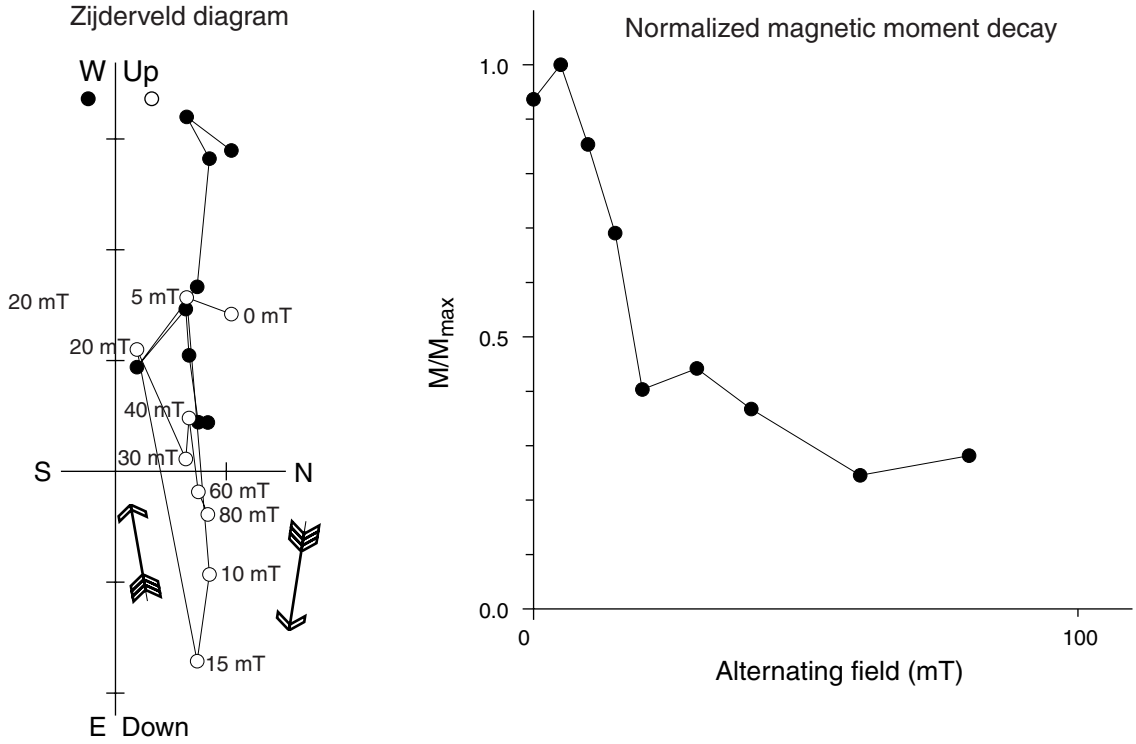

Figure F39. Isothermal remanent magnetization (IRM) acquisition results for two representative samples. The strong acquisition at the beginning is indicative of magnetite, and the gradual increase in acquisition after 300 mT is indicative of minerals of the hematite family.

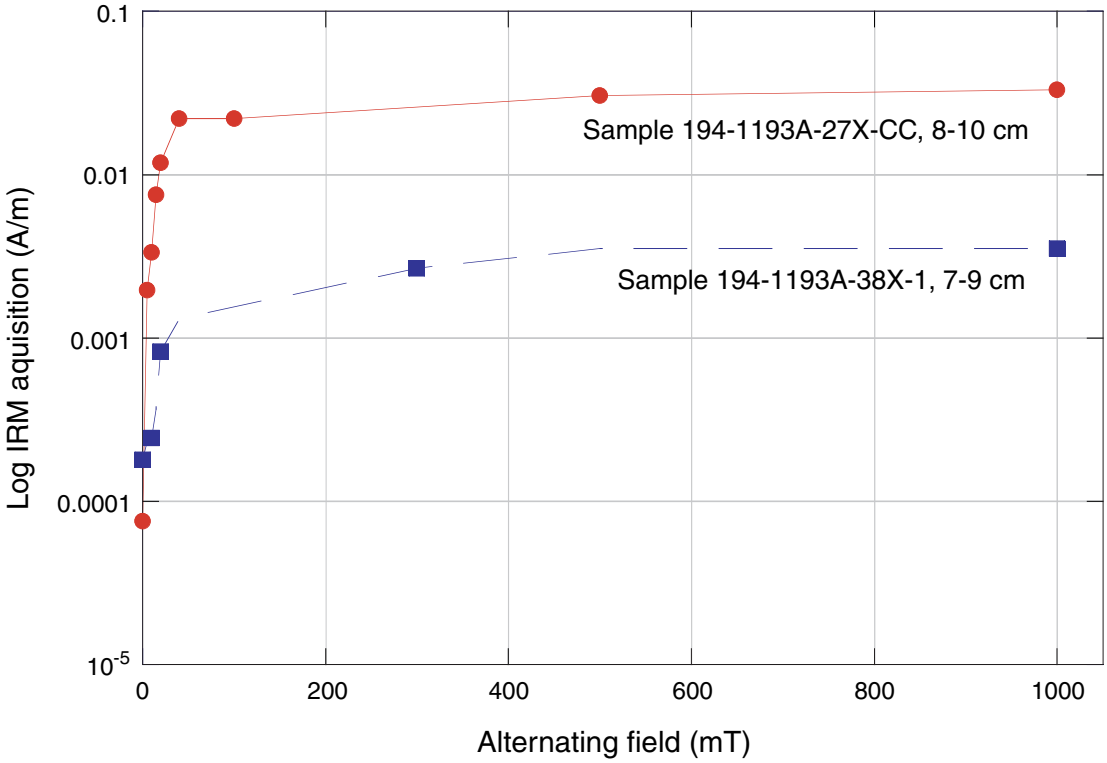

Figure F40. Thermal demagnetization results of IRM showing two antiparallel directions, possibly indicating the presence of goethite and titanomagnetite or magnetite. **A.** Sample 194-1193A-27X-CC, 8–10 cm. **B.** Sample 194-1139A-38X-1, 7–9 cm. NRM = natural remanent magnetization.

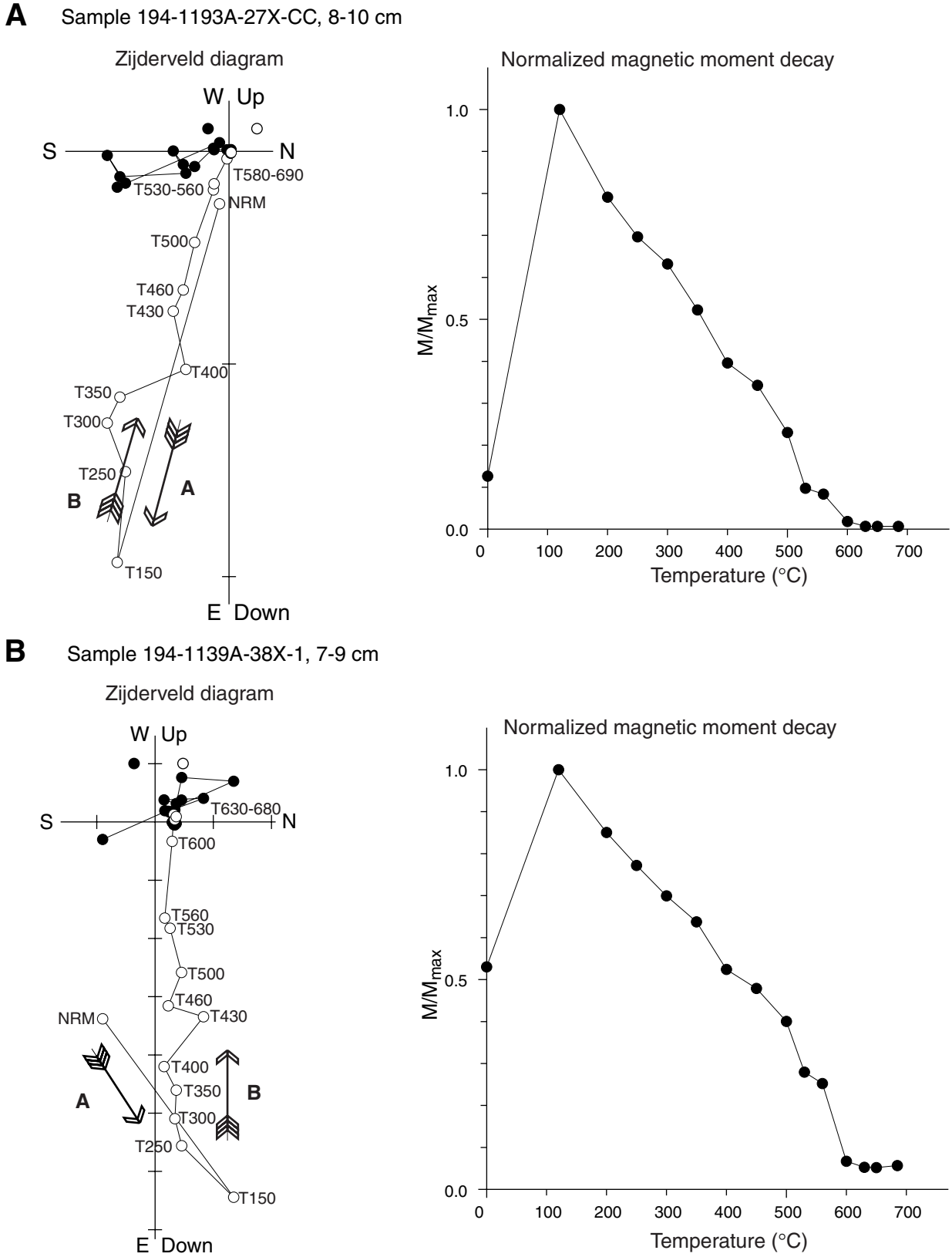

Figure F41. Thermal demagnetization results of IRM showing two components with similar directions, indicating the presence of titanomagnetite and some hematite. **A.** Sample 194-1193B-6Z-1, 102–104 cm. **B.** Sample 194-1193B-8Z-1, 51–53 cm. NRM = natural remanent magnetization.

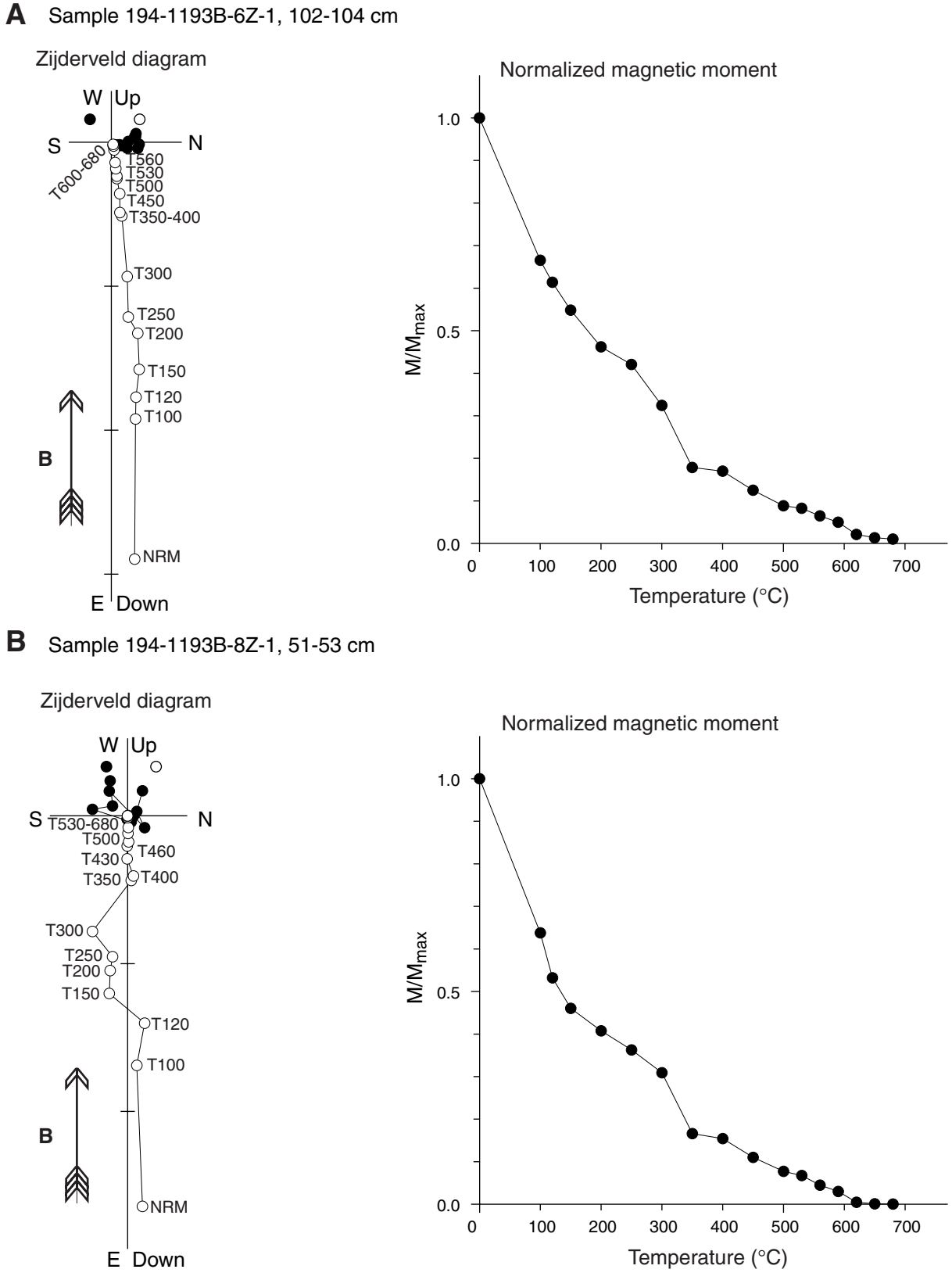

Figure F42. Age-depth model and sedimentation rates at Site 1193. Horizontal lines spanning from the left figure margin to the age-depth curve are lithologic unit (solid) and subunit (dashed) boundaries. Horizontal lines spanning from the right margin of the figure to the age-depth curve are seismic megasequence boundaries (solid) and major reflectors within megasequences (dashed). Vertical lines are epoch boundaries as labeled at the top of the diagram. MS = Megasequence.

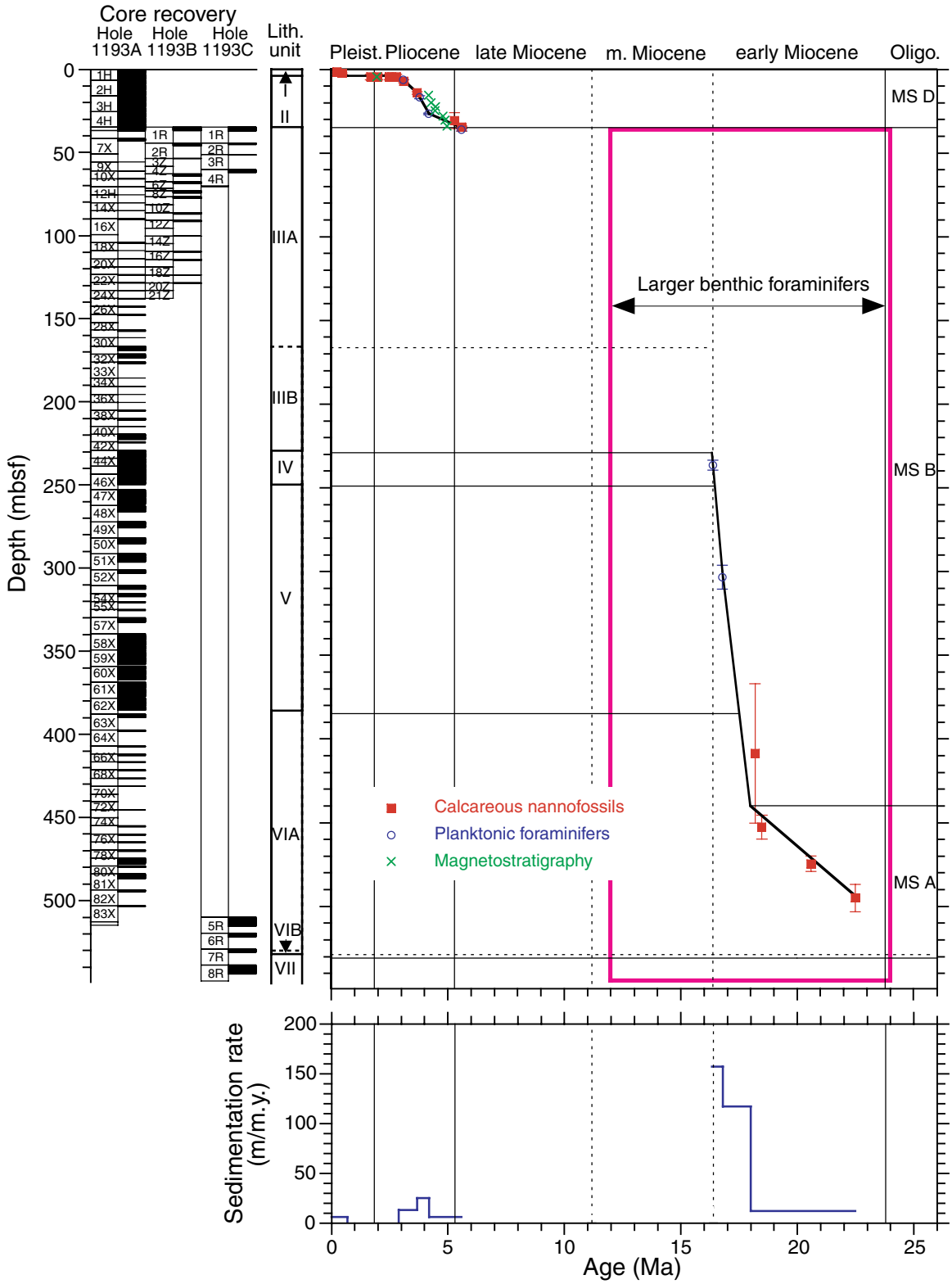

Figure F43. Concentrations of dissolved constituents vs. depth. **A.** Chloride. **B.** Alkalinity. **C.** Potassium. **D.** Magnesium. **E.** Calcium. **F.** Strontium. **G.** Sulfate. **H.** Ammonium.

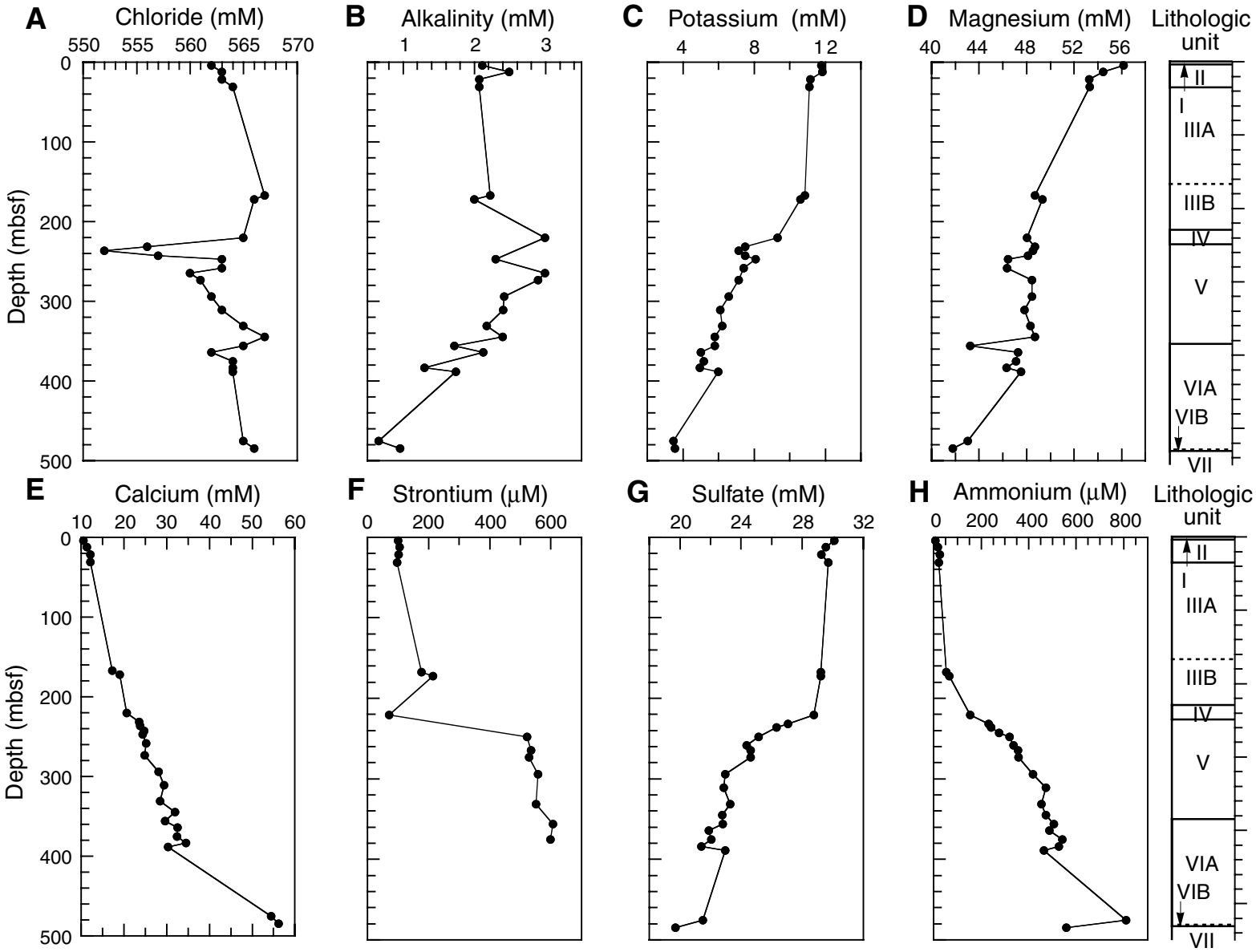

Figure F44. Percentages of dolomite, calcite, and noncarbonate minerals, Site 1193.

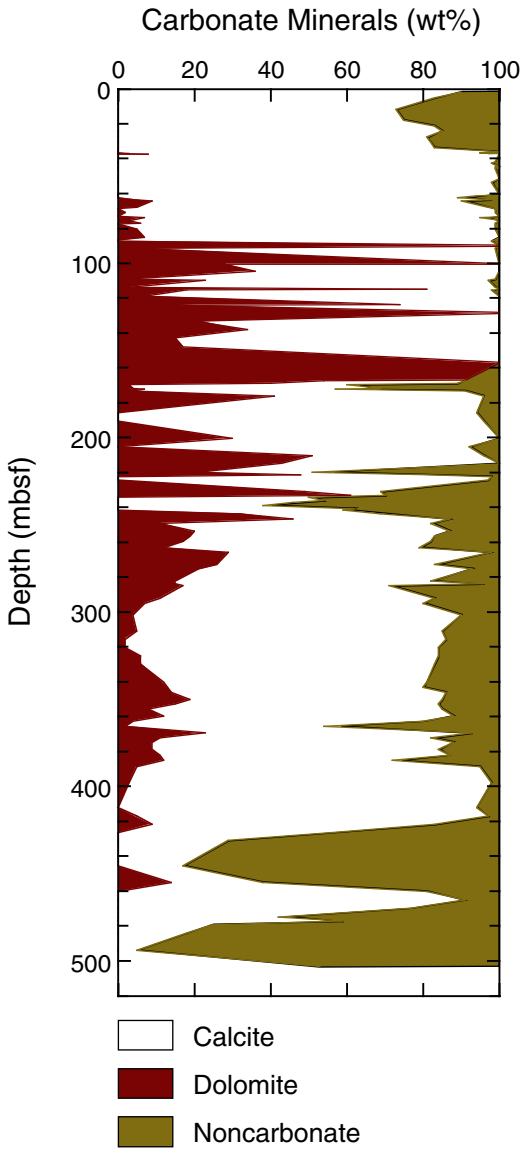

Figure F45. Plots of percent carbonate, percent total organic carbon (TOC), hydrogen index (HI) values, and percent total sulfur at Site 1193. The solid vertical line at HI = 150 marks the approximate boundary between terrigenous (<150) and marine organic matter. CNS = carbon-nitrogen-sulfur.

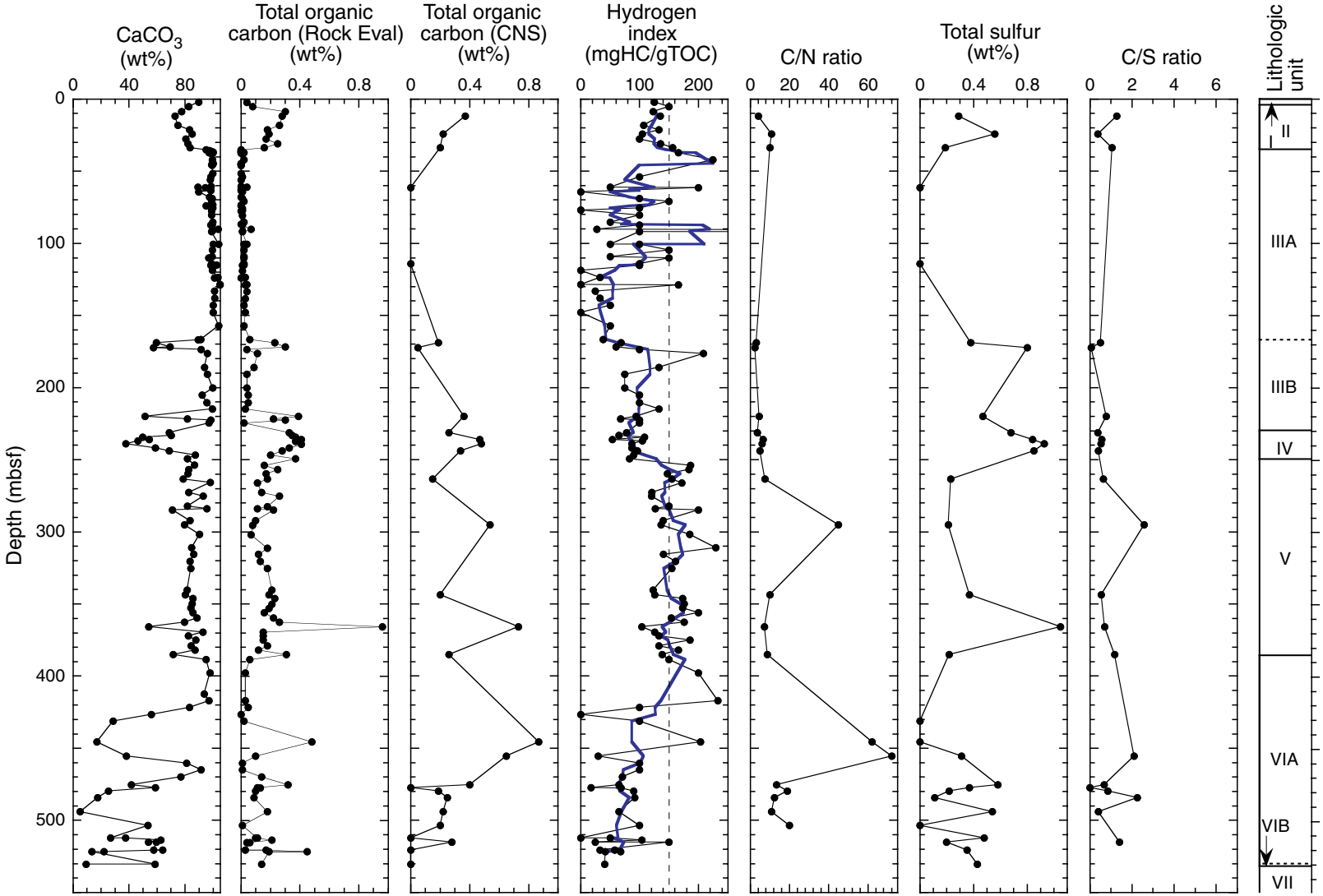

Figure F46. **A.** Bulk density from GRA (solid circles) and MAD (open circles). **B.** Grain density. **C.** Porosity at Site 1193 as a function of depth. Open circles = suspect grain density (B) and corresponding porosity (C) values. Solid line = exponential porosity-decay curve for the nonplatform sediments.

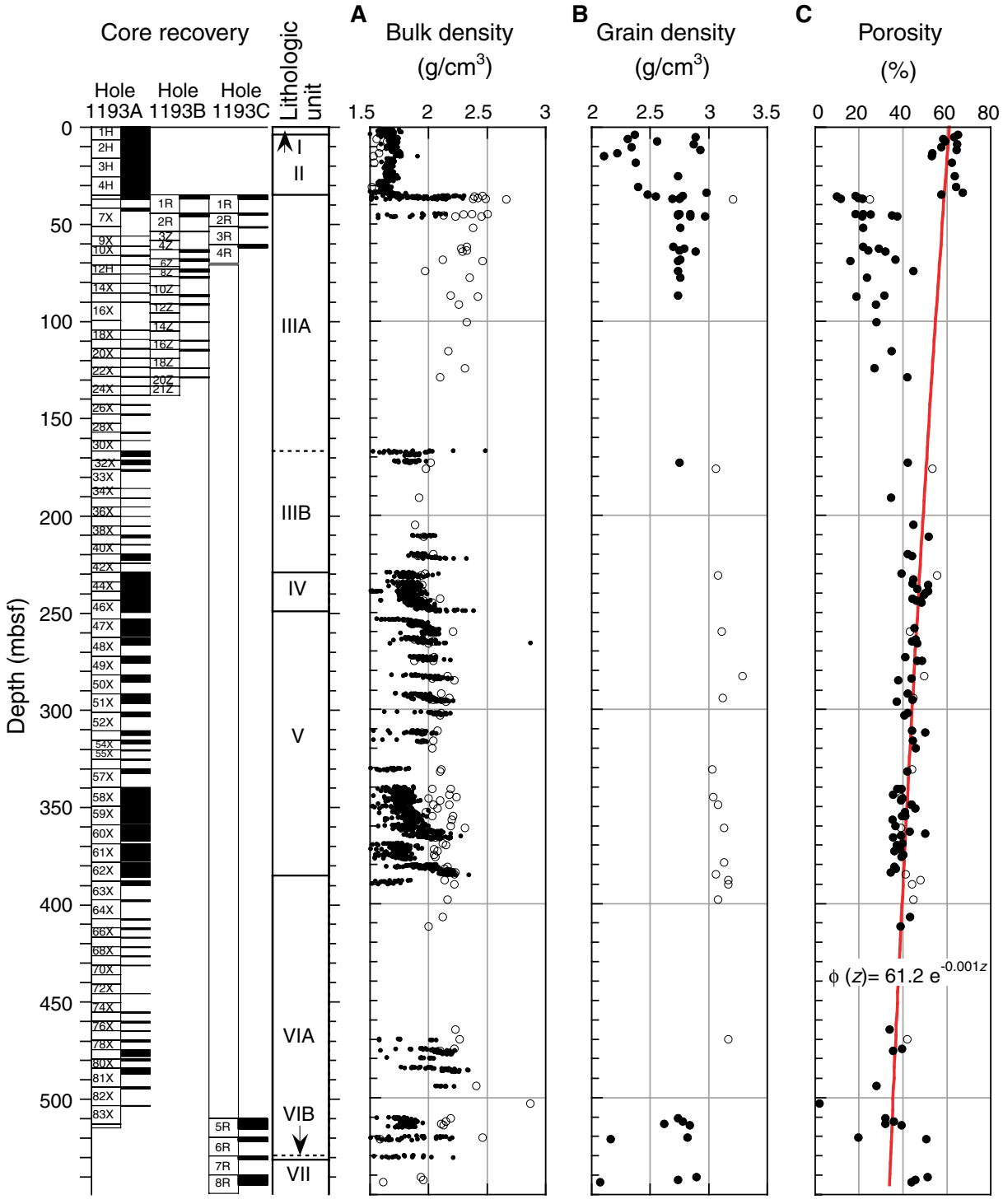

Figure F47. *P*-wave velocity for Site 1193 as a function of depth.

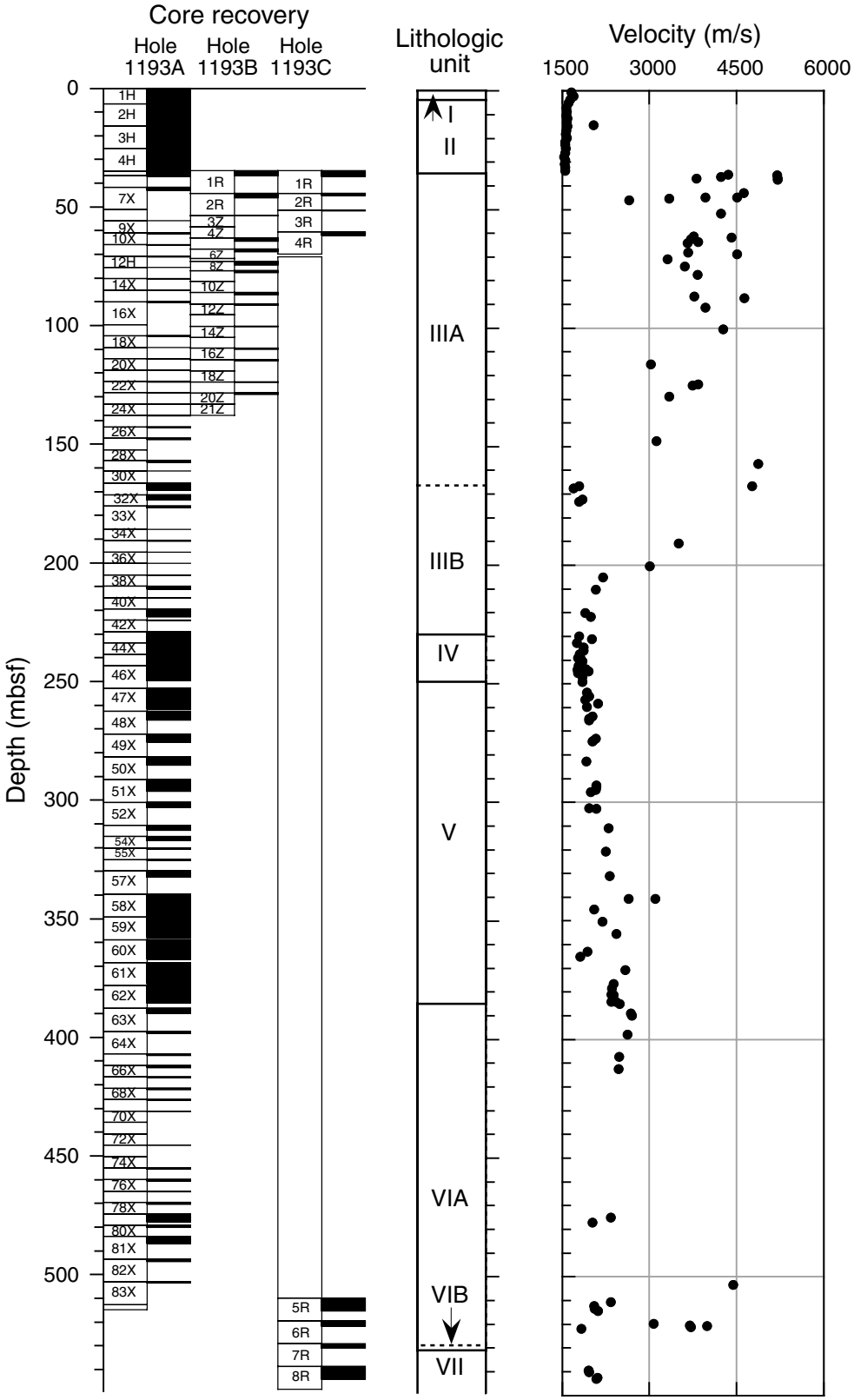

Figure F48. Crossplot of velocity vs. porosity for Site 1193. Solid lines = time-average equations for calcite, dashed lines = time-average equations for dolomite (Wyllie et al., 1956). Symbols represent three different lithologic units (see **"Lithostratigraphy and Sedimentology,"** p. 6): squares = hemipelagic drifts (Units I and II), solid circles = platform (Unit III), circles = upper/middle slope (Units IV and V).

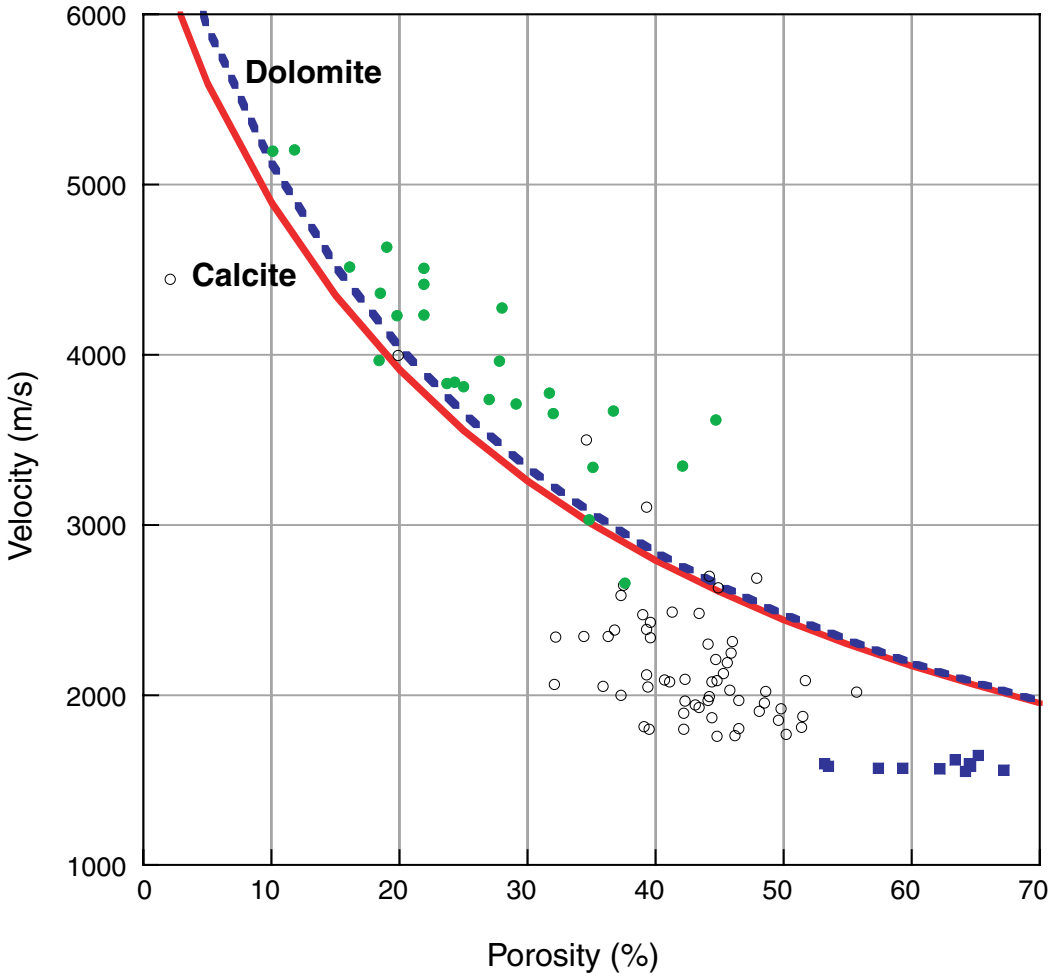

Figure F49. Average thermal conductivity for Site 1193 as a function of depth.

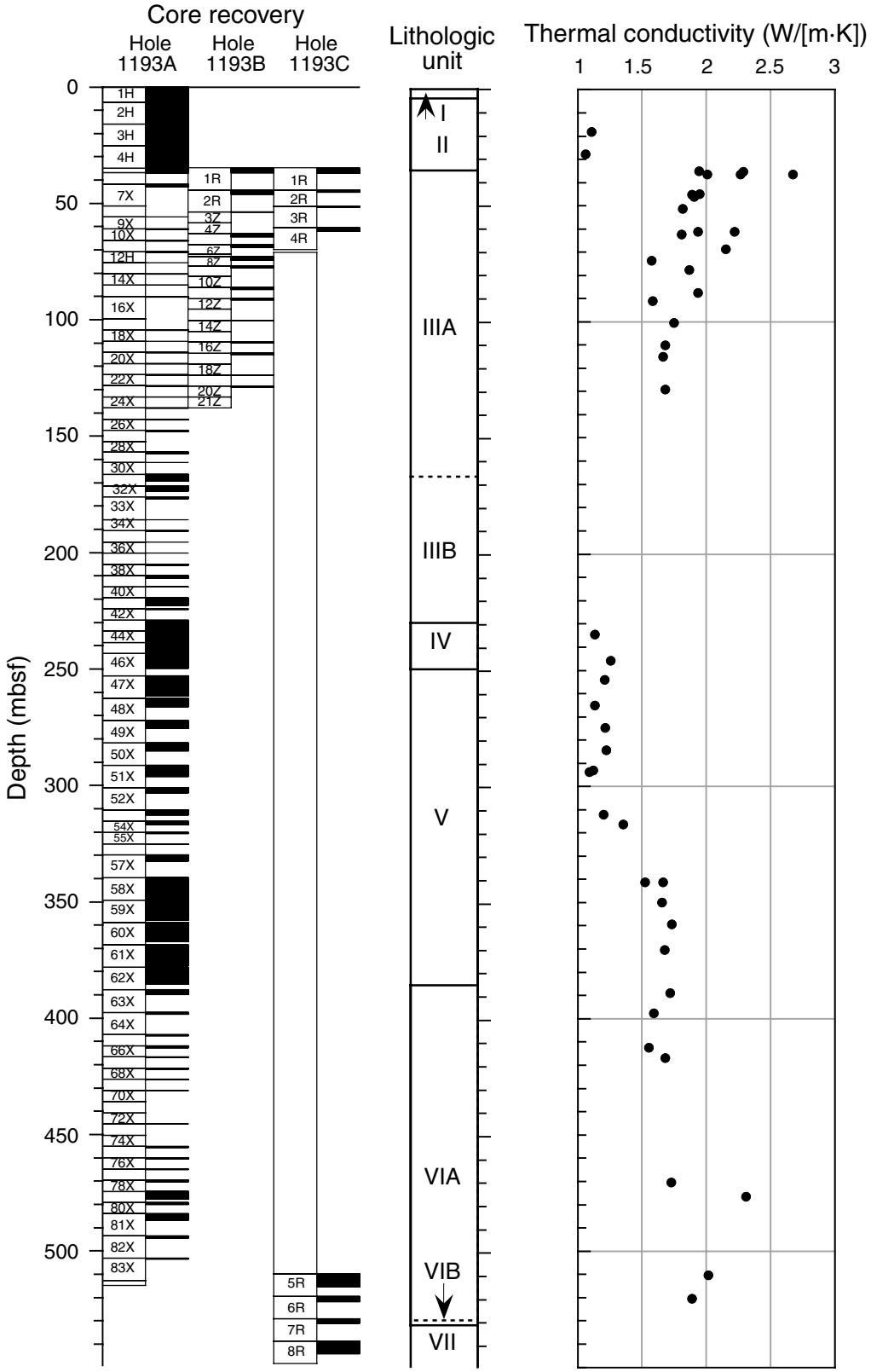

Figure F50. Crossplot of thermal conductivity vs. porosity for Site 1193. Solid lines = theoretical curves for pure unilithology systems.

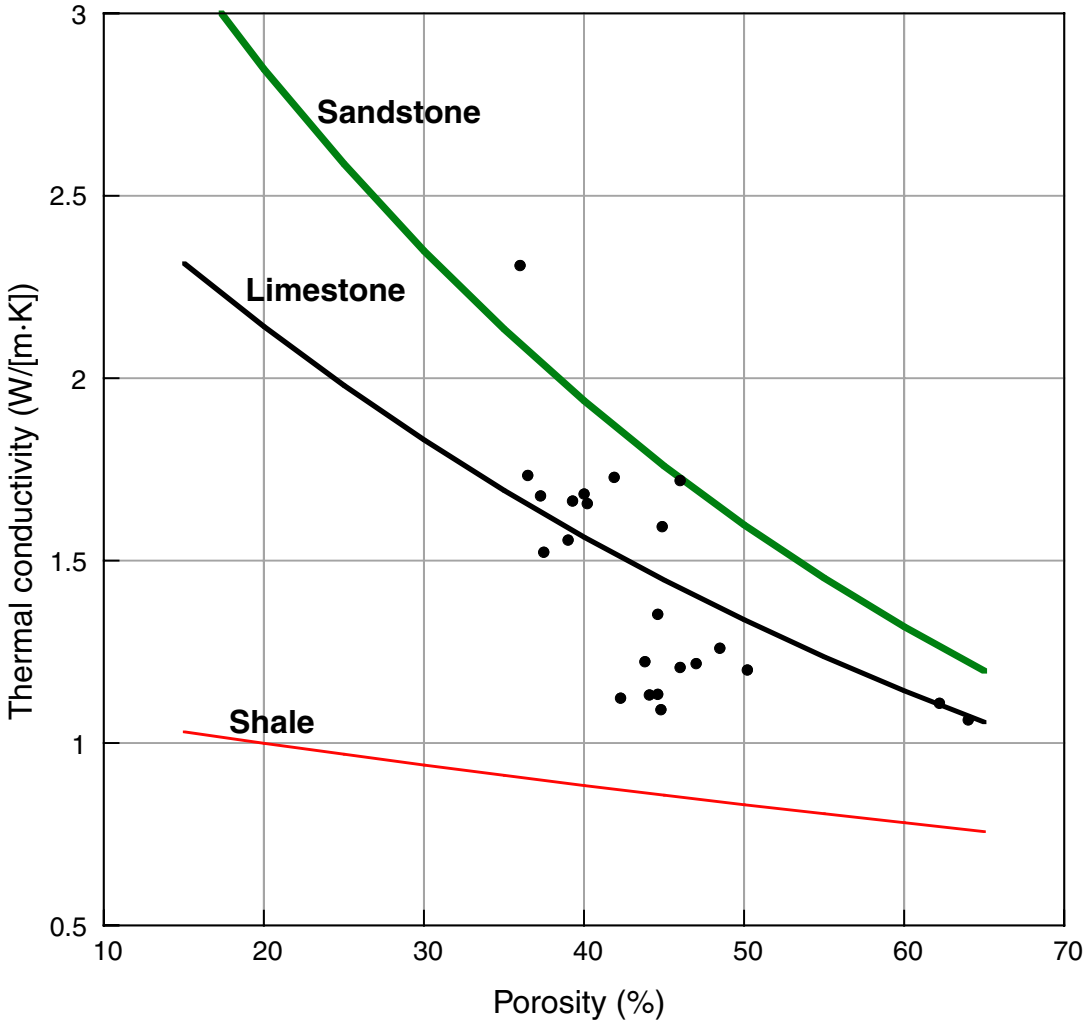

Figure F51. Site 1193 (A) Magnetic susceptibility (MS) and (B) natural gamma radiation (NGR) as a function of depth. Small circles = Hole 1193A, large circles = Hole 1193B, triangles = Hole 1193C. Note the different MS scale below 450 mbsf.

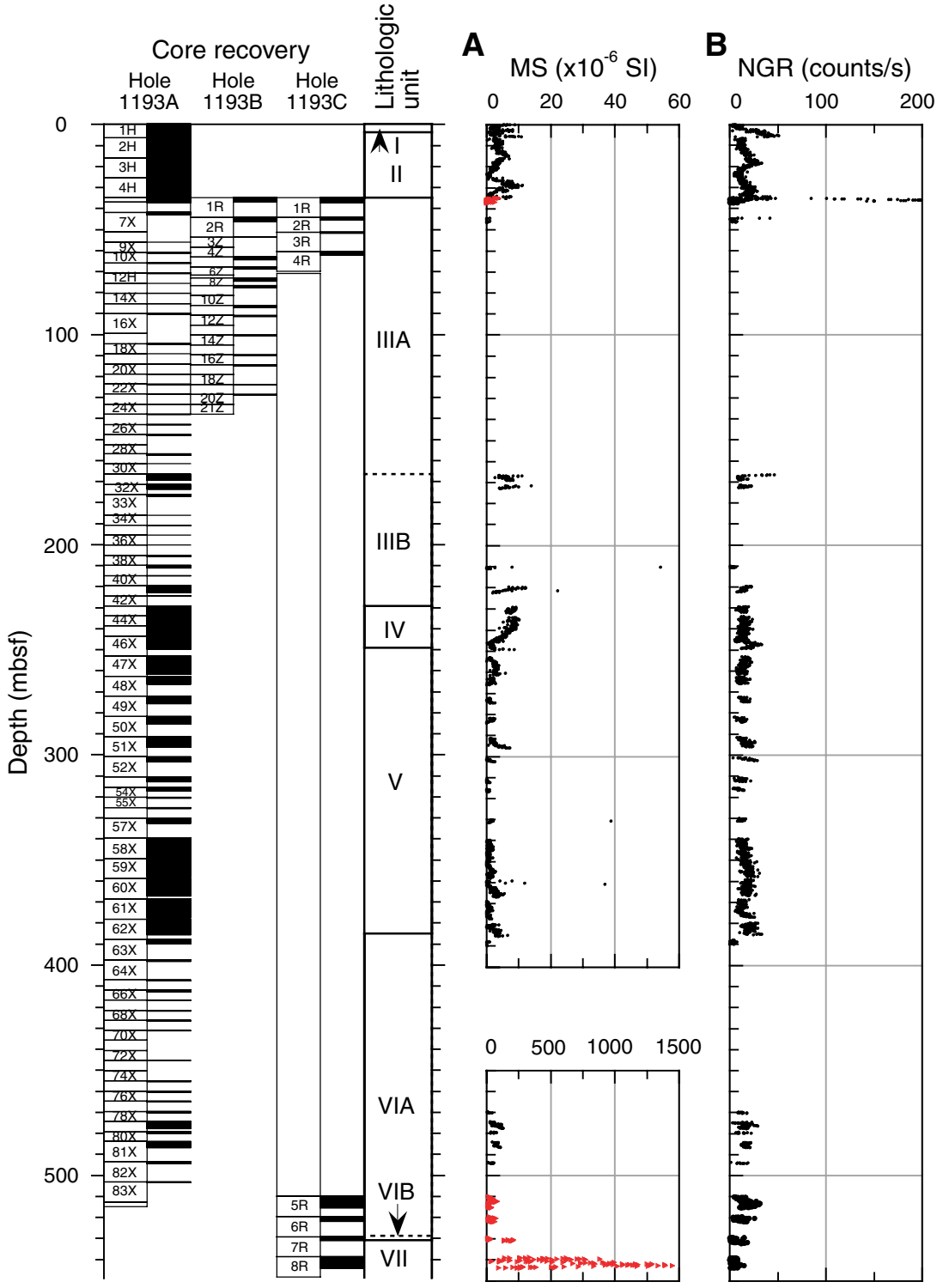

Figure F52. Site 1193 (**A**) bulk density, (**B**) magnetic susceptibility (MS), and (**C**) natural gamma radiation (NGR) from 0 to 35 mbsf.

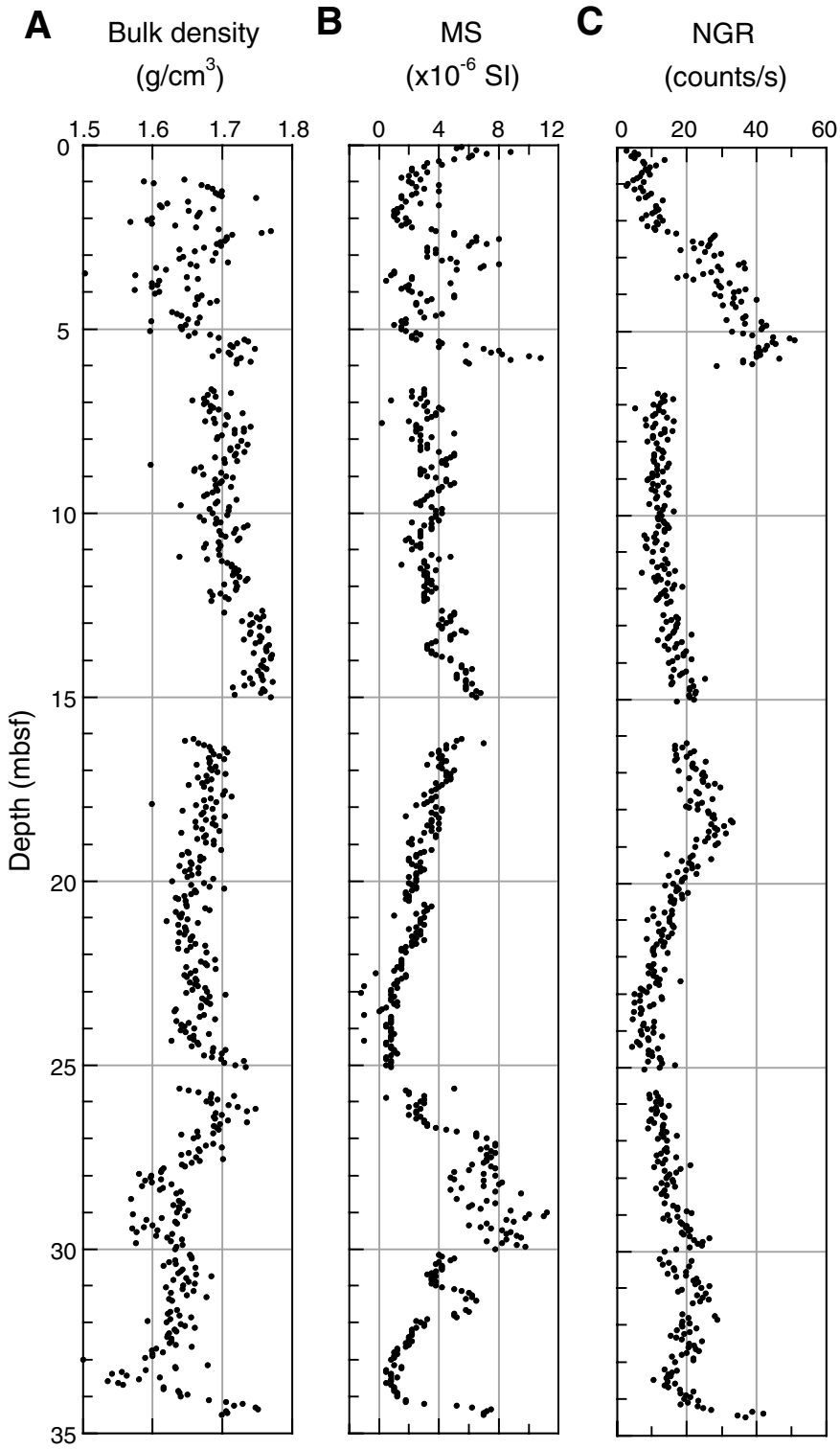

Figure F53. Multichannel line MAR13 with location and penetration depth of Site 1193 located at shotpoint 4755. The seismic megasequences (MS) and the basement are marked and traced along the section. NMP = Northern Marion Platform.

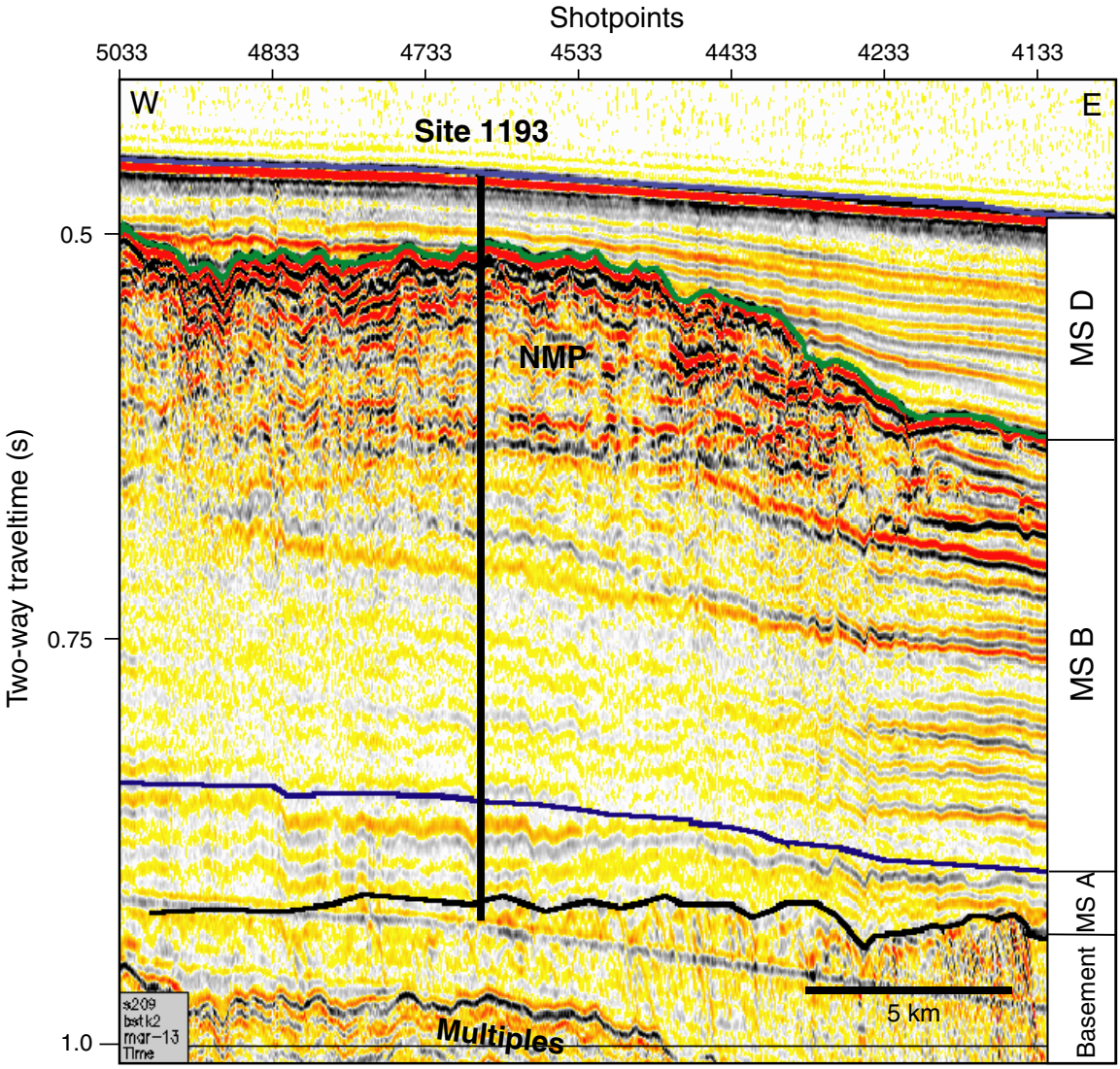

Figure F54. Synthetic seismogram plotted on line MAR13 with two-way traveltime-to-depth velocity data, *P*-wave velocity and gamma ray attenuation bulk densities, extracted sonic wavelet, synthetic seismogram, the megasequence boundaries, and lithologic boundaries. The traveltime-vs.-depth plot was used to correlate seismic reflection events to their location with depth in the sedimentary section.

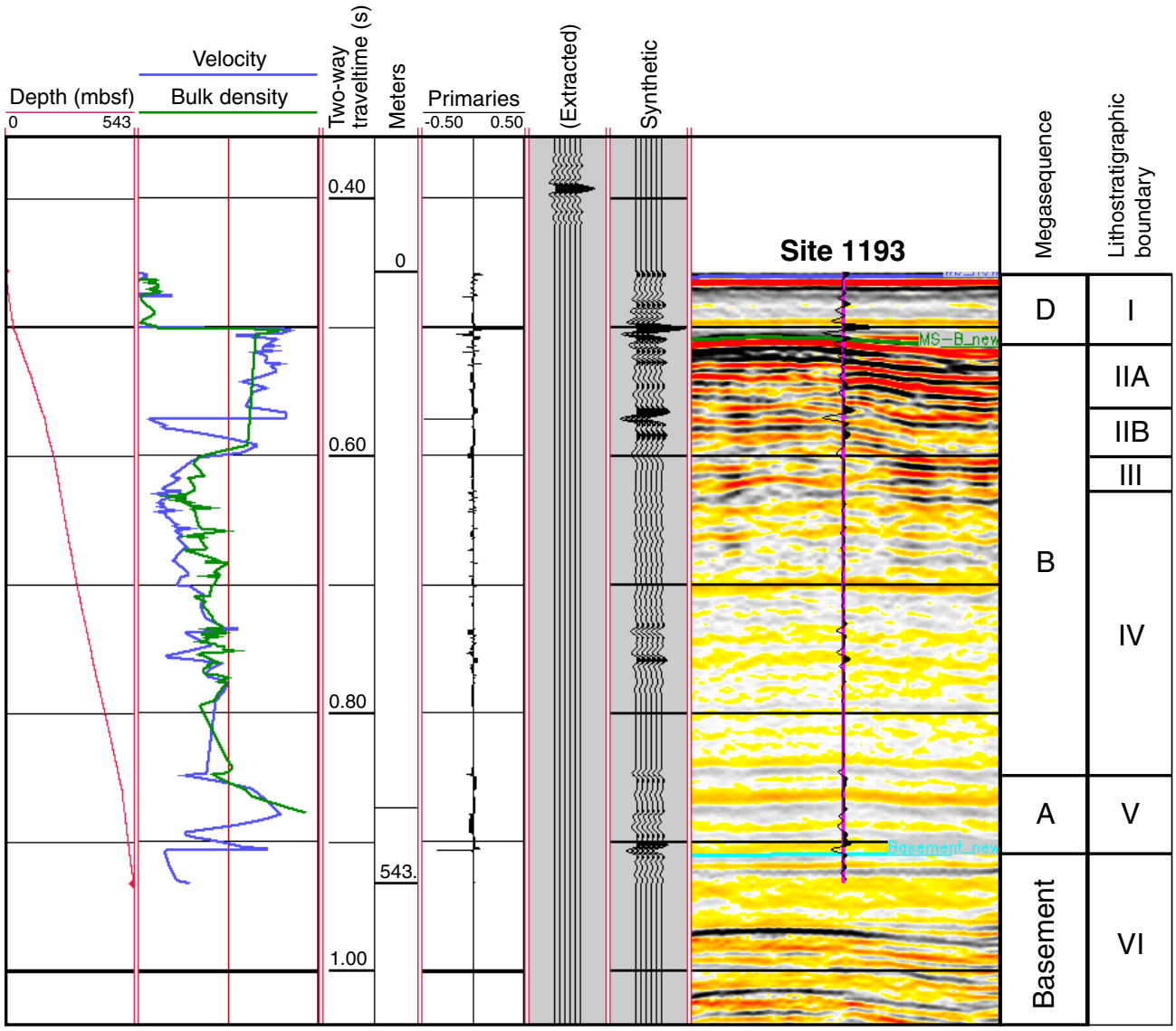

Table T1. Coring summary, Site 1193.

Core	Date (Jan 2001)	Time (local)	Depth (mbsf) Top	Depth (mbsf) Bottom	Length (m) Cored	Length (m) Recovered	Recovery (%)
194-1193A-							
1H	13	0050	0.0	6.6	6.6	6.63	100.5
2H	13	0130	6.6	16.1	9.5	9.42	99.2
3H	13	0205	16.1	25.6	9.5	9.99	105.2
4H	13	0225	25.6	35.1	9.5	9.82	103.4
5H	13	0245	35.1	37.1	2.0	1.55	77.5
6X	13	0525	37.1	41.9	4.8	0.35	7.3
7X	13	0650	41.9	51.3	9.4	1.37	14.6
8X	13	0800	51.3	56.1	4.8	0.00	0.0
9X	13	0900	56.1	61.2	5.1	0.05	1.0
10X	13	1010	61.2	66.1	4.9	0.29	5.9
11X	13	1055	66.1	70.9	4.8	0.25	5.2
12X	13	1155	70.9	75.7	4.8	0.25	5.2
13X	13	1250	75.7	80.5	4.8	0.08	1.7
14X	13	1345	80.5	85.3	4.8	0.10	2.1
15X	13	1440	85.3	90.1	4.8	0.13	2.7
16X	13	1550	90.1	99.7	9.6	0.33	3.4
17X	13	1635	99.7	104.5	4.8	0.00	0.0
18X	13	1720	104.5	109.3	4.8	0.32	6.7
19X	13	1810	109.3	114.1	4.8	0.07	1.5
20X	13	1905	114.1	118.9	4.8	0.21	4.4
21X	13	2005	118.9	123.7	4.8	0.21	4.4
22X	13	2105	123.7	128.5	4.8	0.20	4.2
23X	13	2155	128.5	133.3	4.8	0.23	4.8
24X	13	2240	133.3	138.1	4.8	0.11	2.3
25X	13	2345	138.1	142.9	4.8	0.16	3.3
26X	14	0055	142.9	147.7	4.8	0.26	5.4
27X	14	0205	147.7	152.5	4.8	0.51	10.6
28X	14	0300	152.5	157.0	4.5	0.04	0.9
29X	14	0410	157.0	161.5	4.5	0.78	17.3
30X	14	0455	161.5	166.6	5.1	0.05	1.0
31X	14	0600	166.6	171.5	4.9	2.94	60.0
32X	14	0640	171.5	176.3	4.8	2.26	47.1
33X	14	0750	176.3	186.0	9.7	0.76	7.8
34X	14	0825	186.0	190.8	4.8	0.05	1.0
35X	14	0925	190.8	195.6	4.8	0.28	5.8
36X	14	1005	195.6	200.4	4.8	0.05	1.0
37X	14	1100	200.4	205.2	4.8	0.05	1.0
38X	14	1210	205.2	210.0	4.8	0.54	11.3
39X	14	1305	210.0	214.8	4.8	1.29	26.9
40X	14	1405	214.8	219.6	4.8	0.19	4.0
41X	14	1505	219.6	224.4	4.8	3.29	68.5
42X	14	1600	224.4	229.2	4.8	0.35	7.3
43X	14	1700	229.2	234.0	4.8	4.56	95.0
44X	14	1750	234.0	238.8	4.8	5.60	116.7
45X	14	1845	238.8	243.6	4.8	7.03	146.5
46X	14	1940	243.6	253.1	9.5	6.27	66.0
47X	14	2050	253.1	262.7	9.6	8.76	91.3
48X	14	2140	262.7	272.3	9.6	3.81	39.7
49X	14	2230	272.3	281.9	9.6	3.53	36.8
50X	14	2335	281.9	291.5	9.6	3.57	37.2
51X	15	0025	291.5	301.1	9.6	5.01	52.2
52X	15	0120	301.1	310.7	9.6	2.33	24.3
53X	15	0200	310.7	315.5	4.8	2.18	45.4
54X	15	0245	315.5	320.4	4.9	1.76	35.9
55X	15	0330	320.4	325.2	4.8	0.42	8.8
56X	15	0440	325.2	330.1	4.9	0.45	9.2
57X	15	0620	330.1	339.7	9.6	2.61	27.2
58X	15	0725	339.7	349.4	9.7	9.48	97.7
59X	15	0855	349.4	359.0	9.6	8.75	91.1
60X	15	1050	359.0	368.7	9.7	8.33	85.9
61X	15	1200	368.7	378.3	9.6	8.90	92.7
62X	15	1335	378.3	387.9	9.6	7.49	78.0
63X	15	1455	387.9	397.6	9.7	2.35	24.2
64X	15	1600	397.6	407.2	9.6	0.89	9.3
65X	15	1650	407.2	412.0	4.8	0.52	10.8
66X	15	1745	412.0	416.8	4.8	0.87	18.1
67X	15	1830	416.8	421.6	4.8	0.29	6.0
68X	15	1940	421.6	426.4	4.8	0.57	11.9
69X	15	2035	426.4	431.2	4.8	0.35	7.3
70X	15	2115	431.2	436.0	4.8	0.15	3.1
71X	15	2200	436.0	440.8	4.8	0.00	0.0
72X	15	2235	440.8	445.6	4.8	0.00	0.0
73X	15	2335	445.6	450.4	4.8	0.12	2.5
74X	16	0815	450.4	455.2	4.8	0.00	0.0
75X	16	0945	455.2	460.1	4.9	0.51	10.4
76X	16	1045	460.1	464.9	4.8	0.60	12.5
77X	16	1200	464.9	469.7	4.8	0.33	6.9
78X	16	1310	469.7	474.5	4.8	0.75	15.6
79X	16	1420	474.5	479.3	4.8	3.54	73.8
80X	16	1545	479.3	484.1	4.8	1.02	21.3
81X	16	1720	484.1	493.7	9.6	2.90	30.2
82X	16	1850	493.7	503.3	9.6	1.05	10.9
83X	16	2020	503.3	512.9	9.6	0.41	4.3
84X	17	1245	512.9	515.0	2.1	0.00	0.0
				Cored total:	515.0	173.87	33.8
				Drilled total:	0.0		
				Total:	515.0		
194-1193B-							
10	17	1800	0.0	35.0	0.0	0.00	NA
1R	17	2045	35.0	44.4	9.4	2.13	22.7
2R	17	2200	44.4	53.8	9.4	1.85	19.7
3Z	18	1645	53.8	58.5	4.7	0.24	5.1
4Z	19	0210	58.5	63.2	4.7	0.00	0.0
5Z	19	1015	63.2	67.9	4.7	1.39	29.6
6Z	19	1140	67.9	71.8	3.9	1.11	28.5
7Z	19	1330	71.8	73.2	1.4	0.00	0.0
8Z	19	1440	73.2	76.9	3.7	1.48	40.0
9Z	19	1550	76.9	81.6	4.7	0.93	19.8
10Z	19	1650	81.6	86.3	4.7	0.00	0.0
11Z	19	1815	86.3	91.0	4.7	0.96	20.4
12Z	19	2340	91.0	95.7	4.7	0.73	15.5
13Z	20	0050	95.7	100.4	4.7	0.00	0.0
14Z	20	0155	100.4	105.1	4.7	0.27	5.7
15Z	20	0310	105.1	109.8	4.7	0.00	0.0
16Z	20	0420	109.8	114.5	4.7	0.31	6.6
17Z	20	0540	114.5	119.2	4.7	0.69	14.7
18Z	20	0640	119.2	123.9	4.7	0.00	0.0
19Z	20	0730	123.9	128.6	4.7	0.20	4.3
20Z	20	0935	128.6	133.3	4.7	0.48	10.2
21Z	20	1055	133.3	138.0	4.7	0.00	0.0
				Cored total:	103.0	12.77	12.4
				Drilled total:	35.0		
				Total:	138.0		
194-1193C-							
10	20	1840	0.0	35.0	0.0	0.00	NA
1R	20	2230	35.0	44.4	9.4	2.49	26.5
2R	21	0040	44.4	51.4	7.0	1.06	15.1
3R	21	0200	51.4	60.6	9.2	0.50	5.4
4R	21	0300	60.6	70.1	9.5	1.66	17.5
50	21	2330	70.1	510.0	0.0	0.00	NA
5R	22	0110	510.0	519.6	9.6	5.59	58.2
6R	22	0225	519.6	529.3	9.7	2.40	24.7
7R	22	0345	529.3	538.9	9.6	1.92	20.0
8R	22	0525	538.9	548.5	9.6	5.45	56.8
				Cored total:	73.6	21.07	28.6
				Drilled total:	474.9		
				Total:	548.5		

Note: NA = not applicable (wash core).

Table T2. Expanded coring summary, Site 1193. (See table notes. Continued on next seven pages.)

Core	Date (Jan 2001)	Time (local)	Core depth (mbsf) Top	Core depth (mbsf) Bottom	Length (m) Cored	Length (m) Recovered	Recovery (%)	Section	Length (m) Liner	Length (m) Curated	Section depth (mbsf) Top	Section depth (mbsf) Bottom	Catwalk samples	Comment
194-1193A-														
1H	13	0050	0.0	6.6	6.6	6.63	100.5							
								1	1.50	1.50	0.00	1.50		
								2	1.50	1.50	1.50	3.00		
								3	1.50	1.50	3.00	4.50	IW	
								4	1.50	1.50	4.50	6.00	HS	
								5	0.45	0.45	6.00	6.45		
								CC (w/5)	0.18	0.18	6.45	6.63	PAL	
								Totals:	6.63	6.63				
2H	13	0130	6.6	16.1	9.5	9.42	99.2							
								1	1.50	1.50	6.60	8.10		
								2	1.50	1.50	8.10	9.60		
								3	1.50	1.50	9.60	11.10		
								4	1.50	1.50	11.10	12.60	IW	
								5	1.50	1.50	12.60	14.10	HS	
								6	1.01	1.01	14.10	15.11		
								7	0.63	0.63	15.11	15.74		
								CC (w/7)	0.28	0.28	15.74	16.02	PAL	
								Totals:	9.42	9.42				
3H	13	0205	16.1	25.6	9.5	9.99	105.2							
								1	1.50	1.50	16.10	17.60		
								2	1.50	1.50	17.60	19.10		
								3	1.50	1.50	19.10	20.60		
								4	1.50	1.50	20.60	22.10	IW	
								5	1.50	1.50	22.10	23.60	HS	
								6	1.50	1.50	23.60	25.10		
								7	0.72	0.72	25.10	25.82		
								CC (w/7)	0.27	0.27	25.82	26.09	PAL	
								Totals:	9.99	9.99				
4H	13	0225	25.6	35.1	9.5	9.82	103.4							
								1	1.50	1.50	25.60	27.10		
								2	1.50	1.50	27.10	28.60		
								3	1.50	1.50	28.60	30.10		
								4	1.50	1.50	30.10	31.60	IW	
								5	1.50	1.50	31.60	33.10	HS	
								6	1.50	1.50	33.10	34.60		
								7	0.65	0.65	34.60	35.25		
								CC (w/7)	0.17	0.17	35.25	35.42	PAL	
								Totals:	9.82	9.82				
5H	13	0245	35.1	37.1	2.0	1.55	77.5							
								1	1.50	1.50	35.10	36.60		
								CC (w/CC)	0.05	0.05	36.60	36.65	PAL	
								Totals:	1.55	1.55				
6X	13	0525	37.1	41.9	4.8	0.35	7.3							
								CC (w/CC)	0.35	0.50	37.10	37.60		
								Totals:	0.35	0.50				
7X	13	0650	41.9	51.3	9.4	1.37	14.6							
								1	0.98	1.47	41.90	43.37		
								2	0.39	0.0				
								Totals:	1.37	1.47				
8X	13	0800	51.3	56.1	4.8	0.00	0.0							
9X	13	0900	56.1	61.2	5.1	0.05	1.0							
								1	0.05	0.05	56.10	56.15		
								Totals:	0.05	0.05				
10X	13	1010	61.2	66.1	4.9	0.29	5.9							
								1	0.29	0.31	61.20	61.51		
								Totals:	0.29	0.31				
11X	13	1055	66.1	70.9	4.8	0.25	5.2							
								1	0.25	0.25	66.10	66.35		
								Totals:	0.25	0.25				
12X	13	1155	70.9	75.7	4.8	0.25	5.2							
								1	0.25	0.29	70.90	71.19		
								Totals:	0.25	0.29				
13X	13	1250	75.7	80.5	4.8	0.08	1.7							
								1	0.08	0.08	75.70	75.78		
								Totals:	0.08	0.08				

Table T2 (continued).

Core	Date (Jan 2001)	Time (local)	Core depth (mbsf) Top	Core depth (mbsf) Bottom	Length (m) Cored	Length (m) Recovered	Recovery (%)	Section	Length (m) Liner	Length (m) Curated	Section depth (mbsf) Top	Section depth (mbsf) Bottom	Catwalk samples	Comment
14X	13	1345	80.5	85.3	4.8	0.10	2.1							
								1	0.10	0.10	80.50	80.60	PAL	
								Totals:	0.10	0.10				
15X	13	1440	85.3	90.1	4.8	0.13	2.7							
								1	0.13	0.13	85.30	85.43	PAL	
								Totals:	0.13	0.13				
16X	13	1550	90.1	99.7	9.6	0.33	3.4							
								1	0.33	0.33	90.10	90.43		
								Totals:	0.33	0.33				
17X	13	1635	99.7	104.5	4.8	0.00	0.0							
18X	13	1720	104.5	109.3	4.8	0.32	6.7							
								1	0.32	0.32	104.50	104.82		
								Totals:	0.32	0.32				
19X	13	1810	109.3	114.1	4.8	0.07	1.5							
								CC (w/CC)	0.07	0.07	109.30	109.37		
								Totals:	0.07	0.07				
20X	13	1905	114.1	118.9	4.8	0.21	4.4							
								CC (w/CC)	0.21	0.21	114.10	114.31	PAL	
								Totals:	0.21	0.21				
21X	13	2005	118.9	123.7	4.8	0.21	4.4							
								CC (w/CC)	0.21	0.30	118.90	119.20	PAL	
								Totals:	0.21	0.30				
22X	13	2105	123.7	128.5	4.8	0.20	4.2							
								CC (w/CC)	0.20	0.28	123.70	123.98	PAL	
								Totals:	0.20	0.28				
23X	13	2155	128.5	133.3	4.8	0.23	4.8							
								CC (w/CC)	0.23	0.22	128.50	128.72	PAL	
								Totals:	0.23	0.22				
24X	13	2240	133.3	138.1	4.8	0.11	2.3							
								CC (w/CC)	0.11	0.14	133.30	133.44	PAL	
								Totals:	0.11	0.14				
25X	13	2345	138.1	142.9	4.8	0.16	3.3							
								CC (w/CC)	0.16	0.23	138.10	138.33	PAL	
								Totals:	0.16	0.23				
26X	14	0055	142.9	147.7	4.8	0.26	5.4							
								1	0.26	0.26	142.90	143.16	PAL	
								Totals:	0.26	0.26				
27X	14	0205	147.7	152.5	4.8	0.51	10.6							
								CC (w/CC)	0.51	0.57	147.70	148.27	PAL	
								Totals:	0.51	0.57				
28X	14	0300	152.5	157.0	4.5	0.04	0.9							
								CC (w/CC)	0.04	0.04	152.50	152.54	PAL	All to PAL
								Totals:	0.04	0.04				
29X	14	0410	157.0	161.5	4.5	0.78	17.3							
								1	0.78	0.94	157.00	157.94	PAL	
								Totals:	0.78	0.94				
30X	14	0455	161.5	166.6	5.1	0.05	1.0							
								1	0.05	0.05	161.50	161.55	PAL	
								Totals:	0.05	0.05				
31X	14	0600	166.6	171.5	4.9	2.94	60.0							
								1	1.50	1.50	166.60	168.10	IW	
								2	1.08	1.08	168.10	169.18	HS	
								CC (w/CC)	0.36	0.36	169.18	169.54	PAL	
								Totals:	2.94	2.94				
32X	14	0640	171.5	176.3	4.8	2.26	47.1							
								1	1.50	1.50	171.50	173.00	IW	
								2	0.55	0.55	173.00	173.55		
								CC (w/2)	0.21	0.21	173.55	173.76	PAL	
								Totals:	2.26	2.26				
33X	14	0750	176.3	186.0	9.7	0.76	7.8							
								1	0.30	0.30	176.30	176.60		
								CC (w/1)	0.46	0.46	176.60	177.06	PAL	
								Totals:	0.76	0.76				
34X	14	0825	186.0	190.8	4.8	0.05	1.0							
								1	0.05	0.05	186.00	186.05		
								Totals:	0.05	0.05				

Table T2 (continued).

Core	Date (Jan 2001)	Time (local)	Core depth (mbsf) Top	Core depth (mbsf) Bottom	Length (m) Cored	Length (m) Recovered	Recovery (%)	Section	Length (m) Liner	Length (m) Curated	Section depth (mbsf) Top	Section depth (mbsf) Bottom	Catwalk samples	Comment
35X	14	0925	190.8	195.6	4.8	0.28	5.8							
								1	0.28	0.28	190.80	191.08		
								Totals:	0.28	0.28				
36X	14	1005	195.6	200.4	4.8	0.05	1.0							
								1	0.05	0.05	195.60	195.65	PAL	
								Totals:	0.05	0.05				
37X	14	1100	200.4	205.2	4.8	0.05	1.0							
								1	0.05	0.05	200.40	200.45		
								Totals:	0.05	0.05				
38X	14	1210	205.2	210.0	4.8	0.54	11.3							
								1	0.54	0.54	205.20	205.74	PAL	
								Totals:	0.54	0.54				
39X	14	1305	210.0	214.8	4.8	1.29	26.9							
								1	1.04	1.04	210.00	211.04	HS	
								CC (w/1)	0.25	0.25	211.04	211.29	PAL	
								Totals:	1.29	1.29				
40X	14	1405	214.8	219.6	4.8	0.19	4.0							
								1	0.19	0.19	214.80	214.99	PAL	
								Totals:	0.19	0.19				
41X	14	1505	219.6	224.4	4.8	3.29	68.5							
								1	1.50	1.50	219.60	221.10	IW	
								2	1.42	1.42	221.10	222.52	HS	
								CC (w/CC)	0.37	0.37	222.52	222.89	PAL	
								Totals:	3.29	3.29				
42X	14	1600	224.4	229.2	4.8	0.35	7.3							
								1	0.35	0.35	224.40	224.75		
									0.35	0.35				
43X	14	1700	229.2	234.0	4.8	4.56	95.0							
								1	1.50	1.50	229.20	230.70		
								2	1.50	1.50	230.70	232.20	IW	
								3	1.15	1.15	232.20	233.35	HS	
								CC (w/CC)	0.41	0.41	233.35	233.76	PAL	
								Totals:	4.56	4.56				
44X	14	1750	234.0	238.8	4.8	5.60	116.7							
								1	1.50	1.50	234.00	235.50		
								2	1.50	1.50	235.50	237.00	IW	
								3	1.50	1.50	237.00	238.50	HS	
								4	0.73	0.73	238.50	239.23		
								CC (w/4)	0.37	0.37	239.23	239.60	PAL	
								Totals:	5.60	5.60				
45X	14	1845	238.8	243.6	4.8	7.03	146.5							
								1	1.50	1.50	238.80	240.30		
								2	1.50	1.50	240.30	241.80		
								3	1.50	1.50	241.80	243.30	IW	
								4	1.50	1.50	243.30	244.80	HS	
								5	0.59	0.59	244.80	245.39		
								CC (w/5)	0.44	0.44	245.39	245.83	PAL	
								Totals:	7.03	7.03				
46X	14	1940	243.6	253.1	9.5	6.27	66.0							
								1	1.50	1.50	243.60	245.10		
								2	1.50	1.50	245.10	246.60		
								3	1.50	1.50	246.60	248.10	IW	
								4	1.38	1.38	248.10	249.48	HS	
								CC (w/CC)	0.39	0.39	249.48	249.87		
								Totals:	6.27	6.27				
47X	14	2050	253.1	262.7	9.6	8.76	91.3							
								1	1.50	1.50	253.10	254.60		
								2	1.50	1.50	254.60	256.10		
								3	1.50	1.50	256.10	257.60		
								4	1.50	1.50	257.60	259.10	IW	
								5	1.50	1.50	259.10	260.60	HS	
								6	0.92	0.92	260.60	261.52		
								CC (w/6)	0.34	0.34	261.52	261.86	PAL	
								Totals:	8.76	8.76				
48X	14	2140	262.7	272.3	9.6	3.81	39.7							
								1	1.50	1.50	262.70	264.20		
								2	1.00	1.00	264.20	265.20	IW	
								3	0.86	0.86	265.20	266.06	HS	

Table T2 (continued).

Core	Date (Jan 2001)	Time (local)	Core depth (mbsf) Top	Core depth (mbsf) Bottom	Length (m) Cored	Length (m) Recovered	Recovery (%)	Section	Length (m) Liner	Length (m) Curated	Section depth (mbsf) Top	Section depth (mbsf) Bottom	Catwalk samples	Comment
								CC (w/3)	0.45	0.45	266.06	266.51	PAL	
								Totals:	3.81	3.81				
49X	14	2230	272.3	281.9	9.6	3.53	36.8							
								1	1.50	1.50	272.30	273.80	IW	
								2	1.00	1.00	273.80	274.80	HS	
								3	0.63	0.63	274.80	275.43		
								CC (w/3)	0.40	0.40	275.43	275.83	PAL	
								Totals:	3.53	3.53				
50X	14	2335	281.9	291.5	9.6	3.57	37.2							
								1	1.50	1.50	281.90	283.40	IW	
								2	1.00	1.00	283.40	284.40	HS	
								3	0.68	0.68	284.40	285.08		
								CC (w/3)	0.39	0.39	285.08	285.47	PAL	
								Totals:	3.57	3.57				
51X	15	0025	291.5	301.1	9.6	5.01	52.2							
								1	1.50	1.50	291.50	293.00		
								2	1.50	1.50	293.00	294.50	IW	
								3	1.00	1.00	294.50	295.50	HS	
								4	0.64	0.64	295.50	296.14		
								CC (w/4)	0.37	0.37	296.14	296.51	PAL	
								Totals:	5.01	5.01				
52X	15	0120	301.1	310.7	9.6	2.33	24.3							
								1	1.50	1.50	301.10	302.60		
								2	0.42	0.42	302.60	303.02		
								CC (w/2)	0.41	0.41	303.02	303.43	PAL	
								Totals:	2.33	2.33				
53X	15	0200	310.7	315.5	4.8	2.18	45.4							
								1	1.00	1.00	310.70	311.70	HS, IW	
								2	0.96	0.96	311.70	312.66		
								CC (w/2)	0.22	0.22	312.66	312.88		
								Totals:	2.18	2.18				
54X	15	0245	315.5	320.4	4.9	1.76	35.9							
								1	1.39	1.39	315.50	316.89		
								CC (w/CC)	0.37	0.37	316.89	317.26	PAL	
								Totals:	1.76	1.76				
55X	15	0330	320.4	325.2	4.8	0.42	8.8							
								CC (w/CC)	0.42	0.42	320.40	320.82	PAL	
								Totals:	0.42	0.42				
56X	15	0440	325.2	330.1	4.9	0.45	9.2							
								CC (w/CC)	0.45	0.45	325.20	325.65	PAL	
								Totals:	0.45	0.45				
57X	15	0620	330.1	339.7	9.6	2.61	27.2							
								1	1.50	1.50	330.10	331.60		
								2	0.67	0.67	331.60	332.27	IW	
								CC (w/2)	0.44	0.44	332.27	332.71	PAL	
								Totals:	2.61	2.61				
58X	15	0725	339.7	349.4	9.7	9.48	97.7							
								1	1.50	1.50	339.70	341.20		
								2	1.50	1.50	341.20	342.70		
								3	1.50	1.50	342.70	344.20		
								4	1.36	1.36	344.20	345.56	IW	
								5	1.47	1.47	345.56	347.03	HS	
								6	1.12	1.12	347.03	348.15		
								7	0.80	0.80	348.15	348.95		
								CC (w/7)	0.23	0.23	348.95	349.18	PAL	
								Totals:	9.48	9.48				
59X	15	0855	349.4	359.0	9.6	8.75	91.1							
								1	1.52	1.52	349.40	350.92		
								2	1.30	1.30	350.92	352.22		
								3	1.50	1.50	352.22	353.72		
								4	1.53	1.53	353.72	355.25		
								5	1.46	1.46	355.25	356.71	IW	
								6	1.22	1.22	356.71	357.93		
								CC (w/6)	0.22	0.22	357.93	358.15	PAL	
								Totals:	8.75	8.75				
60X	15	1050	359.0	368.7	9.7	8.33	85.9							
								1	1.47	1.47	359.00	360.47		
								2	1.45	1.45	360.47	361.92		

Table T2 (continued).

Core	Date (Jan 2001)	Time (local)	Core depth (mbsf) Top	Core depth (mbsf) Bottom	Length (m) Cored	Length (m) Recovered	Recovery (%)	Section	Length (m) Liner	Length (m) Curated	Section depth (mbsf) Top	Section depth (mbsf) Bottom	Catwalk samples	Comment
								3	1.50	1.50	361.92	363.42		
								4	1.50	1.50	363.42	364.92	IW	
								5	1.50	1.50	364.92	366.42	HS	
								6	0.50	0.50	366.42	366.92		
								CC (w/6)	0.41	0.41	366.92	367.33	PAL	
								Totals:	8.33	8.33				
61X	15	1200	368.7	378.3	9.6	8.90	92.7							
								1	1.35	1.35	368.70	370.05		
								2	1.39	1.39	370.05	371.44		
								3	1.50	1.50	371.44	372.94		
								4	1.46	1.46	372.94	374.40		
								5	1.40	1.40	374.40	375.80	IW	
								6	1.37	1.37	375.80	377.17	HS	
								CC (w/CC)	0.43	0.43	377.17	377.60	PAL	
								Totals:	8.90	8.90				
62X	15	1335	378.3	387.9	9.6	7.49	78.0							
								1	1.53	1.53	378.30	379.83		
								2	1.50	1.50	379.83	381.33		
								3	1.50	1.50	381.33	382.83		
								4	1.50	1.50	382.83	384.33	IW	
								5	1.07	1.07	384.33	385.40	HS	
								CC (w/5)	0.39	0.39	385.40	385.79	PAL	
								Totals:	7.49	7.49				
63X	15	1455	387.9	397.6	9.7	2.35	24.2							
								1	1.33	1.33	387.90	389.23	IW	
								2	0.81	0.81	389.23	390.04	HS	
								CC (w/2)	0.21	0.21	390.04	390.25	PAL	
								Totals:	2.35	2.35				
64X	15	1600	397.6	407.2	9.6	0.89	9.3							
								1	0.46	0.46	397.60	398.06		
								CC (w/1)	0.43	0.43	398.06	398.49	PAL	
								Totals:	0.89	0.89				
65X	15	1650	407.2	412.0	4.8	0.52	10.8							
								CC (w/CC)	0.52	0.52	407.20	407.72	PAL	
								Totals:	0.52	0.52				
66X	15	1745	412.0	416.8	4.8	0.87	18.1							
								1	0.62	0.62	412.00	412.62		
								CC (w/1)	0.25	0.25	412.62	412.87	PAL	
								Totals:	0.87	0.87				
67X	15	1830	416.8	421.6	4.8	0.29	6.0							
								CC (w/CC)	0.29	0.29	416.80	417.09	PAL	
								Totals:	0.29	0.29				
68X	15	1940	421.6	426.4	4.8	0.57	11.9							
								CC (w/CC)	0.57	0.57	421.60	422.17	PAL	
								Totals:	0.57	0.57				
69X	15	2035	426.4	431.2	4.8	0.35	7.3							
								CC (w/CC)	0.35	0.35	426.40	426.75	PAL	
								Totals:	0.35	0.35				
70X	15	2115	431.2	436.0	4.8	0.15	3.1							
								CC (w/CC)	0.15	0.15	431.20	431.35	PAL	
								Totals:	0.15	0.15				
71X	15	2200	436.0	440.8	4.8	0.00	0.0							
72X	15	2235	440.8	445.6	4.8	0.00	0.0							
73X	15	2335	445.6	450.4	4.8	0.12	2.5							
								CC (w/CC)	0.12	0.12	445.60	445.72	PAL	
								Totals:	0.12	0.12				
74X	16	0815	450.4	455.2	4.8	0.00	0.0							
75X	16	0945	455.2	460.1	4.9	0.51	10.4							
								CC (w/CC)	0.51	0.51	455.20	455.71	PAL	
								Totals:	0.51	0.51				
76X	16	1045	460.1	464.9	4.8	0.60	12.5							
								1	0.60	0.60	460.10	460.70	PAL	
								Totals:	0.60	0.60				
77X	16	1200	464.9	469.7	4.8	0.33	6.9							
								CC (w/CC)	0.33	0.33	464.90	465.23	PAL	
								Totals:	0.33	0.33				

Table T2 (continued).

Core	Date (Jan 2001)	Time (local)	Core depth (mbsf) Top	Core depth (mbsf) Bottom	Length (m) Cored	Length (m) Recovered	Recovery (%)	Section	Length (m) Liner	Length (m) Curated	Section depth (mbsf) Top	Section depth (mbsf) Bottom	Catwalk samples	Comment
78X	16	1310	469.7	474.5	4.8	0.75	15.6							
								1	0.75	0.75	469.70	470.45	PAL	
								Totals:	0.75	0.75				
79X	16	1420	474.5	479.3	4.8	3.54	73.8							
								1	1.50	1.50	474.50	476.00	IW	
								2	1.00	1.00	476.00	477.00	HS	
								3	0.68	0.68	477.00	477.68		
								CC (w/3)	0.36	0.36	477.68	478.04	PAL	
								Totals:	3.54	3.54				
80X	16	1545	479.3	484.1	4.8	1.02	21.3							
								1	0.61	0.61	479.30	479.91	HS	
								CC (w/CC)	0.41	0.41	479.91	480.32	PAL	
								Totals:	1.02	1.02				
81X	16	1720	484.1	493.7	9.6	2.90	30.2							
								1	1.50	1.50	484.10	485.60	IW	
								2	1.18	1.18	485.60	486.78	HS	
								CC (w/2)	0.22	0.22	486.78	487.00	PAL	
								Totals:	2.90	2.90				
82X	16	1850	493.7	503.3	9.6	1.05	10.9							
								1	0.66	0.66	493.70	494.36		
								CC (w/1)	0.39	0.39	494.36	494.75	PAL	
								Totals:	1.05	1.05				
83X	16	2020	503.3	512.9	9.6	0.41	4.3							
								CC (w/CC)	0.41	0.41	503.30	503.71	PAL	
								Totals:	0.41	0.41				
84X	17	1245	512.9	515.0	2.1	0.00	0.0							
				Totals:	515.0	173.87	33.8							
194-1193B-														
10	17	1800	0.0	35.0	0.0	0.00	NA							
1R	17	2045	35.0	44.4	9.4	2.13	22.7							
								1	1.50	1.50	35.00	36.50		
								2	0.60	0.94	36.50	37.44		
								CC (w/2)	0.03	0.03	37.44	37.47	PAL	
								Totals:	2.13	2.47				
2R	17	2200	44.4	53.8	9.4	1.85	19.7							
								1	1.00	1.42	44.40	45.82		
								2	0.85	0.70	45.82	46.52		
								Totals:	1.85	2.12				
3Z	18	1645	53.8	58.5	4.7	0.24	5.1							
								1	0.24	0.37	53.80	54.17	PAL	
								Totals:	0.24	0.37				
4Z	19	0210	58.5	63.2	4.7	0.00	0.0							
5Z	19	1015	63.2	67.9	4.7	1.39	29.6							
								1	1.24	1.24	63.20	64.44		
								CC (w/1)	0.15	0.15	64.44	64.59	PAL	
								Totals:	1.39	1.39				
6Z	19	1140	67.9	71.8	3.9	1.11	28.5							
								1	1.05	1.31	67.90	69.21		
								CC (w/1)	0.06	0.06	69.21	69.27	PAL	
								Totals:	1.11	1.37				
7Z	19	1330	71.8	73.2	1.4	0.00	0.0							
8Z	19	1440	73.2	76.9	3.7	1.48	40.0							
								1	1.48	1.20	73.20	74.40		
								2	0.00	0.58	74.40	74.98		
								Totals:	1.48	1.78				
9Z	19	1550	76.9	81.6	4.7	0.93	19.8							
								1	0.86	0.84	76.90	77.74		
								CC (w/1)	0.07	0.07	77.74	77.81	PAL	
								Totals:	0.93	0.91				
10Z	19	1650	81.6	86.3	4.7	0.00	0.0							
11Z	19	1815	86.3	91.0	4.7	0.96	20.4							
								1	0.96	1.36	86.30	87.66	PAL, HS	
								Totals:	0.96	1.36				

Table T2 (continued).

Core	Date (Jan 2001)	Time (local)	Core depth (mbsf) Top	Core depth (mbsf) Bottom	Length (m) Cored	Length (m) Recovered	Recovery (%)	Section	Length (m) Liner	Length (m) Curated	Section depth (mbsf) Top	Section depth (mbsf) Bottom	Catwalk samples	Comment
12Z	19	2340	91.0	95.7	4.7	0.73	15.5							
								1	0.71	1.01	91.00	92.01	PAL	
								CC (NS)	0.02	0.02	92.01	92.03	PAL	
								Totals:	0.73	1.03				
13Z	20	0050	95.7	100.4	4.7	0.00	0.0							
14Z	20	0155	100.4	105.1	4.7	0.27	5.7							
								1	0.27	0.35	100.40	100.75	PAL	
								Totals:	0.27	0.35				
15Z	20	0310	105.1	109.8	4.7	0.00	0.0							
16Z	20	0420	109.8	114.5	4.7	0.31	6.6							
								1	0.31	0.45	109.80	110.25	PAL	
								Totals:	0.31	0.45				
17Z	20	0540	114.5	119.2	4.7	0.69	14.7							
								1	0.67	0.93	114.50	115.43		
								CC (w/1)	0.02	0.02	115.43	115.45	PAL	
								Totals:	0.69	0.95				
18Z	20	0640	119.2	123.9	4.7	0.00	0.0							
19Z	20	0730	123.9	128.6	4.7	0.20	4.3							
								1	0.20	0.24	123.90	124.14		
								Totals:	0.20	0.24				
20Z	20	0935	128.6	133.3	4.7	0.48	10.2							
								1	0.48	0.59	128.60	129.19		
								Totals:	0.48	0.59				
21Z	20	1055	133.3	138.0	4.7	0.00	0.0							
				Totals:	103	12.77	12.4							
194-1193C-														
10	20	1840	0.0	35.0	0.0	0.00	NA							
1R	20	2230	35.0	44.4	9.4	2.49	26.5							
								1	1.38	1.35	35.00	36.35		
								2	1.06	1.47	36.35	37.82	VASC	
								CC (w/2)	0.05	0.05	37.82	37.87	PAL	All to PAL
								Totals:	2.49	2.87				
2R	21	0040	44.4	51.4	7.0	1.06	15.1							
								1	1.03	1.19	44.40	45.59		
								CC (w/CC)	0.03	0.03	45.59	45.62	PAL	
								Totals:	1.06	1.22				
3R	21	0200	51.4	60.6	9.2	0.50	5.4							
								1	0.48	0.52	51.40	51.92		
								CC (w/1)	0.02	0.02	51.92	51.94	PAL	
								Totals:	0.50	0.54				
4R	21	0300	60.6	70.1	9.5	1.66	17.5							
								1	0.19	1.47	60.60	62.07	VASC	
								2	1.45	0.68	62.07	62.75		
								CC (w/2)	0.02	0.02	62.75	62.77	PAL	
								Totals:	1.66	2.17				
51	21	2330	70.1	510.0	0.0	0.00	NA							
5R	22	0110	510.0	519.6	9.6	5.59	58.2							
								1	1.32	1.32	510.00	511.32		
								2	1.36	1.36	511.32	512.68		
								3	1.36	1.36	512.68	514.04		
								4	1.31	1.31	514.04	515.35		
								CC (w/CC)	0.24	0.24	515.35	515.59	PAL	
								Totals:	5.59	5.59				
6R	22	0225	519.6	529.3	9.7	2.40	24.7							
								1	1.50	1.50	519.60	521.10		
								2	0.88	0.88	521.10	521.98		
								CC (w/CC)	0.02	0.02	521.98	522.00	PAL	
								Totals:	2.40	2.40				
7R	22	0345	529.3	538.9	9.6	1.92	20.0							
								1	0.25	1.50	529.30	530.80		
								2	1.38	1.05	530.80	531.85	PAL	
								CC (w/2)	0.29	0.00				
								Totals:	1.92	2.55				

Table T2 (continued).

Core	Date (Jan 2001)	Time (local)	Core depth (mbsf) Top	Core depth (mbsf) Bottom	Length (m) Cored	Length (m) Recovered	Recovery (%)	Section	Length (m) Liner	Length (m) Curated	Section depth (mbsf) Top	Section depth (mbsf) Bottom	Catwalk samples	Comment
8R	22	0525	538.9	548.5	9.6	5.45	56.8							
								1	1.26	1.26	538.90	540.16		
								2	1.42	1.42	540.16	541.58		
								3	1.49	1.49	541.58	543.07		
								4	0.99	0.99	543.07	544.06		
								CC (w/4)	0.29	0.29	544.06	544.35	PAL	
								Totals:	5.45	5.45				
				Totals:	73.6	21.07	28.6							

Notes: CC = core catcher (number in parentheses indicates which section the core catcher is stored with). Catwalk samples: IW = interstitial water, HS = headspace, VASC = sample request code, PAL = paleontology sample, NS = all of the core catcher was used for the paleontology sample, NA = not available.

Table T3. Lithologic units and subunits, Site 1193.

		Hole 1193A				Hole 1193B				Hole 1193C					
		Core, section, interval (cm)		Depth (mbsf)		Core, section, interval (cm)		Depth (mbsf)		Core, section, interval (cm)		Depth (mbsf)			
Unit	Subunit	Top	Base	Top	Base	Top	Base	Top	Base	Top	Base	Top	Base	Description	Interpretation
I		1H-1, 0	1H-3, 100	0.0	3.5									Skeletal grainstone/mudstone/packstone with planktonic foraminifers. Light brown to yellow.	Hemipelagic (open plateau), high energy
II		1H-3, 100	4H-7, 40	3.5	35.0									Skeletal packstone/wackestone with clay, planktonic foraminifers. Light olive-gray.	Hemipelagic (open plateau), mixed energy
III	IIIA	4H-7, 40	31X-1, 30	35.0	167.0	1R-1, 100				1R-1, 100				Skeletal rudstone/floatstone/grainstone with bryozoans and benthic foraminifers. White, yellow, reddish white, subordinate dolostone.	Platform, high energy, inner to middle neritic
III	IIIB	31X-1, 30	42X-1, 30	167.0	229.2									Skeletal rudstone/floatstone/grainstone with bryozoans, red algae, benthic foraminifers, variable clay content, and subordinate clay-rich mudstone. Light greenish gray.	Platform, high energy, inner to middle neritic, mudstones from bay/lagoonal setting
IV		42X-1, 30	46X-4, 90	229.2	249.0									Mudstone/claystone, minor planktonic and benthic foraminifers. Dark to light greenish gray.	Upper to middle platform slope, low influx of coarse neritic debris
V		46X-7, 90	62X-5, 77	249.2	385.1									Skeletal packstone with clay, fine sand to silt-sized bioclastics, benthic foraminifers. Light olive-gray.	Upper to middle platform slope, moderate to high influx of coarse neritic debris
VI	VIA	62X-5, 77		385.1							7R-1, 100		529.3	Grainstone with quartz, phosphate, and glauconite sand, sandstone beds, benthic foraminifers, echinoderms, red algae. Greenish gray to brown.	Shallow, high-energy shelf with varying carbonate production, siliciclastic influx, and periods of condensed sedimentation
VI	VIB									7R-1, 0	7R-2, 20	529.3	531.4	Sandstone/conglomerate with large oyster shells. Greenish gray.	Transgressive shoreline
VII										7R-2, 20	8R-5, 30	531.4	544	Volcaniclastic conglomerate/breccia, basaltic composition, highly fractured with calcite veins and extensive low-temperature alteration. Reddish brown to dark green.	Basement

Table T4. Biostratigraphic datums, Site 1193.

Datum	Core, section, interval (cm)	Depth (mbsf)		Mean depth (mbsf)	Age (Ma)
		First absence or presence	Last presence or absence		
	194-1193A-				
FO *Emiliania huxleyi*	1H-1, 90, to 1H-2, 80	0.90	2.30	1.60	0.26
LO *Pseudoemiliania lacunosa*	1H-2, 80, to 1H-3, 10	2.30	3.10	2.70	0.46
LO *Calcidiscus macintyrei*	1H-3, 30, to 1H-5, 30	3.30	6.30	4.80	1.70
LO *Discoaster brouweri*	1H-3, 30, to 1H-5, 30	3.30	6.30	4.80	2.00
LO *Discoaster pentaradiatus*	1H-3, 30, to 1H-5, 30	3.30	6.30	4.80	2.50
LO *Discoaster surculus*	1H-3, 30, to 1H-5, 30	3.30	6.30	4.80	2.60
LO *Discoaster tamalis*	1H-3, 30, to 1H-5, 30	3.30	6.30	4.80	2.80
LO *Dendoglobigerina altispira*	1H-5, 18, to 1H-CC	6.18	6.58	6.38	3.09
LO *Sphaeroidinellopsis seminulina*	1H-CC to 2H-2, 10	6.58	8.20	7.39	3.12
LO *Reticulofenestra pseudoumbilica*	2H-5, 90, to 2H-6, 98	13.50	15.08	14.29	3.70
LO *Globorotalia margaritae*	2H-CC, to 3H-2, 10	15.97	17.70	16.84	3.80
LO *Globigerina nepenthes*	4H-1, 80, to 4H-2, 10	26.40	27.20	26.80	4.18
FO *Sphaeroidinella dehiscens*	3H-CC to 4H-CC	26.06	35.39	30.73	5.30
FO *Globorotalia tumida*	4H-CC to 5H-CC	35.39	36.06	35.73	5.60
LO *Discoaster quinqueramus*	4H-6, 80, to 4H-CC	33.90	35.39	34.65	5.60
FO *Discoaster surculus*	5H-CC to 39X-CC	36.06	211.27	123.67	7.50
LO *Cyclicargolithus floridanus*	5H-CC to 39X-CC	36.06	211.27	123.67	11.90
LO *Globigerina connecta*	43X-CC to 44X-CC	233.74	239.58	236.66	16.40
LO *Globigerinoides parawoodi*	51X-CC to 52X-CC	296.42	303.38	299.90	16.80
FO *Sphenolithus heteromorphus*	60X-CC to 73X-CC	367.31	445.70	406.51	18.20
LO *Sphenolithus belemnos*	73X-CC to 75X-CC	445.70	455.54	450.62	18.50
FO *Sphenolithus belemnos*	78X-CC to 79X-CC	470.03	478.02	474.03	20.60
LO *Zygrhablithus bijugatus*	81X-CC to 82X-CC	486.92	494.70	490.81	22.50

Note: FO = first occurrence, LO = last occurrence.

Table T5. Summary of biostratigraphic and paleoenvironmental interpretations, Site 1193. (See table notes. Continued on next page.)

Core, section, interval (cm)	Depth (mbsf)	Age (Ma)	Foraminiferal assemblages				Comments on constituents >63 µm	Paleowater depth (m)					Depositional setting	Lithologic unit
			PF	ONBF	ESBF	LBF		<30	<60	<100	>100	>200		
194-														
1193A-1H-CC	6.63	3.6–4.8*	D	R			Foraminifer-nannofossil ooze					X	Hemipelagic	II
1193A-2H-CC	16.02	3.6–5.6*	D	C			Foraminifer-nannofossil ooze, *Cibicidoides*					X	Hemipelagic	
1193A-3H-CC	26.09	4.8–5.6*	D	C			Foraminifer-nannofossil ooze, *Cibicidoides*					X	Hemipelagic	
1193A-4H-CC	35.42	4.8–5.6*	D	R		D	Foraminifer-nannofossil ooze					X	Hemipelagic	
1193A-5H-CC	36.65	12–24	A	C	C	C	Reworked material; LBF	?	X	X			Platform	IIIA
1193A-6X-CC	37.60	12–24	R		C	A	Bryozoan with LBF		?	X			Platform	
1193B-1R-CC	37.47	12–24	R		R	A	Reworked material; LBF	?	X	X			Platform	
1193C-1R-CC	37.87	12–24				C	Reworked material; LBF	?	X	X			Platform	
1193C-2R-CC	45.62	12–24				A	Abundant larger foraminifers		X	X			Platform	
1193C-3R-CC	51.94	12–24				A	*Amphistegina, Cycloclypeus*		X	X			Platform	
1193C-4R-CC	62.77	12–24				C	LBF robust to large and flat	X	X	X			Platform	
1193B-5Z-CC	64.59	12–24			R	A	LBF relatively flat to very flat		X	X			Platform	
1193B-6Z-CC	69.27	12–24				A	LBF relatively flat to very flat		X	X			Platform	
1193B-9Z-CC	77.81	12–24			C	C	LBF relatively flat to very flat		X	X			Platform	
1193A-14X-CC	80.60	12–24			R	R	LBF relatively flat to very flat		X	X			Platform	
1193A-15X-CC	85.40	12–24				C	Exposure surface to flat LBF	X	X	X			Platform	
1193B-11Z-CC	87.20	12–24				A	LBF robust to large and flat	X	X	X			Platform	
1193B-12Z-CC	92.03	12–24				C	LBF robust to large and flat	X	X	X			Platform	
1193A-19X-CC	109.37	12–24				A	Bryozoan with large *Cycloclypeus*		X	X			Platform	
1193A-20X-CC	114.31	12–24				A	Bryozoan with large *Cycloclypeus*		X	X			Platform	
1193B-17Z-CC	115.45	12–24				A	Bryozoan with large *Cycloclypeus*		X	X			Platform	
1193A-21X-CC	119.20	12–24				C	Bryozoan with large *Cycloclypeus*		X	X			Platform	
1193A-22X-CC	123.98	12–24				C	Bryozoan with large *Cycloclypeus*		X	X			Platform	
1193A-23X-CC	128.72	12–24				C	Dolomitized bryozoan with LBF		X	X			Platform	
1193A-24X-CC	133.44	12–24			R	R	Dolomitized bryozoan with LBF		X	X			Platform	
1193A-25X-CC	138.33	12–24			C	C	Dolomitized bryozoan with LBF		X	X			Platform	
1193A-27X-CC	148.27	12–24				C	Dolomitized bryozoan with LBF		X	X			Platform	
1193A-28X-CC	152.54	12–24				C	Dolomitized bryozoan with LBF		X	X			Platform	
1193A-29X-CC	157.80	12–24				C	Dolomitized bryozoan with LBF		X	X			Platform	
1193A-31X-CC	169.54	12–24			C	C	Clay, calc silt with transported LBF	?	?	?			Platform	IIIB
1193A-32X-CC	173.76	12–24			C	C	Clay, calc silt with transported LBF	?	?	?			Platform	
1193A-33X-CC	177.06	12–24			R	A	Clay, calc silt with transported LBF	?	?	?			Platform	
1193A-36X-CC	195.60	12–24				C	Bryozoan with large *Cycloclypeus*		X	X			Platform	
1193A-37X-CC	196.00	12–24				C	Bryozoan with large *Cycloclypeus*		X	X			Platform	
1193A-38X-CC	205.70	12–24			C	C	Dolomitized bryozoan with LBF		X	X			Platform	
1193A-39X-CC	211.29	12–24				C	Bryozoan with *N. howchini,* others		X	X			Platform	
1193A-40X-CC	215.00	12–24				C	Bryozoan with large *Cycloclypeus*		X	X			Platform	
1193A-41X-CC	222.89	12–24				C	Bryozoan with large *Cycloclypeus*		X	X			Platform	
1193A-43X-CC	233.76			C			Calc silt/vfs, terrigenous clays				X		Distal periplatform	IV
1193A-44X-CC	239.60	16.4*		C			Calc silt/vfs, terrigenous clays				X		Distal periplatform	
1193A-45X-CC	245.83			C			Calc silt/vfs, terrigenous clays				X		Distal periplatform	
1193A-46X-CC	249.87			C			Calc silt/vfs, terrigenous clays				X		Distal periplatform	
1193A-47X-CC	261.86	12–24		R	R		Calc silt/vfs, bioclastic fragments				X		Proximal periplatform	V
1193A-48X-CC	266.51	12–24		R	R	C	Calc silt/vfs, bioclastic fragments				X		Proximal periplatform	
1193A-49X-CC	275.83	12–24		R	R	R	Calc silt/vfs, bioclastic fragments				X		Proximal periplatform	
1193A-50X-CC	285.47	12–24		R	R	R	Calc silt/vfs, bioclastic fragments				X		Proximal periplatform	

Table T5 (continued).

Core, section, interval (cm)	Depth (mbsf)	Age (Ma)	Foraminiferal assemblages				Comments on constituents >63 µm	Paleowater depth (m)					Depositional setting	Lithologic unit
			PF	ONBF	ESBF	LBF		<30	<60	<100	>100	>200		
1193A-5X1-CC	296.51	12–24		R	R	R	Calc silt/vfs, bioclastic fragments				X		Proximal periplatform	
1193A-52X-CC	303.43	16.8*		R	R	C	Calc silt/vfs, bioclastic fragments				X		Proximal periplatform	
1193A-54X-CC	317.26			R			Calc silt/vfs, bioclastic fragments				X		Proximal periplatform	
1193A-55X-CC	320.82						Calc silt/vfs, nondescript				X		Proximal periplatform	
1193A-56X-CC	325.65			R		R	Calc silt/vfs, bioclastic fragments				X		Proximal periplatform	
1193A-57X-CC	332.71			R			Calc silt/vfs, bioclastic fragments				X		Proximal periplatform	
1193A-58X-CC	349.18			R			Calc silt/vfs, bioclastic fragments				X		Proximal periplatform	
1193A-59X-CC	358.15	12–24		R			Calc silt/vfs, bioclastic fragments				X		Proximal periplatform	
1193A-60X-CC	367.33	18.2*		R	R	R	Calc silt/vfs, bioclastic fragments				X		Proximal periplatform	
1193A-61X-CC	377.60	12–24		R	R	C	Calc silt/vfs, bioclastic fragments				X		Proximal periplatform	
1193A-62X-CC	385.79	12–24		R	R	C	Calc silt/vfs, bioclastic fragments				X		Proximal periplatform	
1193A-63X-CC	390.25	12–24				Dom	Imbricated *Lepidocyclina* sands	X					Platform	VI
1193A-64X-CC	398.49	12–24				A	Bioclastic sands; robust LBF	X					Platform	
1193A-65X-CC	407.72	12–24				A	Bioclastic sands; robust LBF	X					Platform	
1193A-66X-CC	412.87	12–24				C	Floatstone with bryozoans, LBF		X	X			Platform	
1193A-67X-CC	417.09	12–24				C	Bryozoan with LBF		X	X			Platform	
1193A-68X-CC	422.17					R	Calc silt/vfs, nondescript						Platform	
1193A-69X-CC	426.75	12–24				C	Carbonate/quartz sands; LBF		X				Platform	
1193A-70X-CC	431.35	12–24				C	Bioclastic/arkosic sands; *Cycloclypeus*		X	X			Platform	
1193A-73X-CC	445.72						Arkosic sandstone, no fossils evident						Platform	
1193A-75X-CC	455.71	18.5*				C	Siliciclastic sands with LBF		X	X			Platform	
1193A-76X-CC	460.70	12–24				C	Grainstone: bryozoans, LBF		X				Platform	
1193A-77X-CC	465.23	12–24			C	C	Grainstone: bryozoans, LBF		X				Platform	
1193A-78X-CC	470.40	20.6*			C	C	Carbonate/quartz sands; LBF		X				Platform	
1193A-79X-CC	478.04	12–24			C	C	Pyritized LBF and miliolids		X				Platform	
1193A-80X-CC	480.32	12–24			R	C	Carbonate/quartz sands; LBF		X				Platform	
1193A-81X-CC	487.00	12–24			R	R	Carbonate/quartz sands; LBF		X				Platform	
1193A-82X-CC	494.75	22.5*			R	R	Carbonate/quartz sands; LBF		X				Platform	
1193A-83X-CC	503.71	12–24			R	R	Carbonate/quartz sands; LBF		X				Platform	
1193C-5X-CC	515.59	12–24				R	Siliciclastic sands with LBF		X				Platform	
1193C-6X-CC	522.00	12–24				R	Siliciclastic sands with LBF		X				Platform	
1193C-7X-CC	531.83	12–24				R	Siliciclastic sands with rare LBF		X				Platform	VII
1193C-8X-CC	544.35	12–24				R	Siliciclastic sands with rare LBF		X				Platform	

Notes: Based on microscopic analysis of biogenic sediment constituents, particularly benthic foraminifers, from core catcher samples and augmented by thin sections and selected core descriptions. Age: * = age from planktonic foraminifers or nannofossils (see Table T4, p. 102). Foraminiferal assemblages: PF = planktonic foraminifers, ONBF = outer neritic to upper bathyal benthic foraminifers, ESBF = middle to inner neritic smaller benthic foraminifers, LBF = larger benthic foraminifers, Dom = dominant, R = rare, C = common, A = abundant. Comments: Calc silt/vfs = silt-sized and very fine sand-sized bioclastic carbonate sediments. Paleowater depth: ? = uncertain.

Table T6. Magnetic polarity transitions, Hole 1193A.

Chron	Top observation		Bottom observation		Average		
	Core, section, interval (cm)	Depth (mbsf)	Core, section, interval (cm)	Depth (mbsf)	Depth (mbsf)	Error	Age (Ma)
	194-1193A-		194-1193A-				
C2n	1H-3, 50	3.5	1H-4, 150	6.0	4.8	1.25	1.95
C3n.1n (T)	2H-6, 90	15.0	2H-6, 90	15.0	15.5	0.50	4.18
C3n.1n (O)	3H-3, 90	20.0	3H-3, 90	20.0	20.0	0.00	4.29
C3n.2n (T)	3H-4, 140	22.0	3H-5, 90	23.0	22.5	0.50	4.48
C3n.2n (O)	3H-6, 40	24.0	4H-1, 40	26.0	25.0	1.00	4.46
C3n.3n (T)	4H-1, 140	27.0	4H-3, 40	29.0	28.0	1.00	4.80
C3n.3n (O)	4H-3, 140	30.0	4H-4, 90	31.0	30.5	0.50	4.89
C3n.4n (T)	4H-6, 90	34.0	4H-6, 140	34.5	34.3	0.25	4.98

Note: (T) = termination, (O) = onset.

Table T7. Age-depth control points, Site 1193.

Source	Datum	Age (Ma)	Top: FO presence or LO absence		Bottom: LO presence or FO absence		Average depth (mbsf)	Uncertainty (m)	
			Core, section, interval (cm)	Depth (mbsf)	Core, section, interval (cm)	Depth (mbsf)		Upsection	Downsection
			194-1193A-		194-1193A-				
CN	FO *Emiliania huxleyi*	0.26	1H-1, 90	0.90	1H-2, 80	2.30	1.60	0.70	0.70
CN	LO *Pseudoemiliania lacunosa*	0.46	1H-2, 80	2.30	1H-3, 10	3.10	2.70	0.40	0.40
CN	LO *Calcidiscus macintyrei*	1.7	1H-3, 30	3.30	1H-5, 30	6.30	4.80	1.50	1.50
CN	LO *Discoaster brouweri*	2	1H-3, 30	3.30	1H-5, 30	6.30	4.80	1.50	1.50
CN	LO *Discoaster pentaradiatus*	2.5	1H-3, 30	3.30	1H-5, 30	6.30	4.80	1.50	1.50
CN	LO *Discoaster surculus*	2.6	1H-3, 30	3.30	1H-5, 30	6.30	4.80	1.50	1.50
CN	LO *Discoaster tamalis*	2.8	1H-3, 30	3.30	1H-5, 30	6.30	4.80	1.50	1.50
PF	LO *Dentoglobigerina altispira*	3.09	1H-5, 18	6.18	1H-CC	6.58	6.38	0.20	0.20
CN	LO *Sphaeroidinellopsis seminulina*	3.12	1H-CC	6.58	2H-2, 10	8.20	7.39	0.81	0.81
CN	LO *Reticulofenestra pseudoumbilica*	3.7	2H-5, 90	13.50	2H-6, 98	15.08	14.29	0.79	0.79
PF	LO *Globorotalia margaritae*	3.8	2H-CC	15.97	3H-2, 10	17.70	16.84	0.87	0.86
PF	LO *Globorotalia nepenthes*	4.18	4H-1, 80	26.40	4H-2, 10	27.20	26.80	0.40	0.40
CN	FO *Sphaeroidinella dehiscens*	5.30	3H-CC	26.06	4H-CC	35.39	30.73	4.67	4.67
PF	FO *Globorotalia tumida*	5.60	4H-CC	35.39	5H-BCI	37.10	36.25	0.86	0.85
CN	LO *Discoaster quinqueramus*	5.6	4H-6, 80	33.90	4H-CC	35.39	34.65	0.74	0.75
PF	LO *Globoturborotalita connecta*	16.40	43X-CC	233.74	44X-CC	239.58	236.66	2.92	2.92
PF	LO *Globigerinoides parawoodi*	16.80	51X-CC	296.42	52X-BCI	310.70	303.56	7.14	7.14
CN	FO *Sphenolithus heteromorphus*	18.2	60X-CC	367.31	73X-BCI	450.40	408.86	41.55	41.55
CN	LO *Sphenolithus belemnos*	18.5	73X-CC	445.70	75X-BCI	460.10	452.90	7.20	7.20
CN	FO *Sphenolithus belemnos*	20.6	78X-CC	470.03	79X-BCI	479.30	474.67	4.63	4.64
CN	LO *Zygrhablithus bijugatus*	22.5	81X-CC	486.92	82X-BCI	503.30	495.11	8.19	8.19
			194-1193A-		194-1193C-				
LBF	Range of LBF associations LF5–LF7	12–24.0	5H-CC	37.00	6R-BCI	529.30			

Notes: Source: CN = calcareous nannoplankton, PF = planktonic foraminifers, LBF = large benthic foraminifers. Datum: FO = first occurrence, LO = last occurrence. Core, section, interval: BCI = bottom of cored interval.

Table T8. Interpolated ages of lithologic unit boundaries and seismic reflectors, Site 1193.

	Top of unit		
	Depth (mbsf)	Age (Ma)	Comments
Lithologic unit:			
I	0	0	
II	4 (5.7)	0.7 to 2.9	Hiatus (5.7 mbsf based on core logging)
IIIA	35	5.6 to >12	Hiatus (late Miocene)
IIIB	167	Not defined	
IV	229	16.35	
V	249	16.45	
VIA	385	17.5	
VIB	529	Not defined	late Oligocene?
VII	531	Not defined	late Oligocene?
Seismic sequences and reflectors:			
Megasequence D	0	0	
D-black	Not present		
D-turquoise	Not present		
Megasequence C	Not present		
Megasequence B	35	5.6 to >12	Hiatus (late Miocene)
Megasequence A	440	18	
Basement	531	Not defined	late Oligocene?

Table T9. Headspace gas composition, Site 1193.

Core, section	Depth (mbsf)	C_1 (ppmv)
194-1193A-		
1H-4	4.50	1.7
2H-5	12.60	1.8
3H-5	22.10	1.7
4H-5	31.60	1.7
31X-2	168.10	2.0
39X-1	210.00	1.9
41X-2	221.10	1.9
43X-3	232.20	2.2
44X-3	237.00	1.9
45X-4	243.30	2.3
46X-4	248.10	2.2
47X-5	259.10	2.2
48X-3	265.20	2.5
49X-2	273.80	2.9
50X-2	283.40	3.2
51X-3	294.50	2.7
53X-1	310.70	3.7
58X-5	345.56	2.2
60X-5	364.92	2.3
61X-6	375.80	2.2
62X-5	384.33	3.0
63X-2	389.23	1.9
80X-1	479.30	2.0
81X-2	485.60	6.6
194-1193B-		
11Z-1	86.30	3.7

Note: C_1 = methane.

Table T10. Interstitial water chemistry, Hole 1193A.

Core, section, interval (cm)	Depth (mbsf)	pH	Alk (mM)	Salinity	Cl^- (mM)	SO_4^{2-} (mM)	Na^+ (mM)	Mg^{2+} (mM)	Ca^{2+} (mM)	K^+ (mM)	NH_4^+ (μM)	Sr^{2+} (μM)	Li^+ (μM)	Mn^{2+} (μM)	Fe^{2+} (μM)
194-1193A-															
1H-3, 140–150	4.40	7.72	2.11	35.5	562	30.12	477	56.17	10.61	11.79	8	101	27.86	0.13	5.43
2H-4, 140–150	12.50	7.61	2.49	35.5	563	29.57	479	54.45	11.39	11.83	18	106	31.23	0.14	0.67
3H-4, 140–150	22.00	7.51	2.07	35.5	563	29.29	479	53.29	12.17	11.18	26	102	28.65	0.30	0.92
4H-4, 140–150	31.50	7.52	2.07	36.0	564	29.73	481	53.32	12.19	11.10	23	98	28.00	0.18	2.41
31X-4, 140–150	168.00	7.84	2.22	36.0	567	29.26	482	48.73	17.37	10.86	53	177	31.30	0.14	0.27
32X-1, 140–150	172.90	7.71	2.00	36.0	566	29.25	477	49.34	19.04	10.61	66	215	34.19	0.12	1.73
41X-2, 135–150	220.95	7.75	2.99	36.0	565	28.79	476	48.04	20.70	9.32	155	72	21.22	0.00	0.00
43X-2, 135–150	232.05			35.5	556	27.10	458	48.71	23.66	7.50	232				
44X-2, 135–150	236.85			35.5	552	26.34	453	48.53	23.81	7.13	242				
45X-3, 135–150	243.15			35.5	557	25.36	454	48.11	24.84	7.52	276				
46X-3, 140–150	248.00	7.54	2.30	35.5	563	25.18	463	46.47	24.48	8.10	320	523	45.47	0.19	0.37
47X-4, 140–150	259.00			35.5	563	24.38	461	46.38	25.21	7.42	338				
48X-2, 090–100	265.10	7.52	2.99	35.5	560	24.66	457	46.45	25.91	7.20	356	536	48.96	0.18	0.00
49X-1, 140–150	273.70	7.52	2.89	35.5	561	24.66	457	48.48	24.87	7.13	358	529	48.51	0.20	0.00
51X-2, 135–150	294.35	7.70	2.42	35.5	562	22.97	448	48.47	28.15	6.57	419	559	54.68	0.25	0.29
53X-1, 085–100	311.55	7.73	2.41	35.5	563	22.88	448	47.85	29.42	6.10	474				
57X-2, 000–017	331.60	7.73	2.18	36.0	565	23.32	452	48.32	28.55	6.22	455	553	54.93	0.18	0.24
58X-4, 120–136	345.40	7.67	2.40	35.5	567	22.79	445	48.71	32.00	5.79	474				
59X-5, 136–146	356.61	7.76	1.72	35.5	565	22.82	459	43.27	29.65	5.79	506	608	59.60	0.23	6.17
60X-4, 140–150	364.82	7.65	2.13	35.5	562	21.90	441	47.30	32.62	5.02	489				
61X-5, 130–150	375.70			35.5	564	22.06	444	47.14	32.43	5.17	543	600	66.45	0.16	0.28
62X-4, 140–150	384.23	8.00	1.30	35.5	564	21.40	440	46.31	34.60	4.97	527				
63X-1, 121–133	389.11	7.57	1.74	35.5	564	22.99	448	47.54	30.36	5.99	466				
79X-1, 140–150	475.90	7.98	0.66	35.5	565	21.50	409	43.07	54.56	3.49	810				
81X-1, 135–150	485.45	7.75	0.96	35.5	566	19.71	406	41.79	56.25	3.57	559				

Note: Alk = alkalinity.

Table T11. Percentages of aragonite, calcite, dolomite, and noncarbonate minerals, Site 1193. (Continued on next page.)

Core, section, interval (cm)	Depth (mbsf)	Aragonite (wt%)	Calcite (wt%)	Dolomite (wt%)	Non-carbonate (wt%)
194-1193A-					
1H-2, 75–76	2.25	0	90	0	10
1H-4, 75–76	5.25	0	83	0	17
2H-2, 75–76	8.85	0	78	0	22
2H-4, 75–76	11.85	0	73	0	27
3H-2, 75–76	18.35	0	75	0	25
3H-4, 75–76	21.35	0	83	0	17
3H-6, 75–76	24.35	0	85	0	15
4H-2, 75–76	27.85	0	81	0	19
4H-4, 75–76	30.85	0	82	0	18
4H-6, 75–76	33.85	0	83	0	17
6X-CC, 11–12	37.21	0	94	3	3
6X-CC, 37–38	37.47	0	98	0	2
6X-CC, 46–47	37.56	0	92	8	0
7X-1, 12–13	42.02	0	99	0	1
7X-1, 82–83	42.72	0	98	0	2
10X-1, 25–26	61.45	0	94	0	6
12X-1, 3–4	70.93	0	97	2	1
13X-1, 1–2	75.71	0	96	3	0
14X-1, 8–9	80.58	0	94	5	1
15X-1, 3–4	85.33	0	92	7	0
16X-1, 23–24	90.33	0	0	100	0
18-1, 16–17	104.66	0	64	36	0
19X-CC, 5–6	109.35	0	97	3	1
20X-CC, 5–6	114.15	0	96	3	1
21X-CC, 9–10	118.99	0	93	7	0
22X-CC, 6–7	123.76	0	26	78	0
23X-CC, 13–14	128.63	0	0	100	0
24X-CC, 3–4	133.33	0	80	20	0
25X-CC, 18–19	138.28	0	66	36	0
26X-1, 7–8	142.97	0	85	15	0
27X-CC, 23–24	147.93	0	83	17	0
29X-1, 11–12	157.11	0	0	100	0
31X-1, 3–4	166.63	0	0	91	9
31X-1, 43–44	167.03	0	38	54	9
31X-2, 89–90	168.99	0	49	40	11
31X-2, 89–90	168.99	0	57	3	40
32X-1, 36–37	171.86	0	65	4	31
32X-1, 99–100	172.49	0	50	7	43
32X-2, 46–47	173.46	0	87	4	9
33X-1, 10–11	176.40	0	55	41	4
34X-1, 3–4	186.03	0	94	0	6
35X-1, 5–6	190.85	0	96	0	4
37X-1, 3–4	200.43	0	70	30	0
38X-1, 11–12	205.31	0	92	0	8
39X-1, 62–63	210.62	0	45	51	4
40X-1, 8–9	214.88	0	57	43	0
41X-1, 38–39	219.98	0	30	21	49
41X-2, 57–58	221.67	0	34	48	18
41X-CC, 2–4	222.54	0	98	0	2
42X-1, 7–8	224.47	0	97	0	3
43X-2, 49–50	231.19	0	20	49	31
43X-3, 89–90	233.09	0	9	61	30
44X-1, 38–39	234.38	0	50	0	50
44X-2, 58–59	236.08	0	54	0	46
44X-3, 10–11	237.10	0	46	0	54
45X-1, 38–40	239.18	0	38	0	62
45X-2, 57–58	240.87	0	62	0	38
45X-3, 10–11	241.90	0	59	0	41
46X-1, 38–39	243.98	0	37	32	31
46X-3, 23–24	246.83	0	41	46	13
46X-4, 134–135	249.44	0	70	11	18
47X-1, 75–76	253.85	0	67	20	13
47X-3, 76–77	256.86	0	64	19	17
47X-5, 74–75	259.84	0	65	17	18
48X-1, 75–76	263.45	0	67	12	21
48X-3, 75–76	265.95	0	69	29	2
49X-1, 50–51	272.80	0	56	26	17
49X-3, 50–51	275.30	0	72	21	7
50X-1, 50–51	282.40	0	67	15	18
50X-2, 50–52	283.90	0	80	15	4
50X-3, 50–51	284.90	0	54	17	29
51X-1, 75–76	292.25	0	72	11	17
51X-3, 77–78	295.27	0	73	7	20
52X-1, 77–78	301.87	0	86	4	10
53X-1, 47–48	311.17	0	80	5	15
54X-1, 30–31	315.80	0	84	2	14
55X-CC, 18–19	320.58	0	81	2	16
56X-CC, 17–19	325.37	0	78	6	16
57X-CC, 17–18	330.27	0	77	6	17
58X-1, 75–76	340.45	0	69	12	19
58X-3, 75–76	343.45	0	67	13	20
58X-5, 75–76	346.31	0	72	14	14
59X-1, 75–76	350.15	0	66	19	15
59X-3, 75–76	352.97	0	69	15	16
59X-5, 75–76	356.00	0	78	8	15
60X-1, 76–77	359.76	0	76	12	12
60X-3, 80–81	362.72	0	75	4	20
60X-5, 75–76	365.67	0	52	2	46
61X-1, 75–76	369.45	0	69	23	7
61X-3, 79–80	372.23	0	71	11	18
61X-5, 75–76	375.15	0	79	9	12
62X-1, 78–79	379.08	0	76	9	16
62X-3, 78–80	382.11	0	77	11	13
62X-5, 74–76	385.07	0	60	12	28
63X-1, 75–76	388.65	0	90	5	5
64X-1, 24–25	397.84	0	95	3	2
66X-1, 42–43	412.42	0	94	0	6
67X-CC, 15–16	416.95	0	92	5	3
68X-CC, 17–18	421.77	0	74	9	17
69X-CC, 16–17	426.56	0	56	0	44
70X-CC, 7–8	431.27	0	29	0	71
73X-CC, 7–8	445.67	0	17	0	83
75X-CC, 23–24	455.43	0	24	14	62
76X-1, 25–26	460.35	0	81	0	19
77X-CC, 13–14	465.03	0	91	0	9
78X-1, 26–27	469.96	0	77	0	23
79X-1, 78–79	475.28	0	42	0	58
79X-3, 46–47	477.46	0	59	0	41
80X-1, 30–31	479.60	0	25	0	75
81X-1, 30–31	484.40	0	18	0	82
82X-1, 30–31	494.00	0	5	0	95
83X-CC, 15–16	503.45	0	53	0	47
194-1193B-					
1R-1, 86–87	35.86	0	97	0	3
1R-1, 133–134	36.33	0	99	0	1
1R-2, 12–13	36.62	0	100	0	0
1R-2, 49–50	36.99	0	99	0	1
2R-1, 61–62	45.01	0	99	0	1
2R-1, 124–125	45.64	0	99	0	1
2R-2, 29–30	46.11	0	99	0	1
3Z-1, 18–20	53.98	0	98	0	2
5Z-1, 41–43	63.61	0	94	4	2
5Z-1, 107–109	64.27	0	81	9	10
6Z-1, 23–25	68.13	0	92	5	3
6Z-1, 103–105	68.93	0	99	0	1
8Z-1, 21–23	73.41	0	100	0	0
8Z-1, 91–93	74.11	0	88	7	5
9Z-1, 25–27	77.15	0	93	6	1
9Z-1, 76–78	77.66	0	99	0	1
11Z-1, 44–45	86.74	0	99	0	1
11Z-1, 120–121	87.50	0	98	0	2
12Z-1, 55–56	91.55	0	91	9	1

Table T11 (continued).

Core, section, interval (cm)	Depth (mbsf)	Aragonite (wt%)	Calcite (wt%)	Dolomite (wt%)	Non-carbonate (wt%)
12Z-1, 92–93	91.92	0	90	8	1
14Z-1, 24–25	100.64	0	0	100	0
14Z-1, 32–33	100.72	0	72	28	0
16Z-1, 27–28	110.07	0	74	23	3
17Z-1, 43–44	114.93	0	19	81	0
17Z-1, 87–88	115.37	0	81	18	2
19Z-1, 23–24	124.13	0	84	16	0
20Z-1, 30–31	128.90	0	0	100	0
194-1193C-					
1R-2, 63–64	36.98	0	95	0	5
1R-2, 134–135	37.69	0	100	0	0
2R-1, 43–44	44.83	0	100	0	0
2R-1, 85–86	45.25	0	100	0	0
3R-1, 17–18	51.57	0	100	0	0
4R-1, 16–17	60.76	0	100	0	0
4R-1, 49–50	61.09	0	99	0	1
4R-2, 52–53	62.59	0	89	0	11

Table T12. Carbon, nitrogen, sulfur, and hydrogen values and C/N and C/S ratios in sediments, Site 1193. (See table notes. Continued on next two pages.)

Core, section	Depth (mbsf)	IC (wt%)	$CaCO_3$ (wt%)	TC (wt%)	TOC (wt%)	Total N (wt%)	Total S (wt%)	Total H (wt%)	C/N ratio	C/S ratio
194-1193A-										
1H-2	2.25	10.77	89.7	—	—	—	—	—	—	—
1H-4	5.25	9.94	82.8	—	—	—	—	—	—	—
2H-2	8.85	9.32	77.7	9.58	0.26	0.06	0.45	0.25	4.33	0.57
2H-4	11.85	8.72	72.7	9.10	0.37	0.09	0.29	0.37	4.11	1.28
3H-2	18.35	8.99	74.9	9.11	0.12	0.07	0.45	0.27	1.71	0.27
3H-4	21.35	9.99	83.2	—	—	—	—	—	—	—
3H-6	24.35	10.22	85.1	10.40	0.22	0.02	0.56	0.21	11.00	0.39
4H-2	27.85	9.68	80.6	—	—	—	—	—	—	—
4H-4	30.85	9.85	82.1	—	—	—	—	—	—	—
4H-6	33.85	10.02	83.4	10.2	0.20	0.02	0.19	0.25	10.00	1.05
6X-CC	37.21	11.67	97.2	—	—	—	—	—	—	—
6X-CC	37.47	11.82	98.4	—	—	—	—	—	—	—
7X-1	42.13	11.96	99.6	—	—	—	—	—	—	—
7X-1	42.83	11.94	99.5	—	—	—	—	—	—	—
9X-1	56.11	11.77	98.0	—	—	—	—	—	—	—
10X-1	61.45	11.34	94.5	11.30	0.00	0.00	0.00	0.09	—	—
12X-1	70.93	11.89	99.0	—	—	—	—	—	—	—
13X-1	75.71	11.97	99.7	—	—	—	—	—	—	—
14X-1	80.58	11.88	98.9	—	—	—	—	—	—	—
15X-1	85.33	11.97	99.7	—	—	—	—	—	—	—
16X-1	90.33	12.43	103.5	—	—	—	—	—	—	—
18X-1	104.66	11.97	99.7	—	—	—	—	—	—	—
19X-CC	109.35	11.90	99.1	—	—	—	—	—	—	—
20X-CC	114.15	11.89	99.0	11.80	0.00	0.00	0.00	0.06	—	—
21X-CC	118.99	11.96	99.6	—	—	—	—	—	—	—
22X-CC	123.76	12.41	103.4	—	—	—	—	—	—	—
23X-CC	128.63	12.58	104.8	—	—	—	—	—	—	—
24X-CC	133.33	12.10	100.8	—	—	—	—	—	—	—
25X-CC	138.28	12.17	101.4	—	—	—	—	—	—	—
26X-1	142.97	12.02	100.2	—	—	—	—	—	—	—
27X-CC	147.93	12.00	100.0	—	—	—	—	—	—	—
29X-1	157.11	12.46	103.8	—	—	—	—	—	—	—
31X-1	166.61	10.94	91.2	—	—	—	—	—	—	—
31X-1	166.63	10.94	91.2	—	—	—	—	—	—	—
31X-1	167.03	10.73	89.4	—	—	—	—	—	—	—
31X-2	168.99	7.15	59.6	7.34	0.19	0.06	0.38	0.48	3.17	0.50
32X-1	171.86	8.30	69.1	—	—	—	—	—	—	—
32X-1	172.49	6.88	57.3	6.93	0.05	0.02	0.80	0.55	2.50	0.06
32X-2	173.46	10.97	91.4	—	—	—	—	—	—	—
33X-1	176.40	11.53	96.0	—	—	—	—	—	—	—
34X-1	186.03	11.26	93.8	—	—	—	—	—	—	—
35X-1	190.85	11.53	96.0	—	—	—	—	—	—	—
37X-1	200.43	11.99	99.9	—	—	—	—	—	—	—
38X-1	205.31	11.07	92.2	—	—	—	—	—	—	—
39X-1	210.62	11.47	95.5	—	—	—	—	—	—	—
40X-1	214.88	11.96	99.7	—	—	—	—	—	—	—
41X-1	219.98	6.17	51.4	6.53	0.36	0.08	0.47	0.55	4.50	0.77
41X-2	221.67	9.81	81.7	—	—	—	—	—	—	—
41X-CC	222.54	11.81	98.4	—	—	—	—	—	—	—
42X-1	224.47	11.65	97.0	—	—	—	—	—	—	—
43X-2	231.19	8.25	68.8	8.52	0.26	0.07	0.68	0.44	3.71	0.38
43X-3	233.09	8.43	70.2	—	—	—	—	—	—	—
44X-1	234.38	5.97	49.7	—	—	—	—	—	—	—
44X-2	236.08	6.51	54.2	6.98	0.47	0.07	0.84	0.58	6.71	0.56
44X-3	237.10	5.56	46.4	—	—	—	—	—	—	—
45X-1	239.18	4.54	37.8	5.02	0.48	0.08	0.93	0.82	6.00	0.52
45X-3	241.90	7.07	58.9	—	—	—	—	—	—	—
46X-1	243.98	8.24	68.7	8.58	0.34	0.07	0.85	0.46	4.86	0.40
46X-3	246.83	10.49	87.4	—	—	—	—	—	—	—
46X-4	249.43	9.81	81.7	—	—	—	—	—	—	—
47X-1	253.85	10.40	86.6	—	—	—	—	—	—	—
47X-3	256.86	9.92	82.7	—	—	—	—	—	—	—
47X-5	259.84	9.85	82.0	—	—	—	—	—	—	—
48X-1	263.45	9.47	78.9	9.62	0.15	0.02	0.23	0.27	7.50	0.65
48X-3	265.95	11.77	98.1	—	—	—	—	—	—	—

Table T12 (continued).

Core, section	Depth (mbsf)	IC (wt%)	$CaCO_3$ (wt%)	TC (wt%)	TOC (wt%)	Total N (wt%)	Total S (wt%)	Total H (wt%)	C/N ratio	C/S ratio
49X-1	272.80	9.91	82.6	—	—	—	—	—	—	—
49X-3	275.30	11.14	92.8	—	—	—	—	—	—	—
50X-1	282.40	9.81	81.7	—	—	—	—	—	—	—
50X-2	283.90	11.47	95.5	—	—	—	—	—	—	—
50X-3	284.90	10.65	88.5	10.82	0.15	0.02	0.07	0.15	10.00	2.14
51X-1	292.26	10.02	83.5	10.03	0.01	0.04	0.23	0.14	0.29	0.04
51X-3	295.28	9.56	79.7	10.10	0.54	0.01	0.21	0.12	45.00	2.57
52X-1	301.85	10.84	90.3	—	—	—	—	—	—	—
53X-1	311.17	10.15	84.5	—	—	—	—	—	—	—
54X-1	315.80	10.33	86.0	—	—	—	—	—	—	—
55X-CC	320.57	10.03	83.6	10.70	0.67	0.02	0.08	0.09	37.22	8.59
56X-CC	325.37	10.09	84.0	—	—	—	—	—	—	—
58X-1	340.45	9.77	81.4	—	—	—	—	—	—	—
58X-3	343.45	9.64	80.3	9.85	0.20	0.02	0.37	0.27	10.00	0.54
58X-5	346.31	10.28	85.7	—	—	—	—	—	—	—
59X-1	350.15	10.21	85.1	—	—	—	—	—	—	—
59X-3	352.97	10.09	84.0	10.16	0.07	0.02	0.22	0.17	3.18	0.32
59X-5	356.00	10.25	85.4	—	—	—	—	—	—	—
60X-1	359.76	10.62	88.5	—	—	—	—	—	—	—
60X-3	362.72	9.57	79.7	—	—	—	—	—	—	—
60X-5	365.67	6.50	54.1	7.23	0.73	0.10	1.05	0.65	7.30	0.70
61X-1	369.50	11.12	92.6	—	—	—	—	—	—	—
61X-3	372.23	9.88	82.3	—	—	—	—	—	—	—
61X-5	375.15	10.54	87.8	—	—	—	—	—	—	—
62X-1	379.06	10.13	84.4	—	—	—	—	—	—	—
62X-3	382.11	10.47	87.2	—	—	—	—	—	—	—
62X-5	385.07	8.61	71.7	8.87	0.26	0.03	0.22	0.35	8.67	1.18
63X-1	388.65	11.43	95.2	—	—	—	—	—	—	—
64X-1	397.84	11.74	97.8	—	—	—	—	—	—	—
66X-1	412.42	11.23	93.6	—	—	—	—	—	—	—
67X-CC	416.95	11.67	97.2	—	—	—	—	—	—	—
68X-CC	421.77	9.97	83.1	—	—	—	—	—	—	—
69X-CC	426.56	7.36	61.3	7.47	0.11	0.00	0.00	0.07	137.50	—
70X-CC	431.27	3.44	28.7	5.17	1.73	0.00	0.00	0.09	—	—
73X-CC	445.67	2.03	16.9	2.90	0.87	0.01	0.00	0.08	62.14	—
75X-CC	455.43	4.58	38.1	5.23	0.65	0.01	0.31	0.20	72.22	2.10
76X-1	460.35	9.73	81.0	—	—	—	—	—	—	—
77X-CC	465.03	10.97	91.4	—	—	—	—	—	—	—
78X-1	469.96	9.24	76.9	—	—	—	—	—	—	—
79X-1	475.28	5.01	41.7	5.41	0.40	0.03	0.58	0.50	13.33	0.69
79X-3	477.46	7.07	58.9	7.01	0.00	0.00	0.37	0.29	—	0.00
80X-1	479.60	3.04	25.3	3.23	0.19	0.01	0.22	0.42	19.00	0.86
81X-1	484.40	2.13	17.7	2.38	0.25	0.02	0.11	0.41	12.50	2.27
82X-1	494.00	0.61	5.1	0.83	0.22	0.02	0.54	0.47	11.00	0.41
83X-CC	503.45	6.42	53.5	6.62	0.20	0.01	0.00	0.03	20.00	—
194-1193B-										
1R-1	35.85	11.68	97.3	—	—	—	—	—	—	—
1R-1	36.33	11.86	98.8	—	—	—	—	—	—	—
1R-2	36.61	11.96	99.6	—	—	—	—	—	—	—
1R-2	36.99	11.93	99.3	—	—	—	—	—	—	—
2R-1	45.02	11.92	99.3	—	—	—	—	—	—	—
2R-1	45.63	11.86	98.8	—	—	—	—	—	—	—
2R-2	46.11	11.92	99.3	—	—	—	—	—	—	—
3Z-1	53.98	11.81	98.4	—	—	—	—	—	—	—
5Z-1	63.61	11.81	98.3	—	—	—	—	—	—	—
5Z-1	64.27	10.77	89.7	—	—	—	—	—	—	—
6Z-1	68.13	11.69	97.4	—	—	—	—	—	—	—
6Z-1	68.93	11.91	99.2	—	—	—	—	—	—	—
8Z-1	73.41	11.99	99.9	—	—	—	—	—	—	—
8Z-1	74.11	11.41	95.1	—	—	—	—	—	—	—
9Z-1	77.15	11.85	98.7	—	—	—	—	—	—	—
9Z-1	77.66	11.86	98.8	—	—	—	—	—	—	—
11Z-1	86.74	11.92	99.3	—	—	—	—	—	—	—
11Z-1	87.50	11.79	98.2	—	—	—	—	—	—	—
12Z-1	91.55	11.94	99.5	—	—	—	—	—	—	—
12Z-1	91.92	11.86	98.8	—	—	—	—	—	—	—
14Z-1	100.64	12.48	104.0	—	—	—	—	—	—	—
14Z-1	100.72	12.02	100.2	—	—	—	—	—	—	—
16Z-1	110.07	11.64	96.9	—	—	—	—	—	—	—

Table T12 (continued).

Core, section	Depth (mbsf)	IC (wt%)	$CaCO_3$ (wt%)	TC (wt%)	TOC (wt%)	Total N (wt%)	Total S (wt%)	Total H (wt%)	C/N ratio	C/S ratio
17Z-1	114.93	12.28	102.3	—	—	—	—	—	—	—
17Z-1	115.37	11.82	98.4	—	—	—	—	—	—	—
19Z-1	124.13	12.11	100.9	—	—	—	—	—	—	—
20Z-1	128.90	12.56	104.7	—	—	—	—	—	—	—
194-1193C-										
1R-1	35.20	11.39	94.9	—	—	—	—	—	—	—
1R-2	36.98	12.02	100.2	—	—	—	—	—	—	—
1R-2	37.69	11.97	99.7	—	—	—	—	—	—	—
2R-1	44.83	12.01	100.1	—	—	—	—	—	—	—
2R-1	45.25	11.98	99.8	—	—	—	—	—	—	—
3R-1	51.57	11.98	99.8	—	—	—	—	—	—	—
4R-1	60.76	11.85	98.7	—	—	—	—	—	—	—
4R-1	61.09	10.72	89.3	—	—	—	—	—	—	—
4R-2	62.59	11.75	97.9	—	—	—	—	—	—	—
5R-2	512.17	3.21	26.7	—	—	—	—	—	—	—
5R-2	512.24	4.50	37.5	4.28	0.00	0.00	0.48	0.42	—	—
5R-3	513.50	7.54	62.8	—	—	—	—	—	—	—
5R-4	515.18	6.46	53.9	—	—	—	—	—	—	—
5R-4	515.19	7.13	59.4	7.40	0.28	0.00	0.20	0.23	—	1.40
6R-1	520.64	6.92	57.6	6.48	0.00	0.00	0.35	0.25	—	—
6R-1	520.69	7.68	64.0	—	—	—	—	—	—	—
6R-2	521.69	2.67	22.2	—	—	—	—	—	—	—
6R-2	521.87	1.61	13.4	—	—	—	—	—	—	—
7R-1	530.49	7.02	58.5	6.53	0.00	0.00	0.43	0.28	—	—
7R-1	530.49	1.12	9.3	—	—	—	—	—	—	—

Notes: IC = inorganic carbon, TC = total carbon, TOC = total organic carbon, C/N = carbon/nitrogen, C/S = carbon/sulfur. — = not analyzed.

Table T13. Results of Rock-Eval analyses on sediments, Site 1193. (See table notes. Continued on next page.)

Core, section	Depth (mbsf)	T_{max}	S_1	S_2	S_3	HI	OI	TOC (wt%)
194-1193A-								
1H-2	2.25	431	0.05	0.05	0.37	125	925	0.04
1H-4	5.25	399	0.08	0.12	0.71	150	887	0.08
2H-2	8.85	407	0.09	0.37	1.01	123	336	0.30
2H-4	11.85	404	0.11	0.38	1.40	135	500	0.28
3H-2	18.35	398	0.13	0.28	1.44	107	553	0.26
3H-4	21.35	405	0.10	0.24	0.82	133	455	0.18
3H-6	24.35	407	0.07	0.20	0.73	105	384	0.19
4H-2	27.85	409	0.04	0.17	0.15	100	88	0.17
4H-4	30.85	412	0.13	0.34	0.71	136	284	0.25
4H-6	33.85	412	0.08	0.25	0.74	156	462	0.16
6X-CC	37.21	356	0.01	0.03	0.00	166	0	0.02
7X-1	42.13	341	0.01	0.03	0.00	225	0	0.02
9X-1	56.11	—	0.02	0.01	0.00	—	—	0.00
10X-1	61.45	390	0.00	0.02	0.00	200	0	0.01
12X-1	70.93	366	0.01	0.03	0.00	150	0	0.02
13X-1	75.71	361	0.00	0.01	0.00	100	0	0.01
14X-1	80.58	345	0.00	0.01	0.00	100	0	0.01
15X-1	85.33	354	0.01	0.01	0.00	50	0	0.02
16X-1	90.33	328	0.01	0.02	0.00	28	0	0.07
18X-1	104.66	397	0.02	0.02	0.00	150	0	0.02
19X-CC	109.35	324	0.01	0.01	0.00	50	0	0.02
20X-CC	114.15	338	0.02	0.02	0.00	100	0	0.02
21X-CC	118.99	—	0.00	0.00	0.00	0	0	0.01
22X-CC	123.76	356	0.00	0.01	0.00	33	0	0.03
23X-CC	128.63	—	0.00	0.00	0.00	0	0	0.04
24X-CC	133.33	—	0.02	0.01	0.00	25	0	0.04
25X-CC	138.38	—	0.00	0.01	0.00	33	0	0.03
26X-1	142.97	—	0.01	0.01	0.00	50	0	0.02
27X-CC	147.93	—	0.00	0.00	0.00	0	0	0.03
29X-1	157.11	376	0.02	0.01	0.00	50	0	0.02
31X-1	166.61	380	0.05	0.04	0.01	38	6	0.06
31X-2	168.99	395	0.06	0.16	0.49	69	213	0.23
32X-1	171.86	392	0.06	0.18	0.62	60	206	0.30
32X-2	173.46	348	0.02	0.04	0.01	100	25	0.04
33X-1	176.40	419	0.03	0.23	0.00	209	8	0.11
34X-1	186.03	389	0.06	0.12	0.05	133	55	0.09
35X-1	190.85	414	0.02	0.03	0.00	75	0	0.04
37X-1	200.43	382	0.04	0.03	0.05	75	125	0.04
38X-1	205.31	349	0.02	0.05	0.00	100	0	0.05
39X-1	210.62	391	0.02	0.05	0.00	100	0	0.05
40X-1	214.88	323	0.02	0.04	0.00	133	0	0.03
41X-1	219.98	398	0.24	0.37	0.20	94	51	0.39
41X-2	221.67	400	0.08	0.15	0.05	68	22	0.22
41X-CC	222.54	399	0.18	0.30	0.51	100	170	0.30
42X-1	224.47	311	0.01	0.02	0.00	100	0	0.02
43X-2	231.19	405	0.06	0.26	0.34	78	103	0.33
43X-3	233.09	412	0.06	0.23	0.40	65	114	0.35
44X-1	234.38	408	0.12	0.40	0.61	108	164	0.37
44X-2	236.08	409	0.04	0.17	0.26	54	83	0.41
44X-3	237.10	399	0.08	0.39	0.70	105	189	0.37
45X-1	239.18	404	0.11	0.36	0.89	87	217	0.41
45X-3	241.90	406	0.04	0.29	0.54	87	163	0.33
46X-1	243.98	399	0.07	0.27	0.93	96	332	0.28
46X-3	246.83	401	0.05	0.18	0.22	90	110	0.20
46X-4	249.43	412	0.05	0.31	0.39	83	105	0.37
47X-1	253.85	416	0.12	0.30	0.07	187	43	0.16
47X-3	256.86	418	0.11	0.46	0.26	184	104	0.25
47X-5	259.84	418	0.14	0.25	0.00	147	0	0.17
48X-1	263.45	414	0.16	0.28	0.15	155	83	0.18
48X-3	265.95	419	0.03	0.19	0.00	172	0	0.11
49X-1	272.80	409	0.05	0.17	0.10	121	71	0.14
49X-3	275.30	411	0.08	0.27	0.36	120	157	0.26
50X-1	282.40	418	0.08	0.27	0.07	150	38	0.18
50X-2	283.90	401	0.08	0.14	0.23	127	209	0.11
50X-3	284.90	419	0.13	0.44	0.18	200	81	0.22
51X-1	292.26	406	0.06	0.14	0.00	140	0	0.10
51X-3	295.28	416	0.03	0.11	0.10	137	125	0.08
52X-1	301.85	410	0.04	0.13	0.00	185	0	0.07
53X-1	311.17	419	0.14	0.42	0.10	230	56	0.18
54X-1	315.80	417	0.03	0.17	0.00	141	0	0.12
55X-CC	320.57	417	0.07	0.21	0.01	161	7	0.13
56X-CC	325.37	416	0.05	0.28	0.00	155	0	0.18
58X-1	340.45	412	0.06	0.26	0.07	123	33	0.21
58X-3	343.45	413	0.07	0.24	0.09	126	47	0.19
58X-5	346.31	416	0.12	0.40	0.13	173	56	0.23
59X-1	350.15	417	0.11	0.37	0.12	176	57	0.21
59X-3	352.97	412	0.13	0.33	0.01	173	5	0.19
59X-5	356.00	415	0.18	0.32	0.00	200	0	0.16
60X-1	359.76	418	0.07	0.34	0.03	154	13	0.22
60X-3	362.72	416	0.09	0.40	0.12	176	110	0.26
60X-5	365.67	419	0.19	1.00	0.57	104	59	0.96
61X-1	369.50	412	0.11	0.19	0.00	126	0	0.15
61X-3	372.23	414	0.08	0.20	0.02	133	13	0.15
61X-5	375.15	421	0.09	0.28	0.01	186	6	0.15
62X-1	379.06	418	0.06	0.26	0.03	133	0	0.18
62X-3	382.11	416	0.09	0.20	0.00	166	0	0.12
62X-5	385.07	415	0.13	0.42	0.04	139	13	0.31
63X-1	388.65	404	0.04	0.09	0.23	150	383	0.06
64X-1	397.84	403	0.03	0.06	0.21	200	700	0.03
67X-CC	416.95	404	0.05	0.07	0.17	233	566	0.03
68X-CC	421.77	370	0.03	0.05	0.00	100	0	0.05
69X-CC	426.56	—	0.01	0.01	0.00	—	—	0.00
70X-CC	431.27	366	0.02	0.02	0.00	100	0	0.02
73X-CC	445.67	400	0.17	0.98	0.26	204	54	0.48
75X-CC	455.43	391	0.05	0.03	0.00	30	0	0.10
76X-1	460.35	—	0.04	0.01	0.00	100	0	0.01
77X-CC	465.03	322	0.02	0.01	0.00	100	0	0.01
78X-1	469.96	405	0.04	0.10	0.01	71	7	0.14
79X-1	475.28	413	0.08	0.21	0.14	65	43	0.32
79X-3	477.46	327	0.00	0.02	0.17	18	154	0.11
79X-3	477.46	390	0.07	0.09	0.00	69	0	0.13
80X-1	479.60	388	0.09	0.09	0.00	90	0	0.10
81X-1	484.40	382	0.05	0.06	0.00	92	0	0.09
82X-1	494.00	409	0.05	0.12	0.04	65	17	0.18
83X-CC	503.45	—	0.01	0.01	0.00	100	0	0.01
194-1193B-								
1R-1	35.85	—	0.01	0.00	0.00	—	—	0.00
1R-1	36.33	332	0.02	0.02	0.11	—	—	0.00
1R-2	36.61	332	0.01	0.02	0.00	—	—	0.00
1R-2	36.99	370	0.02	0.02	0.00	—	—	0.00
2R-1	45.02	313	0.02	0.02	4.49	—	—	0.00
2R-1	45.63	—	0.00	0.00	0.00	—	—	0.00
2R-2	46.11	332	0.02	0.02	0.00	—	—	0.00
3Z-1	53.98	—	0.11	0.01	0.00	100	0	0.01
5Z-1	63.61	—	0.03	0.00	0.00	—	—	0.00
5Z-1	64.27	—	0.09	0.00	0.00	0	0	0.01
6Z-1	68.13	302	0.04	0.01	0.00	—	—	0.00
6Z-1	68.93	—	0.06	0.01	0.00	100	0	0.01
8Z-1	73.41	301	0.06	0.02	0.00	—	—	0.00
8Z-1	74.11	—	0.04	0.01	0.00	—	—	0.00
9Z-1	77.15	—	0.05	0.00	0.00	0	0	0.01
9Z-1	77.66	—	0.02	0.00	0.00	—	—	0.00
11Z-1	86.74	346	0.03	0.02	0.00	—	—	0.00
11Z-1	87.50	303	0.05	0.01	0.00	100	0	0.01
12Z-1	91.55	365	0.04	0.07	1.19	650	—	0.01
12Z-1	91.92	410	0.03	0.01	0.49	100	4900	0.01
14Z-1	100.64	319	0.08	0.02	0.53	50	1325	0.04
14Z-1	100.72	307	0.11	0.02	0.08	100	400	0.02
16Z-1	110.07	346	0.11	0.03	0.76	150	3800	0.02
17Z-1	114.93	337	0.02	0.02	0.00	100	0	0.02
17Z-1	115.37	311	0.08	0.01	0.53	100	5300	0.01
19Z-1	124.13	—	0.02	0.00	0.00	—	—	0.00
20Z-1	128.90	371	0.03	0.05	0.00	166	0	0.03

Table T13 (continued).

Core, section	Depth (mbsf)	T_{max}	S_1	S_2	S_3	HI	OI	TOC (wt%)
194-1193C-								
1R-1	35.20	329	0.01	0.01	0.00	—	—	0.00
1R-2	36.98	386	0.01	0.01	0.00	—	—	0.00
1R-2	37.69	—	0.00	0.00	20.71	—	—	0.00
2R-1	44.83	—	0.00	0.00	0.00	—	—	0.00
2R-1	45.25	400	0.02	0.02	0.74	—	—	0.00
3R-1	51.57	374	0.01	0.02	1.18	—	—	0.00
4R-1	60.76	—	0.01	0.00	0.00	—	—	0.00
4R-1	61.09	—	0.12	0.02	0.00	50	0	0.04
4R-2	62.59	320	0.05	0.03	0.00	—	—	0.00
5R-2	512.17	—	0.04	0.00	0.00	—	—	0.11
5R-2	512.24	393	0.01	0.05	0.46	50	460	0.10
5R-3	513.50	383	0.23	0.22	0.00	104	0	0.21
5R-4	515.18	343	0.01	0.01	0.17	25	425	0.04
5R-4	515.19	352	0.09	0.09	0.00	150	0	0.06
6R-1	520.64	324	0.00	0.01	0.19	33	633	0.03
6R-1	520.69	386	0.17	0.10	0.00	58	0	0.17
6R-2	521.69	376	0.35	0.31	2.52	68	560	0.45
6R-2	521.87	379	0.22	0.08	1.45	42	763	0.19
7R-1	530.49	362	0.20	0.06	0.21	41	300	0.14

Notes: T_{max} = temperature of maximum hydrocarbon generation during pyrolysis in °C, S_1 = milligrams of free hydrocarbons per gram of rock, S_2 = milligrams of pyrolyzed hydrocarbons per gram of rock, S_3 = milligrams of carbon dioxide per gram of rock, HI = hydrogen index in milligrams of hydrocarbon per gram of TOC, OI = milligrams of carbon dioxide per gram of TOC, TO = total organic carbon. — = not available.